UNIVERSITÉ DU QUÉBEC À MONTRÉAL

SEASONAL DYNAMICS OF THE MAJOR PROCESSES SUSTAINING CO_2 EMISSIONS FROM BOREAL LAKES

DISSERTATION

PRESENTED

AS PARTIAL REQUIREMENT

OF THE DOCTORATE OF BIOLOGY

BY

DOMINIC VACHON

FEBRUARY 2016

UNIVERSITÉ DU QUÉBEC À MONTRÉAL

DYNAMIQUES SAISONNIÈRES DES PRINCIPAUX PROCESSUS QUI SOUTIENNENT LES ÉMISSIONS DE CO_2 DANS LES LACS BORÉAUX

THÈSE

PRESENTÉE

COMME EXIGENCE PARTIELLE

DU DOCTORAT EN BIOLOGIE

PAR

DOMINIC VACHON

FÉVRIER 2016

REMERCIEMENTS

Avant d'écrire une thèse, il y a tout un cheminement qui passe entre autres par la réflexion, l'élaboration de protocole, la préparation de terrain, l'échantillonnage, les manipulations au laboratoire, la compilation de données, l'analyse statistique, la structure des chapitres, les premières versions de manuscrits, les deuxièmes versions…jusqu'aux versions finales puis, finalement, la thèse. Derrière chacune de ces étapes, des collègues, professionnels de recherches, des professeurs, des amis et ma famille y ont tous contribué de manière significative. Sans eux, chacune de ces étapes aurait, soit été un désastre, soit une étape extrêmement pénible et ardue, ou bien tout simplement impossible à réaliser. Je profite donc des quelques lignes qui suivent pour les remercier sincèrement.

Je remercie tout d'abord Paul del Giorgio, mon directeur de recherche, mais avant tout un mentor qui m'a enseigné et transmis sa vision de la science et sa façon bien particulière d'accorder de l'importance à la vue d'ensemble et au contexte de ce que nous faisons. J'aimerais aussi souligner l'importance de la présence de Yves Prairie dans mon cheminement académique. Il m'a non seulement introduit à la limnologie, mais aussi transmis sa passion et je lui serai éternellement reconnaissant. Yves et Paul, par vos apports complémentaires et riches à leurs manières, vous resterez ma référence en limnologie et en sciences pour bien longtemps. Mon cheminement m'a aussi permis de rencontrer d'autres chercheurs/professeurs qui ont eu un impact significatif sur mon développement, notamment Chris Solomon, Paul Hanson et Jan Karlsson. Un profond merci à vous pour votre générosité.

J'aimerais remercier tous mes collègues proches et lointains qui ont aussi eu un rôle à jouer dans mon cheminement. D'abord, tous les étudiants et aides de terrain du CARBBAS. Les anciens : Jérôme, François, Marie-Ève, Rich, Lisa, Véro, Soren,

Delphine et Simon, Martine, je vous remercie de m'avoir initié au GRIL-UQAM et les moins anciens : Audrey, Marilyne, Lennie, J-F, Geneviève, Martin, Cristian (Teo), Justine, Sara, J-P, Nico, Juan-Pablo, Carolina, Matt, Terhi, Adam, Ryan, Clara, Tonya, Shoji, MingFeng, Cyntia, Mathieu, Julien, Sonya, Karelle, Katheri, Marie, et sans oublier les merveilleuses Annick, Alice et Katherine. Je vous remercie tous pour les discussions plus ou moins scientifiques, les heures de passer au Benelux, en congrès, sur le terrain, au SB-1115 ou à brasser de la bière.

Je voudrais aussi remercier les étudiants du GRIL, Marie-Andrée, Claudette et le GRIL en général pour l'appui financier et le GLEON pour faire mousser la science collaborative. Je remercie aussi grandement le personnel des stations de recherche, particulièrement les gérants de station Éric Valiquette au Lac Croche, Patrick Nadeau au Lac Simoncouche et Raynald Julien au Lac Hébécourt. Merci, vous avez toujours été d'une grande aide.

Finalement, je voudrais remercier ma famille pour tout le soutien moral et parfois même financier : mes parents André et Francine et mes frères Philippe et Marc-André, mais surtout ma femme, Andréa et ma fille Mathilde. Merci.

TABLE DES MATIÈRES

LISTE DES FIGURES

Figure Page

LISTE DES TABLEAUX

Tableau Page

RÉSUMÉ GÉNÉRAL

Dans les paysages boréaux, les eaux de surface des lacs sont systématiquement sursaturées en dioxyde de carbone (CO_2) par rapport à l'atmosphère. Les divers processus qui sont impliqués dans ce phénomène sont bien connus, bien que des informations sur la variabilité temporelle et l'importance relative de ces mécanismes sous-jacents qui influencent la dynamique de CO_2 selon les saisons et aussi à travers différents types de lacs restent rares dans la littérature. Dans cette thèse, trois lacs nordiques (c.-à-d. boréal et tempéré du nord) ayant des caractéristiques limnologiques représentatives du paysage québécois ont été échantillonnés mensuellement sur un cycle annuel complet. Les travaux qui émergent de cette thèse portent sur les principaux processus qui influencent la dynamique du CO_2 dans les lacs du nord, en intégrant des mesures de terrain, des incubations en laboratoire et de la modélisation.

Pour soutenir les émissions de CO_2, le lac doit soit "brûler" du carbone organique terrestre ou soit purger le CO_2 qui a été produit dans son bassin versant. Nous avons d'abord (chapitre I) évalué le rôle et les taux de production de CO_2 de la colonne d'eau dans le lac par deux voies principales : la minéralisation photochimique du carbone organique dissous (COD) et la respiration biologique pélagique. Nous avons constaté que les taux de photo-minéralisation ont été principalement générés par la photo-réactivité intrinsèque du COD et les radiations solaires, tous deux montrant une saisonnalité marquée. En conséquence, la contribution de la photo-minéralisation à la production pélagique de CO_2 a atteint un sommet au printemps (> 50 %) et en moyenne de 11 % pour toute la saison libre de glace. Une portion de la minéralisation biologique et photochimique a été alimentée par le COD allochtone (COD_{alloch}) entrant dans le lac (chapitre II). Nous avons conclu que la minéralisation du COD_{alloch} pourrait contribuer jusqu'à 30-40 % de la pression partielle de CO_2 (pCO_2) observée dans un ensemble de lacs boréaux. Nous avons montré que, lorsque la dégradabilité du COD_{alloch} est considérée comme étant un continuum de réactivité, le rôle de l'hydrologie peut en partie moduler la dégradabilité du COD observée dans les lacs boréaux et donc le potentiel de production de CO_2. De plus, nous avons établi que les apports hydrologiques aux lacs boréaux peuvent charger de grandes quantités de CO_2 dérivées des sols, surtout après des événements de tempêtes (chapitre III). L'ampleur de ces flux de CO_2 provenant du bassin versant est en outre influencée par la morphométrie du système, suggérant que les lacs avec un grand bassin versant par rapport à son volume sont plus susceptibles de recevoir des apports directs de CO_2, après des épisodes de pluies intenses.

La variabilité saisonnière des facteurs externes tels que la température, la radiation et de l'hydrologie suggère que les principaux processus soutenant les émissions de CO_2

sont également variables et peuvent se succéder au long d'un cycle annuel. Nous avons combiné tous les processus abordés dans les chapitres I, II et III dans un cadre commun pour évaluer la succession temporelle de l'importance relative de ces processus aux émissions CO_2 (chapitre IV). Nos résultats suggèrent que l'importance relative de chaque processus est non seulement variable selon les lacs, mais aussi très variable selon les saisons au sein d'un même lac. En été, les émissions de CO_2 sont principalement alimentées par les métabolismes pélagique et benthique, tandis que les émissions de CO_2 à l'automne et au printemps sont généralement soutenues par les apports hydrologiques de CO_2. Le travail de cette thèse suggère que la morphologie du lac et le régime hydro-climatique sont des facteurs clés modulant la dynamique temporelle du CO_2 dans les lacs boréaux. Ils déterminent comment ces lacs transforment le COD, leur force de liaison avec l'environnement terrestre environnant, leur sensibilité aux tempêtes et aussi la succession saisonnière des processus qui façonnent la dynamique de CO_2. Une meilleure compréhension des processus temporels qui soutiennent les émissions de CO_2 des systèmes aquatiques boréaux est un pas en avant dans l'évaluation du rôle des lacs et l'ampleur de leur réponse face aux futurs changements environnementaux.

Mots clés : lacs boréaux, dioxyde de carbone, carbone organique dissous, hydrologie, tempêtes

GENERAL SUMMARY

In boreal landscapes, the surface water of lakes has been shown to be systematically oversaturated in carbon dioxide (CO_2) relative to the atmosphere. Various processes are known to be involved in this phenomenon, albeit information regarding the temporal variability in the underlying processes influencing CO_2 dynamics, and how their relative importance to the lake CO_2 dynamics varies seasonally and also across different types of lakes remain scarce in the literature. In the thesis, monthly sampling of three northern (i.e. boreal and temperate) lakes having different limnological characteristics representative of the northern region in the province of Québec was conducted for an annual cycle. The work emerging from this thesis addresses the major processes influencing CO_2 dynamics in northern lakes within a common framework, by integrating field measurements, lab incubations and modeling approaches.

To sustain their CO_2 emissions, lake must either "burn" organic carbon derived from the terrestrial environment or vent the CO_2 which was produced in its catchment. We first (chapter I) evaluated the role and rates of in-lake water column CO_2 production by two major pathways: photo-chemical mineralization of dissolved organic carbon (DOC) and pelagic biological respiration. We found that areal rates of DOC photo-mineralization were mostly driven by the intrinsic DOC photo-reactivity and solar radiation, both showing strong seasonality. As a result, the contribution of DOC photo-mineralization to pelagic CO_2 production peaked during spring (>50%) and averaged 11% for the entire open water season. Part of the pelagic photo-chemical and biological mineralization was fueled by allochthonous DOC (DOC_{alloch}) entering the lake (Chapter II). We concluded that the combined DOC_{alloch} biological and photo-chemical mineralization could potentially contribute up to 30-40% of the observed surface carbon dioxide partial pressure (pCO_2) across a set of boreal lakes. We further showed that, when DOC_{alloch} degradability is considered as a continuum of reactivity, the role of hydrology by itself may modulate the resulting DOC degradability observed in boreal lakes, and thus the potential for producing CO_2. We further established that the hydrologic inputs to boreal lakes can load large amounts of soil-derived CO_2 to lakes, especially after intense storm events (Chapter III). The magnitude of these fluxes of CO_2 from the catchment to the surface of lakes is further influenced by the lake morphometry and catchment size, suggesting that lakes with large watershed to lake volume ratios are more susceptible to receive direct CO_2 inputs after rain storm events.

The seasonal variability in external drivers such as temperature, light and hydrology in boreal lakes suggests that the major processes sustaining CO_2 emissions are also variable and may succeed each other along an annual cycle. We combined all the major processes addressed in Chapters I, II and III within a common framework to evaluate

the temporal succession in the relative importance to CO_2 dynamics and emissions (Chapter IV). Our results suggest that the relative importance of each process sustaining CO_2 emissions is not only variable among lakes, but also highly variable among seasons within one lake. In summer, CO_2 emissions are mostly fueled by pelagic and benthic metabolism, while fall and spring CO_2 emissions were generally sustained by hydrologic CO_2 inputs. The work from this thesis suggests that lake morphology and hydrology are key modulators of the temporal CO_2 dynamics in boreal lakes, and further determine how these lakes process DOC, their linkage strength with the surrounding terrestrial environment, their sensitivity to storms events, and also the seasonal succession of the processes shaping the temporal CO_2 dynamics. A better understanding of temporal processes sustaining CO_2 emissions from boreal aquatic systems is step further in assessing the magnitude and direction of their response to future environmental changes.

Key words: boreal lakes, carbon dioxide, allochthonous dissolved organic carbon, mineralization, hydrology, storms

INTRODUCTION

0.1 LE CYCLE GLOBAL DU CARBONE ET LES LACS BORÉAUX

Une proportion importante de carbone (C) capté par les écosystèmes terrestres est exportée vers les océans par les réseaux aquatiques continentaux. Cependant, au lieu de transporter passivement ce C vers les océans, les écosystèmes aquatiques agissent plutôt comme des réacteurs (Cole *et al.*, 2007), émettant vers l'atmosphère près de 50 % du carbone reçu (Tranvik *et al.*, 2009). La transformation active du C entraîne des émissions de CO_2 disproportionnées par rapport à la petite fraction qu'occupent les écosystèmes aquatiques dans le milieu terrestre (Downing *et al.*, 2006; Downing *et al.*, 2012; Verpoorter *et al.*, 2014). Les émissions globales de C sous forme de dioxyde de carbone (CO_2) des milieux aquatiques d'eau douce ont été récemment estimés à environ 2.1 Pg C a^{-1} (Raymond *et al.*, 2013). Bien que ce chiffre soit associé à de larges incertitudes, ces flux de CO_2 sont à un niveau comparable aux océans et aux milieux terrestres, qui ont la capacité d'absorber environ 2.3 et 2.6 Pg C par année, respectivement (IPCC, 2013). Alors que le rôle des écosystèmes aquatiques d'eau douce dans le cycle global du carbone est maintenant bien accepté, plusieurs incertitudes subsistent concernant la variabilité naturelle des émissions de CO_2 ainsi que la dynamique des processus sous-jacents qui établissent les liens entre le carbone d'origine terrestre et les émissions de CO_2 des milieux aquatiques.

Étant parmi les plus abondants globalement (Verpoorter *et al.*, 2014), les lacs des régions boréale et tempérée du nord (ci-après dénommé « lacs boréaux ») jouent un rôle particulièrement important dans le bilan global du C. La connexion étroite qui existe entre le milieu terrestre et le réseau aquatique boréal occasionne des teneurs élevées en carbone organique dissous (COD) d'origine terrestres dans les lacs (Wilkinson *et al.*, 2013), avec des conséquences importantes sur son fonctionnement

(Prairie, 2008; Seekell *et al.*, 2015). Ayant longtemps été considéré réfractaire à la dégradation, ce carbone organique d'origine terrestre est en fait réactif biologiquement (Ågren *et al.*, 2008; Marin-Spiotta *et al.*, 2014; McCallister et del Giorgio, 2008) et aussi photo-chimiquement (Opsahl et Benner, 1998; Wetzel *et al.*, 1995). De plus, contrairement aux ruisseaux et rivières, le temps de séjour des lacs est plus beaucoup plus long, laissant la possibilité à la surface de l'eau de se réchauffer et de recevoir des radiations solaires importantes (Kalff, 2002), ce qui fait des lacs boréaux des milieux privilégiés pour la transformation du COD terrestre (Algesten *et al.*, 2003; Cole *et al.*, 2007). Ainsi, la concentration de COD des lacs boréaux est souvent corrélée à la pression partielle de CO_2 (pCO_2) à la surface de l'eau (Lapierre et del Giorgio, 2012; Larsen *et al.*, 2011; Roehm *et al.*, 2009), ce qui suggère qu'il existe des liens soit directs ou indirects entre le milieu terrestre et les émissions de CO_2 des lacs boréaux (Lapierre *et al.*, 2013; Lapierre et del Giorgio, 2012).

Le biome boréal est en perpétuelle transition et fait face notamment à d'importants changements au niveau climatique, prévoyant subir des hausses de température moyenne plus prononcée que la tendance globale (IPCC, 2013). À cela s'ajoute une tendance d'augmentation de la concentration en COD dans les lacs et rivières (Monteith *et al.*, 2007; Roulet et Moore, 2006), mais aussi des perturbations naturelles et anthropogéniques telles que les coupes forestières et la création de réservoirs hydroélectriques. De larges incertitudes persistent donc relativement aux impacts que ces perturbations anthropogéniques auront sur les flux de carbone aquatique. Une meilleure compréhension des mécanismes impliqués dans la dynamique du C des lacs est donc nécessaire, non seulement pour prédire avec moins d'incertitude les émissions de CO_2 provenant des milieux aquatiques d'eau douce dans le biome boréal, mais aussi pour évaluer les impacts des perturbations sur les bilans de C aquatique lors des futures efforts d'atténuation des émissions de gaz à effet de serre (Battin *et al.*, 2009; Tranvik *et al.*, 2009).

0.2 PROCESSUS DE RÉGULATION DU CO_2 À LA SURFACE DES LACS BORÉAUX

De nombreux processus biologiques, chimiques et physiques ajoutent et enlèvent du CO_2 dans la colonne d'eau des lacs. Ainsi dans les lacs boréaux, l'équilibre des entrées et des sorties résulte la plupart du temps en un excès en CO_2. Parmi les processus qui ajoutent du CO_2 à la surface des lacs boréaux, nombreux ont été mis en évidence comme étant significatifs aux émissions de CO_2 dans les lacs : la respiration pélagique de la matière organique allochtone (RP), la respiration benthique (RB), la photo-minéralisation du COD (PM) et l'apport hydrique de CO_2 provenant du bassin versant (AH).

0.2.1 Respiration pélagique

La respiration dans les lacs recycle la matière organique produite par photosynthèse vers sa fraction inorganique gazeuse, le CO_2. Ce processus peut prendre place dans la colonne d'eau par la communauté planctonique hétérotrophe (Figure 0.1a). Comme tout processus biologique, la température joue un rôle important pour la respiration (Pace et Prairie, 2005; Yvon-Durocher *et al.*, 2012). Toutefois, les taux de respiration pélagiques sont susceptibles d'être couplés avec l'état trophique du lac et ses apports en matière organique. Ainsi, il existe des relations positives entre la respiration pélagique et la chlorophylle *a* (chl*a*), le phosphore total (TP) et COD (Pace et Prairie, 2005). Cependant, si la respiration pélagique recycle la matière produite localement (COD autochtone), aucun excès de CO_2 ne sera observé. Par conséquent, dans le contexte de sursaturation de CO_2 à la surface des lacs, la question de l'origine du COD respiré est donc cruciale. La matière organique provenant du milieu terrestre peut soutenir la respiration bactérienne pélagique (Karlsson *et al.*, 2007; McCallister et del Giorgio, 2008). En effet, il est de plus en plus accepté que la matière organique allochtone soit labile pour les bactéries aquatiques (Guillemette *et al.*, 2013; Lapierre

et al., 2013; Marin-Spiotta *et al.*, 2014). Cette utilisation du COD allochtone par les bactéries cause un déséquilibre du métabolisme pélagique, résultant en un excès de respiration par rapport à la production primaire (R > P) (del Giorgio *et al.*, 1997), ce qui serait une des causes des émissions de CO_2 des lacs (del Giorgio *et al.*, 1999). Ce phénomène est davantage marqué dans les lacs peu productifs et ayant des concentrations en COD terrestre élevées (del Giorgio et Peters, 1994; Jansson *et al.*, 2008; Prairie *et al.*, 2002).

0.2.2 Photo-minéralisation du COD dans la colonne d'eau

Le carbone organique d'origine terrestre peut aussi absorber les rayons UV provenant des radiations solaires qui pénètrent dans la colonne d'eau et être photo-minéralisé pour produire du CO_2 à la surface des lacs boréaux (Figure 0.1b). Plusieurs études ont d'ailleurs démontré que ce processus peut être significatif à l'échelle de l'écosystème (Cory *et al.*, 2014; Granéli *et al.*, 1996; Koehler *et al.*, 2014). L'importance de la photo-minéralisation est par contre extrêmement variable parmi ces études. Certaines d'entre elles ont montré que la photo-minéralisation du COD est le principal processus de perte de carbone organique dans les lacs boréaux et arctique (Cory *et al.*, 2014; Molot et Dillon, 1997), tandis que d'autres révèlent une contribution plutôt moindre mais significative (Granéli *et al.*, 1996; Koehler et Tranvik, 2015). Lorsque la photo-minéralisation est intégrée dans la colonne d'eau, les taux ne semblent pas être reliés à la quantité de COD des lacs (Koehler *et al.*, 2014). Cette variabilité des taux observés soulève donc certaines questions relatives à la variabilité de la photo-réactivité du COD. Il semble que celle-ci soit changeante selon les saisons (Gonsior *et al.*, 2013; Lindell *et al.*, 2000). Le rôle de la photo-réactivité intrinsèque du COD est loin d'être compris et pourrait potentiellement jouer un rôle important pour en déterminer les tendances à la surface des lacs boréaux.

0.2.3 Minéralisation de la matière organique des sédiments

La minéralisation de la matière organique dans les sédiments par la communauté benthique produit aussi du CO_2 qui est diffusé depuis l'eau interstitielle des sédiments vers la colonne d'eau (Figure 0.1 b). Cette source de production de CO_2 peut contribuer significativement aux émissions de CO_2 des lacs boréaux (Åberg *et al.*, 2007; Algesten *et al.*, 2005; Andersson et Kumblad, 2006; Jonsson *et al.*, 2001; Kortelainen *et al.*, 2006). La contribution relative de la respiration benthique par rapport à la production totale de CO_2 est plus élevée dans les lacs peu productifs, avec beaucoup de COD (Den Heyer et Kalff, 1998; Jonsson *et al.*, 2003), mais aussi dans les lacs peu profonds (Åberg *et al.*, 2007; Jonsson *et al.*, 2001; Jonsson *et al.*, 2003; Kelly *et al.*, 2001) où le temps d'exposition à l'oxygène est plus long (Ferland *et al.*, 2014; Sobek *et al.*, 2009). En contrepartie, les lacs faibles en COD peuvent avoir de la production primaire des sédiments (Algesten *et al.*, 2005), notamment par la production benthique du périphyton (Vadeboncoeur *et al.*, 2008; Vadeboncoeur et Steinman, 2002).

0.2.4 Apports hydrologiques de CO_2 provenant du bassin versant

Les apports hydrologiques en CO_2 provenant des tributaires et de l'eau souterraine peuvent approvisionner la surface des lacs (Figure 0.1d). Ce processus peut être particulièrement important pour soutenir les émissions de CO_2 (McDonald *et al.*, 2013; Stets *et al.*, 2009), notamment dans les lacs pauvres en COD (Dubois *et al.*, 2009; Maberly *et al.*, 2012). En effet, l'eau souterraine a des concentrations élevées en CO_2 et a donc le potentiel d'influencer la dynamique du CO_2 à la surface des lacs. Notamment, Öquist *et al.*, (2009) ont constaté des niveaux en pCO_2 des eaux souterraines dans les sols boréaux 17 fois plus élevés que la concentration atmosphérique. Les ruisseaux et les rivières sont également connus pour contenir de fortes concentrations de CO_2, même si elles peuvent être très variables selon les régions (Campeau et del Giorgio, 2014; Jones *et al.*, 2003; Koprivnjak *et al.*, 2010;

Weyhenmeyer *et al.*, 2012). Subséquemment, une quantité importante de C a le potentiel d'être chargée dans lacs par les rivières, les ruisseaux et l'eau souterraine, ce qui peut grandement affecter son budget de C et ses émissions (Stets *et al.*, 2009).

0.2.5 Autres processus importants

Les processus mentionnés ci-dessus ajoutent du CO_2 à la surface des lacs, mais plusieurs aussi enlèvent du CO_2. Notamment, la production primaire peut avoir lieu dans la colonne d'eau par le phytoplancton, mais aussi dans le milieu littoral par le périphyton et les macrophytes (Figure 0.1e). Cette production primaire est grandement influencée par les nutriments (Pace et Prairie, 2005; Schindler *et al.*, 1971) et les conditions de lumière dans la colonne d'eau, les deux souvent en lien avec le COD (Seekell *et al.*, 2015). De plus, le CO_2 produit dans le lac peut aussi être exporté par l'exutoire vers les systèmes en aval (Figure 0.1f). Finalement, le CO_2 est aussi en constante interaction avec les autres espèces de carbone inorganique, soit les carbonates et bicarbonates (Figure 0.1g). Deux principaux processus peuvent affecter le CO_2, bien que leur magnitude ne soit que minime par rapport aux autres processus mentionnés plus haut (Cole et Prairie, 2009). Un apport en carbonate solide qui se dissout dans l'eau pour créer du bicarbonate (HCO_3) devra donc consommer du CO_2. La réaction inverse (précipitation des carbonates) cause donc une production de CO_2, mais n'est qu'observée dans les océans et les systèmes en teneurs élevées en carbonate dissous (Cole et Prairie, 2009).

Tous ces processus mentionnés ci-dessus ont un lien direct ou indirect avec le milieu terrestre environnant. L'eau de ruissellement apporte avec elle du CO_2 et du COD vers les lacs. Le CO_2 apporté peut directement soutenir les émissions des lacs, tandis que le COD peut jouer différents rôles, en fonction de sa réactivité et des conditions environnementales. D'abord, le COD qui est fraichement produit est plus réactif et aura donc une plus grande probabilité de se faire minéraliser par les bactéries (Guillemette

et del Giorgio, 2011; Koehler *et al.*, 2012) et par les radiations solaires (Gonsior *et al.*, 2013), qui soutiendra ainsi la sursaturation en CO_2 dans la colonne d'eau. Le COD moins réactif peut soit être exporté en aval, soit rejoindre les sédiments pour être reminéralisé par la communauté bactérienne benthique (Gudasz *et al.*, 2012) ou être séquestré à plus long terme (Ferland *et al.*, 2012; Ferland *et al.*, 2014). L'intensité de la connexion avec le milieu terrestre est donc la clé vers la compréhension de la sursaturation en CO_2 des lacs boréaux.

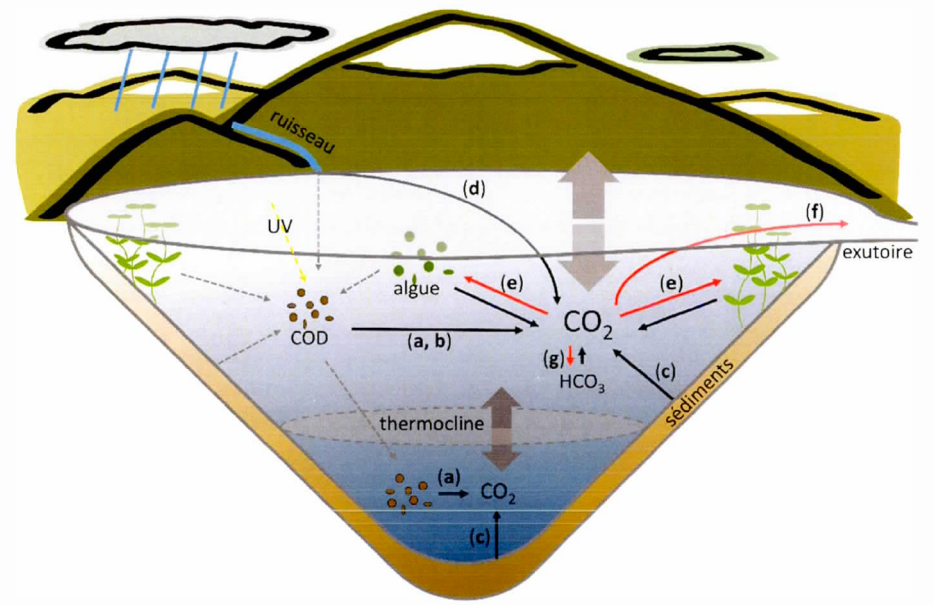

Figure 0.1. Processus impliqués dans la dynamique du CO_2 dans les lacs boréaux

Les flèches noires représentent les processus ajoutant du CO_2, les flèches rouges représentent les processus qui enlèvent du CO_2 et les flèches grises pointillées représentent les flux de COD. Les différents processus impliqués dans la dynamique du CO_2 sont (**a**) la respiration pélagique, (**b**) la photo-minéralisation de la matière organique, (**c**) la respiration benthique (des sédiments), (**d**) les apports hydrologiques externes provenant du bassin versant, (**e**) la production primaire, (**f**) l'exportation par l'exutoire, (**g**) l'équilibre chimique.

0.3 DYNAMIQUE TEMPORELLE DES ÉMISSIONS DE CO_2

Dans les régions boréales et tempérées, la température et les précipitations varient grandement dans l'espace, mais aussi dans le temps, résultant en une vaste gamme de conditions dans lesquelles des mécanismes biologiques et physiques régissant les émissions de CO_2 peuvent avoir lieu. Ces variations climatiques ont un effet sur la dynamique du CO_2 à la surface des lacs, étant au plus élevée l'hiver sous la glace et au printemps et au plus bas l'été, lorsque que le lac est stratifié (Cole *et al.*, 1994; Ducharme-Riel *et al.*, 2015; Huotari *et al.*, 2009; Maberly, 1996; Riera *et al.*, 1999; Striegl et Michmerhuizen, 1998). Cette tendance saisonnière est régulée en grande partie par des phénomènes qui créent des barrières physiques limitant la diffusion (comme le couvert de glace l'hiver et la stratification thermique l'été) et favorisant ainsi l'accumulation du CO_2. Lorsque que ces barrières physiques se rompent, une grande quantité de CO_2 accumulé est donc relâchée et diffusée vers l'atmosphère (Ducharme-Riel *et al.*, 2015; Karlsson *et al.*, 2013; Striegl *et al.*, 2001). À cela s'ajoute l'effet des évènements épisodiques météorologiques (Jennings *et al.*, 2012) comme les tempêtes marquées par de fortes pluies, qui peuvent influencer la structure thermique des lacs (Klug *et al.*, 2012), mais aussi les apports de matières par les eaux de ruissellement soudainement intensifiées (Buffam *et al.*, 2008; Wilson *et al.*, 2013). Ces types d'évènements causent souvent des modifications dans les flux de carbone (Jones *et al.*, 2009) et résultent parfois en émissions de CO_2 plus marquées (Ojala *et al.*, 2011).

Malgré ces informations sur leur variabilité temporelle, les mesures de sursaturation en CO_2 et de ses processus associés sont normalement acquises ponctuellement et la plupart du temps lors de la saison libre de glace, résultant en un instantané qui est peu probable d'être représentatif à l'ensemble du cycle annuel. Malgré plusieurs points d'échantillonnage durant l'année, de grandes incertitudes subsistent dans l'interpolation des processus et des concentrations entre les mesures, notamment en termes d'événements épisodiques, qui peuvent néanmoins être critiques pour le budget

annuel (Ducharme-Riel *et al.*, 2015). L'utilisation croissante des sondes automatisées qui permettent un échantillonnage à haute fréquence des propriétés clés du lac ont considérablement amélioré la couverture temporelle de la dynamique de CO_2 sur les lacs et d'autres données complémentaires (Huotari *et al.*, 2009; Morales-Pineda *et al.*, 2014). Les informations que fournissent ces approches sont cependant limitées quant à la compréhension des mécanismes sous-jacents qui régulent le CO_2 à la surface des lacs. À cet égard, la modélisation mécaniste du cycle du carbone des lacs présente des avantages évidents (Cardille *et al.*, 2007; Hanson *et al.*, 2004; Hanson *et al.*, 2014a), mais les conclusions résultant de cette approche doivent être tirées avec prudence, en particulier lorsque les données mesurées sont limitées et que de nombreuses suppositions sont préalablement établies. En somme, il en résulte donc une compréhension incomplète de la dynamique saisonnière des processus qui régulent le CO_2 des lacs boréaux. De plus, ces procédés qui produisent ou importent du CO_2 sont influencé par d'autres procédés connexes tels que l'exportation de CO_2 aux systèmes en aval, la production primaire et la dissolution des carbonates, qui enlèvent le CO_2 de la surface des lacs. Toutes ces considérations ajoutent de la complexité à l'évaluation de la contribution relative et de la dynamique des processus sous-jacents au maintien des émissions de CO_2 dans les lacs boréaux.

0.4 OBJECTIFS ET HYPOTHÈSE

L'objectif général de cette thèse est d'approfondir les connaissances sur différents aspects des dynamiques temporelles des processus qui influencent les émissions de CO_2 des lacs boréaux, en tenant compte des interactions entre les propriétés spécifiques à chaque lac et de la variabilité des conditions environnementales. En outre, cette thèse cherche à établir des liens entre la variabilité temporelle de la réactivité intrinsèque de la matière organique et des variations de conditions environnementales, dont la température de l'eau, les radiations solaires dans la colonne d'eau et le régime hydrologique. Plus spécifiquement, cette thèse a pour objectifs de :

1) Décrire les dynamiques saisonnières et quantifier la production de CO_2 dans la colonne d'eau des lacs par la respiration biologique et la minéralisation photochimique du COD,

2) Comprendre le rôle du régime hydrologique des lacs sur la variabilité temporelle de la réactivité du COD allochtone, ainsi que sa contribution à la production de CO_2 issue de sa minéralisation dans la colonne d'eau,

3) Évaluer le rôle des épisodes de vents et de pluies intenses sur l'altération des différentes voies de production de CO_2 et sur ses déplacements verticaux et horizontaux dans les lacs,

4) Reconstruire la dynamique saisonnière des principaux processus de production de CO_2 et leurs contributions relatives au maintien de la sursaturation en CO_2 à la surface des lacs boréaux.

Cette thèse se base sur l'hypothèse générale, selon laquelle tous les processus qui influencent la dynamique du CO_2 à la surface des lacs boréaux ont lieu en même temps, dans tous les lacs. Leurs magnitudes et leurs contributions relatives à la production

totale de CO_2 dans les lacs seront par contre influencées par les synchronisations des variabilités de la réactivité de la matière organique et des conditions environnementales, ainsi que par le cadre physico-chimique dans lequel les processus ont lieu. Ainsi, des tendances saisonnières devraient être observées dans ces processus, en raison de la grande variabilité temporelle des conditions environnementales à des latitudes élevées (c.-à-d. température, radiation solaire, précipitation, couverture de glace, productivité des forêts, etc.). Une meilleure compréhension de l'ampleur des processus impliqués dans la dynamique du CO_2 et de leur variabilité temporelle est essentielle pour approfondir les connaissances du fonctionnement des lacs et ainsi fournir des estimations plus précises des émissions annuelles de CO_2 provenant des lacs boréaux.

0.5 APPROCHE GÉNÉRALE

Pour comprendre les processus qui influencent la dynamique du CO_2 dans les lacs, plusieurs approches ont été utilisées. D'abord, trois lacs situés dans le biome boréal ont fait l'objet d'un suivi sur au moins une année complète et sur lesquelles des mesures ont été récoltées manuellement sur place, puis automatiquement par des sondes. Parallèlement, des incubations et expériences ont été menées en laboratoire et des modèles mathématiques et numériques ont été développés en complément à l'étude.

0.5.1 Description des lacs suivis

Les lacs ont été choisis en fonction de leurs différences de morphométrie du bassin, de paramètres physico-chimiques et de régimes hydrologiques. Compte tenu de l'intensité de l'échantillonnage prévu, les lacs ont aussi été sélectionnés en fonction de leur proximité de stations de recherche universitaire pour rendre plus efficaces les travaux. Ainsi, les lacs suivants ont été étudiés : le Lac Croche (Figure 0.2a) est un lac oligo-trophique tempéré sur le Bouclier canadien (45 ° N, 74 ° W) situé à la Station Biologique des Laurentides (SBL) de l'Université de Montréal (http://www.sbl.umontreal.ca), le Lac Simoncouche (Figure 0.2b) est un lac boréal oligo-trophique sur le Bouclier canadien (48 ° N et 71 ° W) situé sur le site de la Forêt d'Enseignement et de Recherche Simoncouche (FERS) de l'Université du Québec à Chicoutimi (http://www.uqac.ca/fers/) et le Lac Hébécourt (Figure 0.2c) est un lac boréal méso-trophique sur la ceinture d'argile abitibienne (48 ° N et 79 ° W) situé sur le site de la Forêt d'Enseignement et de Recherche du Lac Duparquet (FERLD) de l'Université du Québec en Abitibi (http://ferld.uqat.ca/). Ces lacs sont situés suivant un gradient latitudinal et présentent aussi un gradient de COD et de phosphore total, de régime hydrologique et de morphométrie (Tableau 0.1).

Tableau 0.1. Caractéristiques générales des trois lacs à l'étude

Caractéristiques	Lac Croche	Lac Simoncouche	Lac Hébécourt
Coordonnées géographiques (DD)	45.9922° -74.0050°	48.2326° -71.2495°	48.5121° -79.3774°
Aire du lac (ha)	18.1	86.1	775.0
Aire du bassin versant (ha)	88	2633	2800
Profondeur moyenne (m)	5.1	2.1	2.2
Profondeur maximale (m)	12.0	8.2	5.0
Nombre de tributaires	0	2	5
Temps de résidence de l'eau (an)[a]	1.10	0.09	0.48
Formation végétale du bassin versant	Érablière à bouleau jaune	Pessière - sapinière	Sapinière à bouleau blanc
COD (mg C L^{-1})[b]	4.6 ± 0.5	6.9 ± 0.9	9.9 ± 0.8
Chlorophylle *a* (µg L^{-1})[b]	1.4 ± 0.7	1.7 ± 0.8	5.7 ± 3.5
Phosphore total (µg L^{-1})[b]	4.0 ± 1.2	10.0 ± 2.4	27.6 ± 4.7

[a] moyenne annuelle
[b] moyenne de la saison libre de glace ± erreur type

Figure 0.2. Vue aérienne des trois lacs échantillonnés mensuellement entre 2010 et 2012.

(**a**) le Lac Croche de la Station biologique des Laurentides de l'Université de Montréal (crédit photo : Richard Carignan). (**b**) le Lac Simoncouche situé dans la Forêt d'enseignement et de recherche Simoncouche de l'Université du Québec à Chicoutimi (crédit photo : Jean-François Lapierre) et (**c**) le Lac Hébécourt situé dans la Forêt d'enseignement et de recherche du lac Durparquet de l'Université du Québec en Abitibi Témiscamingue (crédit photo : Dominic Vachon).

0.5.2 Mesures et incubations

Dans chaque lac, un budget détaillé de CO_2 a été évalué sur une année complète, selon lequel le changement de masse de CO_2 (ΔCO_2) du lac varie, suivant les entrées et les sorties :

(0.1) $\Delta CO_2 = fCO_2$ + apport hydrologique + respiration pélagique + respiration benthique + photo-minéralisation – production primaire – sorties de CO_2 par l'exutoire.

Dans chaque lac, tous ces processus ont été soit mesurés directement, soit estimés ou modélisés. D'abord, les changements de masse de CO_2 (ΔCO_2) ont été mesurés en suivant la concentration de CO_2 dans la colonne d'eau mensuellement. Ensuite, les flux de CO_2 avec l'atmosphère ont été estimés de deux façons : en estimant la vitesse d'échange gazeux combiné avec la différence de pression partielle de CO_2 entre l'eau et l'atmosphère (Vachon et Prairie, 2013), puis par mesure directe en utilisant une chambre flottante à la surface de l'eau (Vachon *et al.*, 2010). Les entrées et les sorties hydrologiques de CO_2 ont été estimées en combinant les mesures de concentration de CO_2 dans les ruisseaux entrants et de l'eau souterraine avec un budget hydrologique complet. Ce dernier permet d'évaluer les quantités d'eau qui entrent et sortent et a été estimé par surveillance en continu du niveau d'eau du lac, des débits d'eau des ruisseaux et de l'exutoire, combiné aux mesures de précipitations et l'estimation de l'évaporation. La respiration pélagique a été mesurée par incubation dans le noir à température contrôlée (Marchand *et al.*, 2009) et la respiration benthique par des incubations *in situ* de carottes de sédiments (Den Heyer et Kalff, 1998). La photo-minéralisation du COD a été estimée par des incubations sous radiation solaire artificielle contrôlée, combinée avec de la modélisation pour intégrer les taux dans la colonne d'eau (Koehler *et al.*, 2014). La production primaire brute (PPB) a été estimée avec des mesures à haute fréquence de l'oxygène dissous à la surface de l'eau (Cole *et al.*, 2000).

0.5.3 Modélisation

Plusieurs approches par la modélisation ont été combinées en complément aux budgets de CO_2 des lacs. Premièrement, des modèles empiriques ont été développés pour la respiration pélagique et la photo-minéralisation du COD utilisant le COD, la température et les radiations solaires comme principaux prédicteurs. Ensuite, un modèle mécaniste simple a été développé pour comprendre la dynamique du COD allochtone dans les lacs et le potentiel de production de CO_2 (Chapitre II) en laissant le modèle atteindre l'équilibre. Finalement, un modèle mécaniste plus complet utilisant le CO_2 comme variable d'état (« state variable ») a permis de combiner toutes ces mesures et flux de CO_2, et ainsi étudier la dynamique temporelle de ces processus dans un cadre commun (Chapitre IV).

CHAPITRE I

SEASONALITY OF PHOTO-CHEMICAL DISSOLVED ORGANIC CARBON MINERALIZATION AND ITS RELATIVE CONTRIBUTION TO PELAGIC CO_2 PRODUCTION IN NORTHERN LAKES

Dominic Vachon[1], Jean-François Lapierre[1,2] and Paul A. del Giorgio[1]

[1]Groupe de recherche interuniversitaire en limnologie (GRIL), Département des Sciences Biologiques, Université du Québec à Montréal, Montréal, Canada

[2]Now at Department of Fisheries and Wildlife, Michigan State University, East Lansing, USA.

Under review in *Journal of Geophysical Research: Biogeosciences*

Key points

- Both DOC photo-reactivity and irradiance drive the seasonally in photo-mineralization
- Peaks of DOC photo-mineralization was found in spring
- DOC photo-mineralization contributed on average 14% of total pelagic CO_2 production

Key words: carbon cycle, seasonality, boreal lake, CO_2 production, photo-chemistry, dissolved organic carbon

N.B. References cited in this chapter are presented at the end of the thesis

1.1 ABSTRACT

Boreal and northern temperate lakes (hereinafter referred to as northern lakes) are sites of intense processing of dissolved organic carbon (DOC), which is reflected in part in the persistent CO_2 supersaturation of their surface waters. These ecosystems are subjected to strong seasonal fluctuations in both irradiance and DOC amount and quality, which in turn should result in temporal shifts in the magnitude of DOC photo-degradation. Here we explore the temporal patterns in the magnitude of water column DOC photo-mineralization, and its potential contribution to pelagic CO_2 production in three northern lakes of different DOC content. We performed laboratory DOC photo-degradation incubations, and combined the resulting rates with field measurements and modeling to reconstruct the annual cycle in depth-integrated DOC photo-mineralization. We found that areal rates of DOC photo-mineralization were driven by both irradiance and intrinsic DOC photo-reactivity, both of which showed seasonality. Over an annual cycle, depth-integrated DOC photo-mineralization rates were remarkably similar across lakes, averaging 4.4 (SD = 0.7) g C m^{-2} yr^{-1}, and where daily rates followed an apparent seasonal pattern. The contribution of DOC photo-mineralization to total pelagic CO_2 production (as the sum of respiration and DOC photo-mineralization) peaked after ice melt (up to 49%), averaging 14% for the entire open water season. Our study identifies potential hot periods of photochemical activity that result from the interplay between DOC properties and environmental conditions, which should be incorporated into models of lake functioning.

1.2 INTRODUCTION

It is now well established that inland waters emit significant amounts of CO_2 to the atmosphere (Cole *et al.*, 2007; Raymond *et al.*, 2013). One potential source of these emissions is the intense processing of terrestrially-derived organic carbon that occurs in these aquatic ecosystems (Algesten *et al.*, 2003; Tranvik *et al.*, 2009). This terrestrial DOC is mostly composed of colored, aromatic and high molecular weight compounds, which renders it highly photo-degradable (Opsahl et Benner, 1998; Wetzel *et al.*, 1995). In the aquatic network of northern regions, lakes may be prime sites of DOC photochemical degradation due to the combination of dominance of terrestrially-derived DOC (Wilkinson *et al.*, 2013) and extensive exposure to sunlight resulting from longer water residence times. Although many studies have explored various aspects of DOC photo-degradation in lakes, few have placed this process within the context of whole-lake CO_2 production (Cory *et al.*, 2014; Granéli *et al.*, 1996; Jonsson *et al.*, 2001), and even fewer have explored its seasonal variation (Koehler *et al.*, 2014; Lindell *et al.*, 2000). The latter is critical in northern lakes, which are subjected to strong seasonality in both DOC quantity and quality, and irradiance. Although irradiance is predictable, the temporal patterns in DOC photo-reactivity and quantity may not only differ among different lakes, but more importantly, they may not necessarily co-vary with irradiance. There is thus a large degree of uncertainty regarding the relative contribution of photo-chemical DOC mineralization to pelagic CO_2 dynamics over an annual cycle, and this represents a large gap in our understanding of the regulation of CO_2 emissions from lakes.

There has been significant progress over the past decades in our understanding of DOC photo-reactivity and photochemical degradation in aquatic systems. DOC can be photo-degraded into smaller (low molecular weight) and often bio-labile molecules (Anesio *et al.*, 2005; Bertilsson *et al.*, 1999; Lindell *et al.*, 1995; Scully *et al.*, 2003). It can also be photo-mineralized into inorganic carbon species such as CO and CO_2 (Granéli *et*

al., 1998; Granéli *et al.*, 1996; Salonen et Vähätalo, 1994; Stubbins *et al.*, 2008). To understand the intrinsic photo-reactivity of DOC, however, degradation rates must be normalized by the energy (or photons) absorbed by the sample. This is generally expressed as the wavelength-dependent apparent quantum yield (AQY), which is expressed as the moles of DOC mineralized per mol of photons absorbed by the total chromophoric dissolved organic matter (CDOM) pool (Vähätalo *et al.*, 2000; Zepp, 1978). The magnitude of this photo-mineralization efficiency is highly variable among freshwater and marine systems (Johannessen et Miller, 2001; Koehler *et al.*, 2014; Vähätalo *et al.*, 2000; White *et al.*, 2010), but no clear and consistent drivers of this variability have been identified yet. In spite of some high AQY values reported in the open ocean (Johannessen et Miller, 2001), there is an overall inshore to offshore gradient of decreasing AQY, suggesting generally lower apparent DOC photo-mineralization efficiency towards the open ocean (Aarnos *et al.*, 2012; White *et al.*, 2010). Moreover, a recent study in arctic aquatic systems showed high DOC photo-mineralization efficiency in permafrost-derived DOC (Cory *et al.*, 2014). Lapierre et del Giorgio (2014) have reported a disproportionate increase in photo-reactive DOC in highly colored, head water streams relative to larger rivers and lakes. Collectively, this evidence suggests that the degree of connectivity to terrestrial sources of DOC may potentially determine cross-system patterns in the intrinsic photo-reactivity of this carbon. The degree and nature of the connection between lakes and land also varies seasonally as a function of hydrological conditions, and it would thus be expected that the intrinsic photochemical reactivity of the DOC loaded to lakes would therefore also vary seasonally. The few studies to have explicitly addressed this question have indeed reported seasonal patterns in DOC photo-reactivity in boreal lakes (Gonsior *et al.*, 2013; Groeneveld *et al.*, 2015; Lindell *et al.*, 2000), boreal streams (Porcal *et al.*, 2013) and a tropical humic lagoon (Suhett *et al.*, 2007). To our knowledge, however, information on how the seasonality of DOC photo-reactivity affects areal rates of DOC photo-mineralization, and its contribution to the whole water-column CO_2 production in lakes is lacking in the literature.

Determining the role and the relative importance of photo-chemical processes at the whole-lake scale requires integrating the photo-mineralization rates over depth. When light penetrates the water column of lakes, irradiance intensity and its spectral properties are selectively attenuated. Because of the spectral-dependency of the AQY, this in turn will generate a vertical gradient of DOC photo-mineralization, with the highest rates at the near surface (Granéli *et al.*, 1996; Vähätalo *et al.*, 2000). Information on spectral-dependency of DOC photo-mineralization is needed to estimate depth-integrated rates and only a handful of studies have reported such rates in lakes. These studies have usually been based on either in situ measurements at discrete depths (Granéli *et al.*, 1996; Soumis *et al.*, 2008; Vähätalo *et al.*, 2000) or modeled as a function of AQY (Cory *et al.*, 2014; Koehler *et al.*, 2014), and have reported a wide range of values. As a result, the relative contribution of DOC photo-mineralization to the whole-lake CO_2 production appears to be highly variable across systems. For example, photo-chemical processing has been shown to dominate DOC degradation in some boreal and arctic lakes (Cory *et al.*, 2014; Molot et Dillon, 1997), whereas other studies, also in boreal regions, have reported only a modest contribution of photo-chemical processes to the lake CO_2 budget compared to biological rates (Granéli *et al.*, 1996; Jonsson *et al.*, 2001; Koehler *et al.*, 2014; Soumis *et al.*, 2007). This variability is, however, not surprising, since in situ biological and photochemical DOC degradation have different drivers (e.g. temperature vs. light) and the availability of photochemical and biological reactive DOC may also have contrasting drivers (Lapierre et del Giorgio, 2014). This would suggest that the relative contribution of photo-chemical DOC mineralization to the total pelagic CO_2 production may follow a seasonal cycle, where hot moments of photo-chemical activity would not necessary coincide with hot moments of biological degradation. This potential seasonal succession in the relative contribution of depth-integrated DOC photo-mineralization to the whole-lake CO_2 production remains largely unexplored.

Key to reconciling these reported differences in photo-chemical rates is to understand the variability and the relative contribution of the three main components involved in determining total DOC photo-mineralization in lakes: irradiance, DOC amount and DOC reactivity, all of which are highly variable not only across lakes of different regions but also within a single lake throughout the seasons (Gonsior *et al.*, 2013; Lindell *et al.*, 2000). Here we reconstructed the annual cycle of depth-integrated photo-mineralization of DOC in three limnologically distinct northern lakes, explicitly incorporating seasonal shifts in DOC reactivity, DOC amount and irradiance. We further place these photo-mineralization rates in the context of the seasonal variation in the measured pelagic respiration rates. Our aim was to quantify the overall contribution of photochemical degradation of DOC to the water-column CO_2 production and to identify potential hot moments in this contribution, and assess how these may vary across lake types.

1.3 METHODS

1.3.1 Site description and sampling

The study lakes are located in the temperate and boreal regions of Québec (Canada), and were sampled monthly or biweekly during at least one annual cycle (between 2010 and 2012). General lake characteristics are presented in Table 1. Lac Hébécourt (273 m altitude, 48.51°N, 79.38°W) is the shallowest but the largest of the studied lakes, and is situated in the Lac Duparquet Research and Teaching Forest (FERLD), a managed mix forest dominated by balsam fir (*Abies balsamea*) and white birch (*Betula papyrifera*) settled mainly on glacio-lacustrine clays. The lake has five major river/stream inputs, four of which are heavily dammed by beavers (*Castor canadensis*). Lac Simoncouche has a pristine watershed dominated by black spruce (*Picea mariana*) and balsam fir (*Abies balsamea*) settled on podzolic soils (347 m altitude, 48.23°N, 71.25°W). The lake has two major inlet streams (each having an upstream lake) and several headwater ephemeral streams that only flow after heavy rains. The southern part of the lake has extensive development of aquatic macrophytes (*Brasenia schreberi*) from June to October (covering up to about 10-15% of total lake area). Lac Croche is a headwater lake surrounded by a pristine watershed dominated by maple (*Acer saccharum*) and yellow birch (*Betula alleghaniensis*) settled on well-drained Ferro-humic podzols (365 m altitude, 45.99°N, 74.00°W).

Lake water was collected at 0.5m depth at the deepest location of the lake. Samples were immediately brought back to the lab for photochemical DOC mineralization and dark biological respiration incubations, and for further chemical analyses. Additionally, we carried out vertical profiles (each meter) of temperature, dissolved oxygen, conductivity and pH using a multi parameters probe (Yellow Spring Instruments, USA). Chlorophyll samples were analyzed spectrophotometrically following filtration with Whatman (GF/F) filters and hot ethanol (90%) extraction.

DOC concentration was measured on 0.45 μm filtered water samples on an OI-1010 TIC-TOC Analyzer (OI Analytical, College Station, TX, USA) using wet persulfate oxidation. Total phosphorus (TP) was analyzed spectrophotometrically after persulfate digestion.

Table 1.1. General characteristics of the three study lakes.

Characteristics	Lac Hébécourt	Lac Croche	Lac Simoncouche
Lake area (ha)	775.0	18.1	86.1
Watershed area (ha)	2800	88	2633
Mean depth (m)	2.2	5.1	2.1
Mean annual air temperature (°C)[a]	NA	2.65	2.57
Ice-free period (days)	193	217	225
Water Residence Time (year)[b]	0.48	1.10	0.09
DOC (mg C L^{-1})[c]	9.9 ± 0.8	4.6 ± 0.5	6.9 ± 0.9
Absorption coefficient at 440nm (m^{-1})[c]	2.2 ± 0.6	0.8 ± 0.2	1.9 ± 0.5
UV light extinction coefficient (m^{-1})	18.9	10.6	19.7
Chlorophyll a (µg L^{-1})[c]	5.7 ± 3.5	1.4 ± 0.7	1.7 ± 0.8
Total phosphorus (µg L^{-1})[c]	27.6 ± 4.7	4.0 ± 1.2	10.0 ± 2.4

[a] measured in 2011
[b] annual average
[c] ice-free season average ± standard deviation
NA = not available for the whole year

1.3.2 DOC light absorptivity and photo-reactivity

We assessed lake DOC photo-reactivity by determining the magnitude of DOC light absorption and the DOC mineralization during light incubations. After filtering lake water (0.45 μm), light absorption by DOC was measured in the laboratory with an ultraviolet-visible Ultrospec 2100 spectrometer (Biochrom, Cambridge, UK). Absorbance of colored dissolved organic matter ($A_{CDOM,\lambda}$) was measured over the range of 280–800 nm, and then expressed as the Neperian absorption coefficient ($a_{CDOM,\lambda}$; m^{-1}) according to Beer-Lambert's law:

$$a_{CDOM,\lambda} = 2.303 * A_{CDOM,\lambda} / L, \quad (1.1)$$

where L is the path length of the spectrophotometer cell in meters, and the factor ln(10) converts from $\log_{10}$ to ln. As the absorption coefficient typically decreases with increasing wavelength, we fit the absorption spectrum for each sample to a decreasing exponential function described as:

$$a_{CDOM,\lambda} = a_{ref} * e^{S*(\lambda ref - \lambda)} + K, \quad (1.2)$$

where a_{ref} is the absorption coefficient at the reference wavelength (here 290 nm)(m^{-1}), S is the curve shape parameter (nm^{-1}), λ_{ref} is the reference wavelength, and K is the background scattering constant (m^{-1}).

To determine DOC photo-reactivity, we performed irradiation experiments in the laboratory. Water was filtered (2.7 μm nominal pore-size GF/F Whatman filter), and then exposed to artificial light in a solar simulator (Q-sun Xe-1, Q-Lab; light intensity of 0.68W m^{-2} at 340 nm) in borosilicate vials (O.D. x L: 24.8 x 83mm; Volume=40ml) at controlled temperature (24°C). Vials (between 4 and 20 in each incubation) were randomly positioned flat on the tray in the irradiation chamber to ensure uniformity in irradiation intensity and spectra to all the vials. The irradiated surface area was then

assumed to be equivalent to the inner diameter multiplied by the length of the vial. No dark controls were incubated in the irradiation chamber. DOC photo-mineralization (mg C L^{-1} d^{-1} or mol m^{-3} d^{-1}) was measured as the differences in DOC and DIC concentrations between time = 0 (unexposed) and at t = 24 hours. Filtration through 2.7 μm may have left the part of the bacterial community in the vial prior of the light incubation, we further discuss the reason to use this filter and how we accounted for potential bacterial activity in the vials by correcting for dark controls in the Supporting Information section S1.1.

1.3.3 AQY estimation

We estimated the wavelength-integrated AQY (*wi*AQY) for each sample by dividing the DOC loss (and DIC production) during the incubation (mol C) by the photons absorbed by CDOM (mol photon), accounting for self-shading and glass vial transmittance. First, the quantum density flux (Q_{abs}) absorbed in each sample was estimated from the following equation:

$$(1.3) \quad Q_{abs} = bleach \cdot A \cdot T \int_{\lambda=280}^{\lambda=600} \frac{I_{0\lambda}}{(E_\lambda)} \cdot (glass\ trans)_\lambda \cdot \bar{a}_{CDOM,\lambda},$$

where Q_{abs} is the total photons absorbed by CDOM in the vial (mol photons d^{-1}), *bleach* is the average proportion of initial absorption coefficient lost at 375 nm due to bleaching during the incubation. We chose this particular wavelength because it is around 375nm that we found the maximum irradiance energy absorbed (irradiance multiplied by DOC absorption) normally peaks between 350-400nm. A is the surface of the vial exposed to light (0.0018 m^2, estimated as the inner diameter multiplied by the length of the vial), T is the total time of the incubation (s). $I_{0\lambda}$ is the lamp irradiance for a specific wavelength (J s^{-1} m^{-2} or W m^{-2}). Assessing the exact light absorption in cylindrical vials can be highly uncertain, thus a sensitivity analysis was performed to further test the effect of varying the surface area of exposure on the resulting rates of

photo-mineralization (see Supporting Information S1.1 and Table S1.1). We divided the lamp energy by E_λ (J mol photon^{-1}), which is the energy per mol of photons at a specific wavelength (defined as nhc/λ which n is the number of photon in one mol and h is the Planck's constant and c is the speed of light). $(Glass\ trans)_\lambda$ is the wavelength-specific fraction of light that reaches the water sample (Supporting Information Figure S1.1). The mean wavelength-specific fraction of light absorbed in the vial $\bar{\alpha}_{CDOM,\lambda}$ was computed to account for self-shading (Hu *et al.*, 2002) and using the diameter of the vial as the pathlength. Considering the lamp output (750 W m^{-2}) and light absorption by the glass in the vial, we estimated that all water samples received a total of approximately 650 W m^{-2} of radiation (280-800 nm). Detailed information on the spectral characteristics of the light source and the spectral transmittance of the incubation vials (see Supporting Information Figure S1.1).

Our incubation yielded information on the total DOC mineralization per total amount of photons absorbed within the whole UV-visible range. It has been well established that the apparent quantum yield (AQY) is not constant along the spectrum, but rather peaks in the UV range and decreases exponentially with increasing wavelength (Johannessen et Miller, 2001; Stubbins *et al.*, 2011; Vähätalo *et al.*, 2000). It is therefore necessary to estimate the spectral dependency of the DOC photo-mineralization for each sample. In this regard, we can express the total DOC mineralization for a given sample as the sum of the DOC loss rates at each wavelength, which is itself the product of the AQY and the amount of light absorbed by the sample at each wavelength:

$$Total\ DOC\ mineralization = \sum_{\lambda=280}^{\lambda=600} Q_{abs,\lambda}\, AQY_\lambda \,, \tag{1.4}$$

where AQY_λ is the wavelength-specific AQY, and $Q_{abs,\lambda}$ is the wavelength specific photon absorbed by the CDOM during the incubation, corrected for self-shading (Hu *et al.*, 2002). The spectral dependency of AQY (AQY_λ) can be described as an

exponential declining function (Aarnos *et al.*, 2012; Cory *et al.*, 2014; Vähätalo *et al.*, 2000):

$$AQY_{\lambda} = c \times e^{-d\lambda} \quad (1.5)$$

where c (dimensionless) and d (nm^{-1}) are constants, and λ is wavelength in nanometers (nm). Merging equations 1.4 and 1.5 results in:

$$Total\ DOC\ mineralization = \sum_{\lambda=280}^{\lambda=600} Q_{abs,\lambda} \times (c \times e^{-d\lambda}) . \quad (1.6)$$

All the parameters in equation 1.6 are known, except for parameters c (dimensionless) and the slope parameter d (nm^{-1}). Unfortunately, because two parameters (c and d) are unknown, it is impossible to solve equation 1.6, as it results in infinite combinations. Having information on one of these two unknowns, however, allows us to back-calculate the other. Whereas parameter c (in equation 1.5 and 1.6) represents the intercept of the relationship between AQY and wavelength, parameter d describes the shape of the spectral slope, which allows to weigh the relative importance of each wavelength on DOC photo-mineralization. For the purpose of this study only, we assumed that parameter d in equation 1.5 and 1.6 can be replaced by parameter S in equation 1.2 that describes the absorption spectrum. We base this assumption on previous studies that have shown strong relationships between measured AQY and the absorption coefficient of DOC across wavelengths (Xie *et al.*, 2009; Stubbins *et al.*, 2011). Since the quantum yield of DOC mineralization for a given sample is a function of its absorption coefficient, it follows that the spectral slope of the AQY for a given sample should closely follow its absorption spectrum, and this in turn implies that the parameter d of the AQY spectral model (equations 1.5 and 1.6) should be analogous to coefficient S of the absorption spectrum model (equation 1.2). Here we have used this potential equivalence to apportion the total DOC mineralization we measured in the incubation across the spectrum. We thus replaced parameter d by parameter S in equation 1.6 and we iteratively fit parameter c by solving equation 1.6 ('fzero' function

in MATLAB 7, MathWorks). Now having parameters *c* and *S (or d)*, the spectral AQY could then be estimated using equation 1.5. It is important to note that this potential equivalence between CDOM absorption and AQY slopes is an assumption, and although our field comparison of the output of this model with actual DOC photo-degradation supports this assumption (Supporting Information section S1.1), it should be further tested with direct measure of AQY spectra (e.g. using cut-off filters) in future studies. Further details and implication on using this slope parameter, as well as a full sensitivity analysis are presented in the Supporting Information section S1.1 and Table S1.2.

1.3.4 Water-column irradiance

For each sampling day, we estimated the water column irradiance at each depth by combining modeled incident irradiance corrected for cloud cover and surface reflectance, and measurements of diffuse vertical attenuation coefficients (K_d). Hourly data (0:00 to 23:00) of direct and diffuse surface downwelling irradiance were modeled using the Tropospheric Ultraviolet Visible (TUV) model (Madronich et Flocke, 1997) for each sampling date and location, under clear sky conditions and total ozone content retrieved from OMI-AURA (OMI Science Team, 2012). To convert to daily integrated just-below-surface downwelling scalar irradiance (Q_{0^-}), global (direct + diffuse) irradiance from the TUV model was corrected for cloud cover and transmittance at the surface of lake, and converted to scalar irradiance using the average underwater cosine, following Fichot et Miller (2010). We first performed a cloud correction on modeled irradiance using OMI-AURA daily radiative cloud fraction (0-1) on each site (OMI Science Team, 2012), and we parameterized a correction factor using measurements of in situ irradiance just over the lake (see Supporting Information S1.2). Transmittance at the air-water interface for every hour was computed separately for diffuse and direct fractions of irradiance using zenith solar angle and following Fresnel's law (Fichot et Miller, 2010). Finally, conversion to scalar irradiance was computed using the

estimated average underwater cosine for downwelling irradiance, also following Fichot et Miller (2010). Hourly underwater irradiance was interpolated (cubic) to a 1s time resolution to yield daily integrated just-below-water scalar downwelling irradiance (Q_{0-}).

Water column irradiance attenuation was calculated from in situ measurements of underwater cosine-corrected downwelling irradiance using a UV-visible profiler (PUV-2545, Biospherical Instrument Inc., San Diego, USA) at five different wavelengths (313, 320, 340, 443, and 550 nm) (Frenette *et al.*, 2006). Ten measurements per second were recorded as the probe was slowly deployed through the whole water-column. Attenuation coefficients ($K_{d,\lambda}$) were computed for each measured wavelength (λ). For sampling dates for which we did not have the UV profiler, $K_{d,\lambda}$ were estimated using empirical linear models based on our own measurements using DOC or a_{440} as independent variables (*see* Supporting Information S1.3 for details and empirical equations). Attenuation coefficients for each wavelength (1 nm resolution) from 280 to 600 were then estimated by fitting our measured (or estimated) K_d following a model described earlier (Markager et Vincent, 2000). The daily spectral scalar irradiance at each depth (z) ($Q_{0-,z,\lambda,t}$; mol photons nm^{-1} m^{-2} h^{-1}) was determined following the equation:

$$Q_{0-,z,\lambda} = Q_{0-,\lambda} * e^{(-Kd,\lambda * z)} \quad (1.7)$$

where $Q_{0-,\lambda}$ is the cloud-corrected just-below-surface scalar downwelling irradiance (mol photons nm^{-1} m^{-2} d^{-1}), and $K_{d\lambda}$ is the spectral specific vertical irradiance attenuation coefficient.

1.3.5 Areal DOC photo-mineralization rates

The areal DOC photo-mineralization rate (PM, mg C m^{-2} d^{-1}) at each sampling date and lake was calculated as the sum of the volumetric photo-mineralization rates ($PM_{z,t}$) at

each (0.01m) depth intervals, multiplied by the strata volumes derived from lake bathymetry (for each 0.01m depth intervals, in m^3), and divided by lake surface area (m^2). Volumetric DOC photo-mineralization rates at each depth and each hour can be described as:

(1.8) $$PM_z = \int_{\lambda=280}^{\lambda=600} Q_{0^-z,\lambda} \cdot a_{CDOM,\lambda} \cdot AQY_\lambda ,$$

where PM_z is the daily photo-mineralization at depth z (mol C m^{-3} d^{-1}), $Q_{0\text{-}z,\lambda}$ is the spectral scalar irradiance at depth z (mol photons m^{-2} d^{-1}), $a_{CDOM,\lambda}$ is the wavelength-specific absorption coefficient of DOC (m^{-1}), and AQY_λ is the estimated wavelength-specific quantum yield of DOC mineralization (mol DOC loss · mol $photons^{-1}$) estimated for each specific date and lake. A sensitivity analysis revealed that varying the lake-specific AQY spectral slope (*d*) used in equation 1.5 over the entire range of values that were measured resulted in a total variation of *PM* of no more than 10% (see Supporting Information S1.1 for complete sensitivity analysis). Moreover, to validate the model, modeled rates of PM_z was compared to measured rates in quartz vials during two days in July 2015 in Lac Croche (see Supporting Information S1.4 for details on results and the methods). We further estimated the average annual photo-degradation in each lake by recalculating the monthly-averaged *PM* rates and using the natural cubic spline function to integrate over the whole open-water period on each lake. Average monthly *PM* rates were calculated from monthly averaged AQY, cloud cover and irradiance following the same steps as described previously.

1.3.6 Whole-lake pelagic respiration

Pelagic respiration rates were derived from changes in oxygen concentration in unfiltered water samples incubated in 500ml Erlenmeyer at near *in situ* temperature in the dark for 48h (Marchand *et al.*, 2009). Briefly, O_2 concentrations were measured using an optode system, consisting of oxygen-sensitive optical sensors and a fiber optic

meter (Fibox 3, PreSens, Regensburg, Germany), except for Lac Croche samples, where O_2 was measured using a dual-inlet mass spectrometer (Guillemette et del Giorgio, 2011). All samples showed linear decreases of O_2, and respiration rates were derived as the slope of the O_2 concentration versus time plots. All pelagic respiration rates were then converted into C units assuming RQ of 1. It has been previously reported that the bacterial RQ measured in similar systems varies as a function of system trophic status and size, from less than 0.7 to over 1.6 (Berggren *et al.*, 2012). Although the reported average lake bacterial RQ was in the order of 1.2, the predicted RQ for our lakes based on their average chlorophyll and DOC concentrations was somewhat lower, in the order of 0.90 to 1.1, and we have therefore assumed an average RQ of 1 for our three lakes. There was a strong relationship between our measured respiration rates and both DOC and water temperature (see Results section for details), and we used the resulting multivariate regression model to estimate the areal rates of respiration using depth volume-weighted temperature (as $\Sigma(V_Z * T_Z)/$ LV, where Vz is the volume of each stratum, Tz is the temperature at the corresponding depth and LV is the lake volume) and DOC as independent variables, multiplied by the lake mean depth.

1.3.7 Statistical analyses and error assessments

Absorption and irradiance attenuation coefficients fitting were performed using least squared non-linear fitting function ('lsqcurvefit', MathWorks, MATLAB 7). To assess uncertainties in the AQY (resulting *PM* rates), we ran Monte Carlo simulations for each sample (999 iterations), in which each parameter in the calculation is randomly picked from a normal distribution around its mean value. Parameters selected to induce potential uncertainties in the resulting AQY (and thus *PM*) were related to uncertainties in DOC mineralization resulting from variability in the sample replicates and the uncertainties associated with bleaching during incubations in the solar simulator (see Supporting Information S1.2 for further details). For predicted pelagic respiration

values (Eq. 1.11), we used a de-logging correction factor (1.33) calculated from the standard error of the estimate (SEE) (Sprugel, 1983) to remove the bias introduced by the logarithmic transformation (Baskerville, 1974). We calculated the 95% confidence interval around the predicted values in the software R (R Development Core Team, 2008). We evaluated the potential uncertainties in the relative contribution of *PM* by performing a Monte Carlo simulation using the slope parameter errors in the multiple regression predicting pelagic respiration (Eq. 1.11) and uncertainties from *PM*. As a result, this allowed us to having an additional uncertainty estimation for the pelagic respiration itself. To assess the importance of each component in the calculation of *PM* rates, we used partial regression analysis (JMP 7.0, SAS Institute). Variables used in the multiple regression analysis were $\log_{10}$-transformed to adjust to a normal distribution. We compared CDOM (a440), respiration, AQY, *PM* and proportion of *PM* to total CO_2 production values between lakes and seasons (values were clustered by season according to sampling date with n of 2-4 per season) using two-way (with interaction) ANOVA with weighted response when possible (1/variance) using JMP 7.0 statistical software (SAS Institute). Spring refers to measurements made between ice melt until beginning of June, summer refers to samples taken between late June to late September, and fall refers to samples taken during October until the lake is covered with ice (i.e. late November - early December).

1.4 RESULTS

The concentration of DOC and CDOM in the surface waters of the three lakes are presented in Table 1.1. CDOM, measured as absorbance at 440 nm, was significantly different among lakes (see Supporting Information Figure S1.5 for the range in absorption coefficient spectra), but did not show significant seasonal variation (two-way ANOVA). CDOM also directly affected the light penetration in the water column, and the light extinction coefficients ($K_{d,\lambda}$) at different wavelengths were strongly related to CDOM (Table S1.3 in Supporting Information). The average lake UV light extinction coefficient (K_{d320}) was 18.9, 19.7 and 10.6 m^{-1} for Lac Hébécourt, Simoncouche and Croche, respectively.

1.4.1 DOC photo-reactivity and photochemical CO_2 production

The intrinsic photo-reactivity of DOC was estimated using standardized laboratory incubations under simulated sunlight. Average DOC mineralization (as DOC loss and DIC production) during light incubation was 0.41 mg C L^{-1} d^{-1} (ranging from 0.06 to 1.12 mg C L^{-1} d^{-1}) and was weakly but significantly positively related to the initial CDOM (log-normal linear regression, $r^2 = 0.18$, $p = 0.03$). DOC and DIC concentrations after 24 hours of irradiance were generally significantly different from the initial concentration ($p < 0.05$, t-test). We further corrected the DOC loss per amount of photons absorbed in the vial (i.e. *wi*AQY as mol C loss per mol photon absorbed), which yielded an average *wi*AQY of 0.00026 ± 0.00016 (mean ± SD). The average *wi*AQY for Lac Croche (0.00019) and Lac Simoncouche (0.00020) were very similar, whereas Lac Hébécourt showed lower (significantly different, two-way ANOVA, $p = 0.04$) average *wi*AQY (0.00008). Although *wi*AQY seemed to follow a seasonal pattern, being generally higher in spring and autumn and lower in the middle of the summer (Figure 1.1), this was not statistically justified by the two-way ANOVA test ($p > 0.05$). Figure 1.2 further shows the AQY spectra grouped by periods, where

the average spectral AQY for all three lakes peaked after ice melt, and was higher than the summer and fall averages.

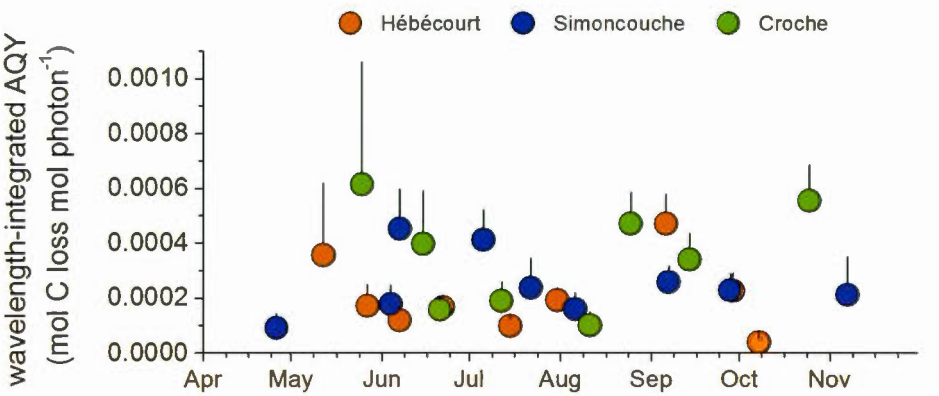

Figure 1.1. Seasonal pattern in total DOC photo-reactivity.

Seasonal pattern in total wavelength-integrated apparent quantum yield (integrated from 280 to 600nm; *wiAQY*) from lakes Hébécourt (orange circles), Croche (green circles) and Simoncouche (blue circles). Error bars (standard deviation) are computed from the Monte Carlo simulation using uncertainties in the light absorption in the vial and variability in the incubation replicates (see Methods section). Note that all measurements from various years are presented on the same timeline.

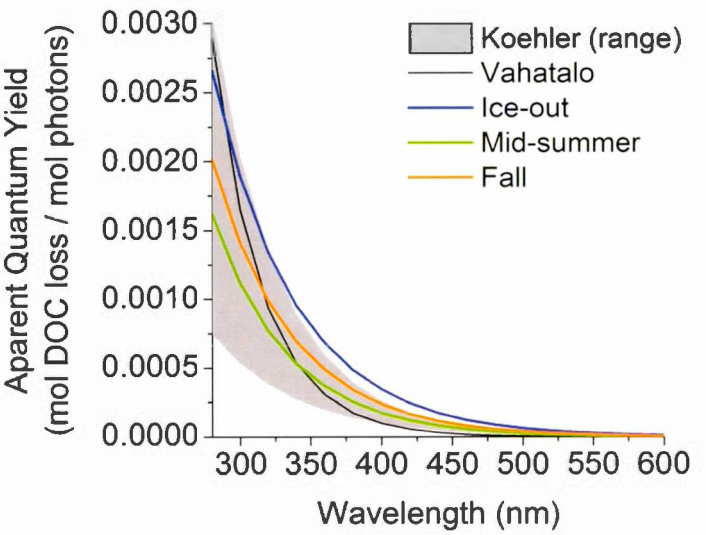

Figure 1.2. Apparent quantum yield spectra of DOC mineralization

Estimated apparent quantum yield spectra based on the assumption that the slope parameter corresponds to the spectral slope of the absorbance spectrum. "Ice out" is the (three lakes) average of the values recorded immediately after ice out (n=3), "Summer" is the (three lakes) average of July and August values (n=6), and "Fall" spectrum (orange line) is the (three lakes) average of September, October and November samples (n=6). The grey area represents the range of measured AQY spectra (n=5) reported in Koehler *et al.*, (2014), and the grey dashed line is the fitted AQY spectrum reported in Vähätälo *et al.*, (2000).

We combined the estimated spectral AQY, ambient irradiance and water column irradiance extinction, to estimate the photochemical DOC mineralization. The modeled volumetric rates (PM_z) were in reasonable agreements with in situ measurements of volumetric photo-mineralization rates (see Supporting Information Figure S1.4). Morphometry-weighted estimates of areal DOC photo-mineralization (PM) averaged 23.8 mg C m^{-2} d^{-1} (ranging from 2.5 to 104.2 mg C m^{-2} d^{-1}) and were not significantly different between lakes (two-way ANOVA, p = 0.92). On an annual basis, PM averaged 4.4 ± 0.7 g C m^{-2} yr^{-1}, and was 4.9, 3.6 and 4.7 g C m^{-2} yr^{-1} for Lac Hébécourt, Lac Croche and Lac Simoncouche, respectively (see Supporting Information Figure S1.6 for the annual integration from monthly rates). PM also followed an apparent seasonal pattern, which was consistent between the different lakes, being typically higher in spring (averaged measured rates of 39.2 mg C m^{-2} d^{-1}), and decreasing during the summer to rates around 18.3 mg C m^{-2} d^{-1} (Figure 1.3a). However, no statistical difference was found between seasons (p = 0.19). There were deviations from this pattern in PM in Lac Simoncouche, where PM peaked in June-July rather than right after ice-out. We performed a series of multiple regression analysis to assess the relative importance of each of the variables involved in the calculation of PM in explaining the variability across lakes and seasons. The best model describing the variability in PM was:

$$(1.9) \quad \log_{10}PM = -0.22 + 1939.09*wi\text{AQY} + 0.07*\text{CDOM} + 0.09*E_{0^-} \quad (r^2 = 0.84)$$

where PM is the areal photochemical DOC mineralization (mg C m^{-2} d^{-1}), wiAQY is the estimated wavelength-integrated AQY (280-600nm), CDOM is the wavelength-integrated (280-600nm) absorption coefficient by colored dissolved organic (m^{-1}), and E_{0^-} is the wavelength-integrated (280-600nm) modeled irradiance just below surface water (MJ m^{-2} d^{-1}). All parameters were statistically different from zero ($p < 0.001$), except for the intercept (p = 0.14). This partial regression model revealed that irradiance (as E_{0^-}) and intrinsic photo-reactivity of DOC (here expressed in terms of

*wi*AQY) explained roughly the same amount of variability (both around 30%), whereas the amount of CDOM explained the remaining variability in *PM*.

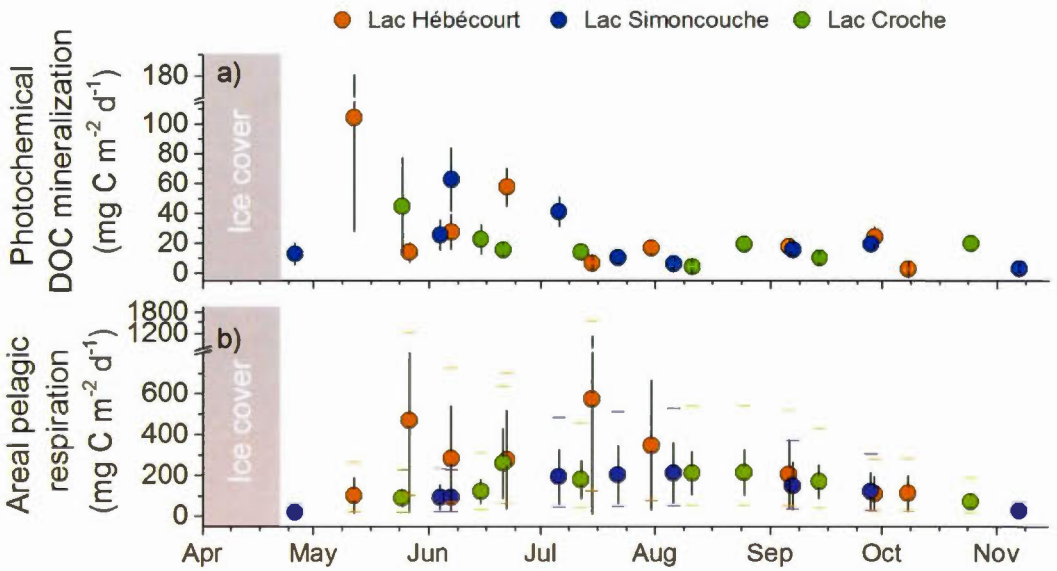

Figure 1.3. Areal rates of photochemical DOC mineralization and pelagic respiration

Panel **a)** is the areal photochemical DOC mineralization (mg C m^{-2} d^{-1}) and panel **b)** is the areal pelagic respiration (mg C m^{-2} d^{-1}) from lakes Hébécourt (orange circles), Croche (green circles) and Simoncouche (blue circles). Error bars for photo-mineralization are the standard deviation around the average values, computed from error in the DOC degradation during the incubation and the uncertainties in the light absorption in the vial (see Methods section for details on the calculations). Error bars on the pelagic respiration are the standard deviation around the average values, computed from the slope parameter error of the multiple regression model (see Methods section). We additionally plotted the lower and upper 95% confidence interval (matching color bars). Note that all measurements from various years are presented on the same timeline.

1.4.2 Water column respiration

Integrated water-column respiration was modeled based on laboratory incubations at near in situ surface water temperature. The measured volumetric pelagic respiration ranged from 4 to 247.5 mg C m^{-3} d^{-1}, and was mainly driven by water temperature:

$$\log_{10}PR = 0.83 + 0.05*T \qquad (r^2 = 0.53) \tag{1.10}$$

where *PR* is the measured pelagic respiration (mg C m^{-3} d^{-1}) and T is the water incubation temperature (°C), which was set to match measured ambient temperature. We used multiple linear regression to explore which additional variables further explained the variability in respiration, and the best predictive model included DOC in addition to temperature:

$$\log_{10}PR = -0.19 + 0.05*T + 1.11*\log_{10}DOC \qquad (r^2_{adj} = 0.67) \tag{1.11}$$

where *PR* is pelagic respiration (mg C m^{-3} d^{-1}), T is water incubation temperature (°C), DOC is dissolved organic carbon (mg C L^{-1}). We used equation 11 to estimate the depth-integrated respiration rates (mg C m^{-2} d^{-1}) using DOC concentration (assuming to be uniform in the water column) and the depth volume-weighted temperature. Measurements of hypolimnetic DOC in Lac Croche during the open water season suggested no significant difference between bottom and surface DOC concentrations (data not shown). Vertical profiles of water temperature and dissolved oxygen are shown in the Supporting Information Figure S1.7. We estimated areal water column respiration for each sampled date, which ranged from 21.5 to 570.6 mg C m^{-2} d^{-1}, averaging 188.6 mg C m^{-2} d^{-1} across all lakes and open water dates. As water temperature is an important driver of water column respiration, whole-lake pelagic respiration rates showed a seasonal pattern (Figure 1.3b) with peak rates in mid-summer (June to August), and with statistical difference between lakes ($p = 0.04$; two-way ANOVA) and seasons ($p = 0.01$; two-ANOVA).

1.4.3 Relative importance of photochemical DOC mineralization to lake pelagic CO_2 production

The relative contribution of *PM* to whole-lake pelagic CO_2 production (photo + respiration) averaged 14% (ranging from 1% to 49%) across all our samples, and followed a seasonal pattern similar to that of *PM* (Figure 1.4), where spring contribution was the highest. The contributions were statistically different between lakes ($p = 0.02$; two-way ANOVA) and seasons ($p = 0.02$; two-way ANOVA), even if there were large uncertainties associated with the spring values. During spring, all lakes showed a greater average contribution of *PM* relative to *PR* (around 26% on average), and the average contribution declined abruptly during the summer to around 7.5%. In all three lakes, there was a slight increase in the contribution of *PM* of up to 12% on average toward the fall period. This seasonal pattern in the relative contribution of *PM* to whole water-column CO_2 production was partly driven by strong shifts in the magnitude of water column respiration (Figure 1.5).

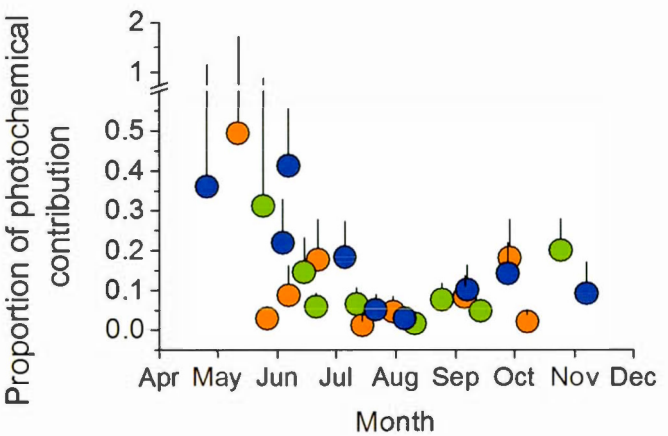

Figure 1.4. Photochemical DOC mineralization relative contribution to the whole water-column CO_2 production.

Photochemical DOC mineralization relative contribution to the whole water-column CO_2 production (as the sum of photo- and biological pelagic processes) of Lac Hébécourt (orange circles), Lac Croche (green circles) and Lac Simoncouche (blue circles). Error bars (for clarity, only upper bars are shown) are the standard deviation estimated by Monte Carlo simulation (see Methods section). Note that all measurements from various years are presented on the same timeline.

1.5 DISCUSSION

1.5.1 Variability in intrinsic DOC photo-reactivity

We carried out incubations with lake water surface samples under simulated sunlight to determine DOC photo-mineralization and to estimate the wavelength-integrated apparent quantum yield (*wi*AQY). Predictably, samples with higher initial CDOM had the highest absolute DOC mineralization rate during light exposure. The relationship between the absolute photo-mineralization and CDOM, however, was weaker (r^2 = 0.18) than the one reported by Lapierre *et al.*, (2013), which used the same approach but worked at the whole network scale, and thus had a much larger DOC and CDOM range. This would suggest that over very large gradients, the absolute amount of photodegradable DOC broadly tracks the bulk DOC (Lapierre *et al.*, 2013). At the scale of individual lakes, however, the temporal variation in the intrinsic properties of the DOC, reflected in seasonal shifts in the apparent quantum yield of this DOC, overshadowed the temporal patterns in the concentration of DOC or CDOM.

In this regard, our results show temporal shifts and an apparent seasonal pattern in the DOC photo-reactivity (reflected as the *wi*AQY; Figure 1.1). The lowest values were usually recorded in mid-summer, presumably because DOC has already undergone significant photochemical processing and there are low inputs of new DOC during this period. Accordingly, photo-reactivity tends to be not only lower, but also less variable within and between lakes during the summer period (Figure 1.1). After ice melt and during fall, however, the DOC photo-reactivity tended to depart from this range (Figure 1.1 and 1.2), which correspond to periods when DOC, which has been relatively photo-protected either under the ice or in the hypolimnion, is brought to the surface and exposed to sunlight. Our results are however partly blurred by the uncertainties in some samples, thus further measurements in time would needed to statistically prove the existing seasonal pattern. Nevertheless, the observed apparent seasonal trend agrees

with previous studies that have reported enhanced photo-reactivity of DOC in spring in both lakes (Gonsior *et al.*, 2013; Lindell *et al.*, 2000) and streams (Porcal *et al.*, 2013). Relatively higher DOC photo-reactivity values in fall were also reported in a small boreal lake in Sweden (Groeneveld *et al.*, 2015). The high values in DOC photo-reactivity recorded in late summer and fall (Figure 1.1 and 1.2) are likely associated to either the mixing of highly photo-reactive hypolimnetic DOC (Gonsior *et al.*, 2013), or from the loading of highly reactive soil DOC following heavy rain events that typically occur in the fall (Raymond et Saiers, 2010). These periods of intense rain result in an increase in both the lake flushing rate and the input of terrestrial DOC that may be fresher and more photo-sensitive, driving an overall increase in photo-reactivity and therefore also in the production and emission of CO_2 (Vachon et del Giorgio, 2014). This may suggest potential hysteresis in intrinsic DOC photo-reactivity, wherein water residence time correlates to the loading of fresh DOC and also determines the light-exposure history of DOC, which in turn shapes its residual photo-sensitivity. We suggest that events that affect water residence time of lakes, such as major storms and the spring freshet, may modulate the dynamics of photo-mineralization in lakes, although this direct link is still to be demonstrated.

Lakes had similar temporal patterns in DOC photo-reactivity (Figure 1.1), except in Lac Simoncouche, where the spring peak in *wi*AQY was delayed compared to the other two lakes. In particular, we observed relatively low DOC photo-reactivity value in Simoncouche after ice melt (Figure 1.1), which suggests that either photo-reactive DOC had already been photo-degraded by the time we sampled, or that it had been diluted by the spring freshet hydrologic load, since both CDOM and DOC also significantly decreased during that period (data not shown). The peak in DOC photo-reactivity in Lac Simoncouche came in late spring (Figure 1.1), when external inputs were already low, suggesting that photo-reactive DOC could have been generated within the lake. Macrophyte-derived DOC leachates have been shown to be highly colored (Lapierre et Frenette, 2009) and photo-reactive (Anesio *et al.*, 1999). Since

nearly 15% of Lac Simoncouche was covered by macrophytes, we suggest that macrophyte leachates could have represented a potential source of photo-reactive DOC in this particular lake, although this hypothesis should be further tested.

Our estimated *wi*AQYs were well within the values reported for boreal lakes in Scandinavia (Groeneveld *et al.*, 2015; Koehler *et al.*, 2014; Vähätalo *et al.*, 2000), yet our estimated rates of *wi*AQY immediately after ice melt were in the upper range (Figure 1.2). This highlights the fact that within a given lake and over an annual cycle, there is considerable variability in *wi*AQY (Groeneveld *et al.*, 2015). Our highest spring AQY were nevertheless, well below the range of values reported by Cory *et al.*, (2014) for arctic lakes and rivers that are influenced by permafrost, which are among the highest ever reported.

1.5.2 Depth-integrated DOC photo-mineralization

By combining estimates of water-column irradiance and DOC properties, we have been able to model the DOC photo-mineralization rates in three northern lakes for the whole open-water season. The in situ measurements of volumetric DOC photo-mineralization performed in July 2015 in Lac Croche further agreed with the modeled rates, thus validating our methods (see Supporting Information S1.4 of complete results). The estimated *PM* ranged from 2.5 to 104.2 mg C m^{-2} d^{-1}, which covers well the averaged measured depth-integrated CO_2 production in boreal lakes in Québec (Soumis *et al.*, 2007), in Swedish (Granéli *et al.*, 1996; Koehler *et al.*, 2014; Vähätalo *et al.*, 2000) as well as arctic lakes (Cory *et al.*, 2014) (Table 1.2). On an annual basis, the average *PM* of the three study lakes was almost identical as the annual average reported by Koehler *et al.*, (2014). Taking only the summer rates, the average *PM* in our three lakes was 18.3 mg C m^{-2} d^{-1}, which is very close to previous estimates for that period of the year (Koehler *et al.*, 2014; Vähätalo *et al.*, 2000), whereas our average spring rates (39.2 mg C m^{-2} d^{-1}) was more similar to estimates from other boreal and arctic lakes (Table 1.2).

Similar to seasonal variability in DOC photo-reactivity, *PM* estimated in three lakes thus covered almost the whole range reported in the literature, although a portion of the reported cross-lake variability in *PM* may be due to differences in the approaches (i.e., measured versus modeled).

The apparent seasonal trends in areal rates of lake photo-chemical processes (Figure 1.3a) resulted from a combination of the seasonal pattern in irradiance and the temporal shifts in DOC photo-reactivity. This pattern was coherent across the different lakes, in spite of major differences in their morphometry and hydrology. Despite the uncertainties and large variability between the rates, we observed an important shift occurred in spring, which could be explain by the combination of greater irradiance and higher photo-reactivity of DOC. There is also a question of scale involved: at very large spatial scales, the gradients in both the amount of CDOM (Lapierre *et al.*, 2013) and of irradiance may overwhelm local differences in DOM reactivity (Koehler *et al.*, 2014), but our results strongly suggest that both irradiance and DOC photo-reactivity are key factors driving ecosystem scale photo-mineralization.

Table 1.2. . Summary of published (and original) values of photo-chemical DOC mineralization and pelagic respiration (average ± standard deviation) and the resulting ratio of photo-chemical DOC mineralization to biological rates.

Study	study period	photo-mineralization	pelagic respiration	photo proportion to bio
		mg C m^{-2} d^{-1}	mg C m^{-2} d^{-1}	
Granéli *et al.*, (1996)	summer, boreal	51.2 ± 5.6[a]	618.3 ± 224.1[a,b]	0.08
Vähätälo *et al.*, (2000)	summer, boreal	11.9 ± 4.1	–	–
Jonsson *et al.*, (2001)	summer, boreal	23.8	161.9	0.15
Soumis *et al.*, (2007)	summer, boreal	74.8 ± 17.2	187.0[a]	0.4
	summer, temperate	74.5 ± 17.2	496.7[a]	0.15
Cory *et al.*, (2014)	Arctic lake (Toolik)	50.9 ± 13.8	77.2 ± 17.4[c]	0.66
	Coastal arctic lakes	109.8 ± 6.0	24.0 ± 3.2[c]	4.58
Koehler *et al.*, (2014)	open water, boreal	16.4 ± 0.2[e]	–	–
This study	**all samples**	23.8 ± 22.6	188.6 ± 126.3	0.13
	summer only	18.3 ± 15.7	244.2 ± 115.1	0.07

[a] average of all the lakes, excluding lake Stråken ,
[b] epilimnetic rates
[c] back calculated from ratio
[d] bacterial respiration only
[e] annual rates divided by 232 of ice free days
[f] average of all (or only summer) samples of the three lakes

1.5.3 Importance of DOC photo-mineralization at the whole lake scale

Having well-constrained estimates of depth-integrated DOC photo-mineralization and assessing its temporal patterns is necessary to adequately quantify the importance of photo-chemical processing of DOC relative to the other C fluxes in lakes. As irradiance and temperature closely track each other on an annual cycle, it could a priori be expected that water column respiration and photo-mineralization should follow the same overall seasonal pattern. This hypothesis, assumes that photo-mineralization is driven entirely by irradiance. We however found an apparent seasonal decoupling in water-column CO_2 production by biological and photochemical processes. Photo-chemical mineralization was enhanced episodically in spring and fall, whereas respiration followed a smoother seasonal pattern (Figure 1.3). As a consequence of the temporal decoupling between respiration and photo-mineralization, the relative contribution of photo-chemical process to the whole water-column CO_2 production (as the sum of photo-chemical and biological processes) also showed a clear seasonal pattern (Figure 1.4), despite of large uncertainties in the spring values. The cold water found in the water-column after ice-out combined with the availability of highly photo-reactive DOC rendered photo-mineralization equally important with respiration as CO_2 contributor in early spring. As the water warms up and the DOC becomes photo-bleached and less photo-reactive, pelagic respiration becomes the main source of CO_2 production in the lake water column in summer (Figure 1.4). It should be pointed out that chemical CO_2 production (i.e. calcite precipitation) is not a significant process in any of these lakes.

Although there was a large temporal variability in *PM* within a given lake, the average open water seasonal values were not significantly different between our study lakes (two-way ANOVA, $p > 0.05$), despite significant differences in bulk DOC and CDOM concentrations (*see* Results section). This low inter-lake variability in *PM* probably reflects the interplay between DOC concentration and light penetration. Because of the

rapid absorption of UV light by DOC in the water-column, rates of DOC photo-mineralization declined rapidly with depth. We evaluated that on average, about 40%, 80% and 90% of the photo-mineralization occurred in the top 0.1, 0.5 and 1m, respectively. This depth-dependency of photo-mineralization is similar to that reported by Koehler *et al.*, (2014), who estimated that 95% of the mineralization in boreal lakes occurred in the top 0.8 m. Because our lakes are deeper than 2 meters on average, most of the UV light is absorbed by both water and mostly DOC, resulting in a reduced influence of morphometry and DOC content on the depth-integrated DOC photo-mineralization across our lakes. In contrast, despite the sometimes large uncertainties around the predicted respiration rates, there was a larger difference in the amplitude of areal water column respiration rates between the lakes relative to that in *PM*, mostly due to lake depth and DOC concentration. As Lac Hébécourt and Lac Simoncouche are both shallow, the difference in amplitude is mainly explained by the DOC concentrations. For Lac Croche, in spite of its oligotrophic condition, its deeper basin results in areal respiration rates that are intermediate between two other lakes (Figure 1.3b), suggesting that deep oligotrophic lakes may still be important sites of biological CO_2 production. It is however important to mention that as respiration rates were measured using surface water samples, extrapolating hypolimnetic rates can be problematic, which is particularly the case in well stratified water column like in Lac Croche (see Supporting Information S1.7 for vertical profiles data). However, because of the smaller volume in the deeper layers (about 30% of the whole lake volume in Lac Croche) together with lower respiration rates because of the lower temperature result in a relatively small contribution of hypolimnetic respiration at the whole lake scale (less than 10% in the case of Lac Croche). As a result, using models derived from surface waters to extrapolate areal respiration rates is unlikely to yield overly biased estimates, and we maintain that the resulting temporal patterns are robust. Nonetheless, because there were still large uncertainties around the predicted values (Figure 1.3b), individual areal respiration rates must be interpreted with caution.

The overall annual contribution of photo-chemical DOC mineralization to the total water-column CO_2 production averaged 14% for all three lakes combined (Figure 1.4). Although *PM* rates were similar between the different lakes, the relative contribution of *PM* was slightly more variable across lakes: *PM* in shallow and unproductive Lac Simoncouche contributed to 17% of the total water-column CO_2 production, whereas in productive Lac Hébécourt and deep Lac Croche *PM* contributed to about 12-13%. This range was mainly due to cross-lake differences in areal pelagic respiration rates, which were significantly different despite their sometimes large uncertainties. Our findings are not incompatible with other studies that have also compared rates of photo-chemical with biological processes. For example, Cory *et al.*, (2014) reported a very high contribution of DOC photo-chemical mineralization in sub-arctic rivers and lakes (sometimes over 100%), and that pattern was a combination of highly reactive DOC in these systems with consistently low respiration rates due to low temperature. In contrast, Granéli *et al.*, (1996) reported a relatively modest contribution (around 8%) of photo-chemical DOC mineralization relative to respiration in Swedish boreal lakes. The cross-system variation in the relative contribution of photo-chemical mineralization reported in these previous studies follows a gradient in pelagic respiration (Figure 1.5), which seems to stabilize at a minimum of around 0.1 (i.e. photo-chemical mineralization is 10% of biological respiration). The underlying reasons are not clear, however, because in our study, periods of low respiration coincided with peaks in photochemical activity and vice versa. Having considered the entire ice-free period, however, allowed us to capture both temporal shifts in DOC photo-reactivity and water temperature that affect DOC processing (biological and photo-chemical) differently, highlighting the importance of spring and fall periods (as well as cold water systems, i.e. left part of Figure 1.5) when DOC processing is not expected to be intense, with implications on our understanding of lake C cycling.

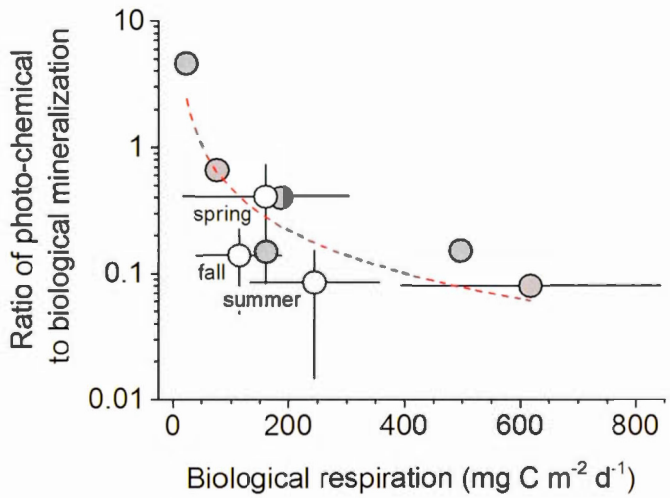

Figure 1.5. Relationship between biological processes (respiration) and the ratio of photo-chemical DOC mineralization to biological respiration.

Relationship between biological processes (respiration) and the ratio of photo-chemical DOC mineralization to biological respiration. Open circles are averaged values from spring, summer and fall of this study (showed with standard deviation) and grey circles are published values with standard deviation of the respiration when available (*see* Table 1.2). Spring refers to measurements made between ice melt until beginning of June, summer refers to samples taken between late June to late September, and fall refers to samples taken during October until the lake is fully covered with ice.

We have shown here, like others studies, that photo-chemical DOC mineralization represents a significant C flux in these northern lakes, and thus potentially a significant component of the CO_2 budget in these lakes. Previous studies have reported relatively high spring emissions from northern lakes, presumably due to the release of CO_2 accumulated under the ice in boreal and sub-arctic regions (Ducharme-Riel *et al.*, 2015; Karlsson *et al.*, 2013). Combining our results of *PM* with the annual CO_2 cycle for these lakes reported by Ducharme-Riel *et al.*, (2015) suggests that photochemical mineralization of photo-sensitive DOC could contribute around 20% of spring CO_2 emissions. We can further express the role of *PM* in terms of its potential to sustain ambient CO_2 concentrations in lake surface waters. We estimate that CO_2 photo-production could potentially contribute to the equivalent of 28 µatm on average, and up to 50 – 150 µatm during peak photo-production in early spring, once gas exchange has been factored in (Vachon et Prairie, 2013). These results suggest that although photo-mineralization cannot by itself sustain the systematic CO_2 supersaturation that has been observed across these temperate and boreal lakes, which typically ranges from 450 to over 1,000 µatm (Lapierre et del Giorgio, 2012; Rasilo *et al.*, 2014), that it is nevertheless a significant contributor to this phenomenon.

1.6 ACKNOWLEDGMENTS

We would like to thank Alice Parkes, Annick St-Pierre, Mathieu Dumais and Jean-Philippe Desindes for field and laboratory assistance. We also thank Sara Mercier-Blais for providing complementary data on Lac Croche, Philippe Massicotte for useful comments on previous version of the manuscript, Drs. J.-J. Frenette and R. Carignan for help with the PUV measurements and Y.T. Prairie for help with statistical analyses. We thank also two anonymous reviewers for constructive comments. This project was part of the large-scale research program of the Industrial Research Chair in Carbon Biogeochemistry in Boreal Aquatic Systems (CarBBAS), co-funded by the Natural Sciences and Engineering Research Council of Canada (NSERC) and Hydro-Québec. NSERC doctoral scholarship and UQAM-FARE scholarship was also attributed to DV.

1.7 SUPPORTING INFORMATION

1.7.1 Uncertainties assessment in the DOC photo-reactivity and AQY calculations

We identified several uncertainties related to some assumptions in the calculation of the DOC photo-mineralization: (1) the potentially unsterilized samples prior to the photo exposure, (2) quantifying photons absorbed by sample and (3) the wavelength dependency of AQY assigned for each sample.

(1) The reason for filtering at 2.7 μm is that we carried out with this same water samples parallel dark incubations to determine bacterial DOC degradation over a large spatial range (Lapierre *et al.*, 2013), and these require a significant proportion of the bacterial community to pass the filter. We hypothesized that bacteria present in the irradiated samples were most likely inactivated by the high UV doses experienced in the solar simulator, and therefore would have not influenced the photochemical results. We however accounted for the potential bacterial activity during the light incubation using results of DOC degradation from parallel dark incubation (*see* Lapierre et del Giorgio (2014) for further details on the dark incubation). Rates of bacterial DOC degradation from dark incubation corresponded on average to only 8% of the photo-chemical DOC degradation rates. We nevertheless used the rates of bacterial degradation for each sample and estimated upper and lower limits of potential DOC degradation (and DIC production) during the light incubation. Those limits corresponded to assuming no bacteria (upper limit) and the majority of the bacteria (lower limit corresponding to subtracting bacterial rate to photo-chemical rate) in the vial during the light incubation. The mean and standard deviation of this range was used in the DOC reactivity calculation.

(2) Additional uncertainties resided in the determination of the absorbed light in the vial. Because we used cylindrical vials in addition to the fact that DOC in the vial was

bleached during the incubation, the exact amount of light absorbed by CDOM after 24 hours of incubation is difficult to estimate with high precision, unless using actinometry methods. We estimated the potential error related to the uncertainty in the quantification of the photo absorbed by the sample. First, we used a subset of data (n=99) from Lapierre et del Giorgio (2014), which also includes some of the data used in this study. We evaluated that CDOM loss during the incubation followed a first order decay of absorption coefficient at 375 nm corresponding to k value of 0.0196 (±0.0184) hr^{-1}. Using this rate, we corrected the mean absorbed photon during the incubation $\bar{\alpha}_{CDOM,\lambda}$ in equation 1.3 of the main manuscript. We then used both uncertainties related to bacterial DOC degradation during the light incubation and related to the quantification of absorbed photon by the sample to estimate the potential error around the DOC photo-reactivity by applying a Monte Carlo simulation with 999 iterations. This simulation allowed us to estimate the total potential error around the AQY calculation. We further evaluated the importance of quantifying the light reaching the sample, which can be difficult to estimate when using cylindrical vials. We performed a sensitivity analysis which explored the potential effect of varying the exposed surface area to the resulting photo-chemical DOC mineralization rates (Table S1.1). The results from this analysis show that the exposed surface area is an important component in the estimation of AQY and thus the resulting areal photo-mineralization rates. In the case of this study, we evaluated that the surface area exposed by the irradiation should well within 20% of variation, because outside this range would mean that the vial would have been irradiated from the below.

Table S1.1. Sensitivity analysis of variation in the assumed exposed surface area of each vial on the resulting *wiAQY*.

Exposed surface area variation					
+5%	+10%	+20%	-5%	-10%	-20%
Resulting variation in *wiAQY*					
-4.8%	-9.0%	-16.7%	+5.3%	+11.1%	+21.9%

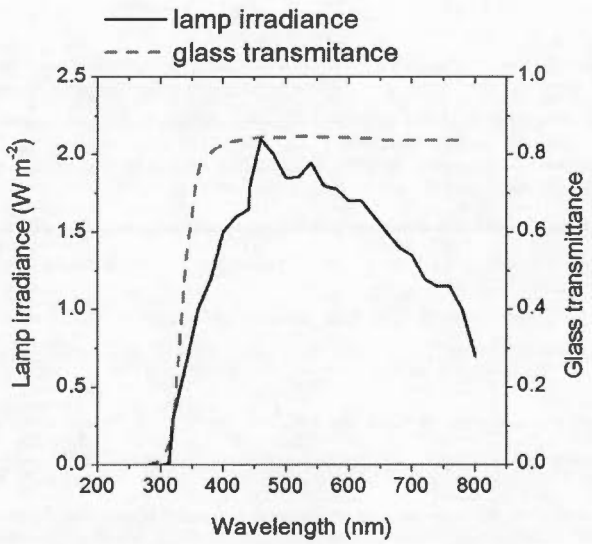

Figure S1.1. Incubation lamp irradiance and incubation tube glass transmittance spectra.

Incubation lamp irradiance and incubation tube glass transmittance spectra used in the calculation of energy absorbed by the sample. The lamp irradiance spectrum was provided by the solar simulator factory, and regularly calibrated using the provided radiometer (CR20 calibration radiometer). Glass transmittance was measured with a spectrophotometer (Biochrom, Cambridge, UK).

(3) We assessed the potential effect of assigning the slope parameter to the AQY equation (Equation 1.5). The parameter *S* was tightly constrained across all our samples (min = 0.016, max = 0.020, C.V. = 5.6%), with an overall average of 0.018. For comparative purposes, we collected AQY data from the literature and recalculate their AQY spectral slopes (parameter *d*) using an exponential equation. The average was 0.018 across a wide range of lakes (Koehler *et al.*, 2014; Vähätalo *et al.*, 2000) and ocean samples (Johannessen et Miller, 2001; White *et al.*, 2010). We however carried out a sensitivity analysis to assess the potential effect on the areal rates of DOC photo-mineralization (Figure S1.2 and Table S1.2). Figure S1.2 shows the implication of varying the slope parameter on the distribution of the AQY along the wavelength axis. For example, increasing the slope parameter give more importance to the smaller wavelengths. Although varying the slope parameter result in significant change in the spectrum of the AQY, the resulting change in areal DOC photo-mineralization is negligible (Table S1.2; up to 5% increase in areal rate).

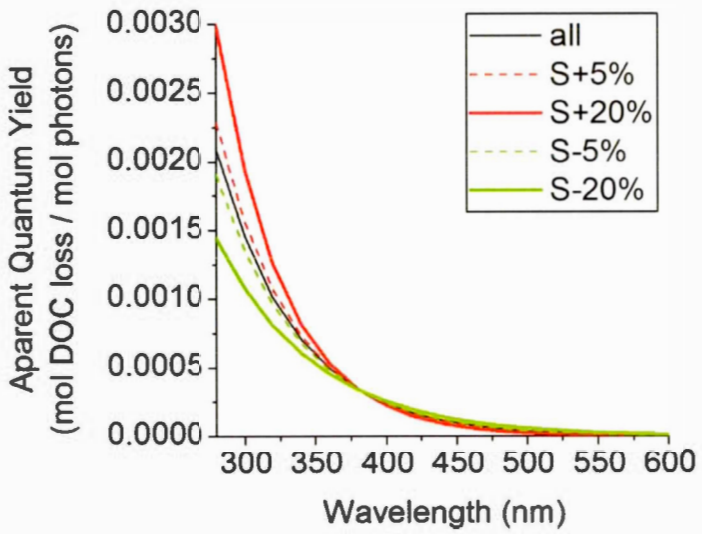

Figure S1.2. Sensitivity analysis on the estimations of the apparent quantum yield (AQY) calculation.

When varying the *S* parameter. Increasing *S* parameter result in steeper decrease with wavelengths, giving more importance to the UV bands.

Table S1.2. Sensitivity analysis of the spectral slope parameter

Sensitivity analysis of the spectral slope parameter on the resulting depth-integrated photochemical DOC mineralization (*PM*) rates. Steeper slopes (as + 5-20%) gives more importance to UV range as shown in Figure S1.5.

Spectral slope (*S*) variation					
+5%	+10%	+20%	-5%	-10%	-20%
Resulting variation in PM					
-1.4%	-2.8%	-5.2%	+1.5%	+3.2%	+6.8%

1.7.2 Determining cloud-corrected downwelling irradiance spectra

We corrected irradiance for cloud attenuation using daily values of OMI/AURA TOMS-Like cloud radiance fraction (CRF) over each lake (OMI Science Team, 2012). CRF is the fraction (0-1) of radiation (measured at 354.1nm) scattered by clouds and is determined as the effective cloud fraction, times cloudy radiance, divided by measured radiance. CRF correction factor (1-CRF) was parameterized using punctual measurements of just-over-water downwelling irradiance at 313nm, 320nm, 340 nm, 443nm and 550nm from our PUV profiler surface (air) probe. We compared correction factors to the ratio of measured to modeled (E_{meas}/E_{mod}) irradiance (W m^{-2} nm^{-1}) for each sampling site at sampling time of the day (Figure S1.3). A linear correction was determined forcing a (1-CRF) value of 0 (clear sky) to correspond to $E_{meas}/E_{mod} = 1$. The linear correction predicted that for a (1-CRF) of 0 (full cloud cover), E_{meas}/E_{mod} would be equal to 0.28. The resulting correction was determined as $E_{cloud} = E_{clear}*(0.72*(1\text{-CRF}) + 0.28)$. The modeled and measured values showed good agreements ($r^2 = 0.67$; Figure S1.3b).

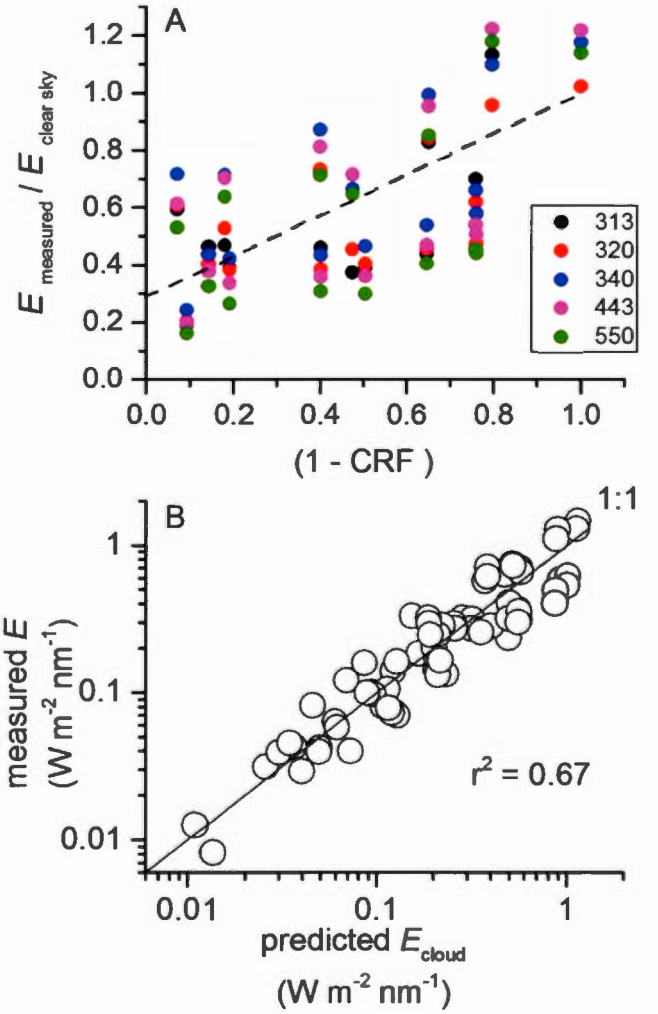

Figure S1.3. Cloud correction empirical relationship and validation.

Panel (a) shows the relationship between the cloud correction factor (1-CRF) and the ratio of measured irradiance ($E_{measured}$) to modeled irradiance under clear sky ($E_{clear\ sky}$) at the corresponding time of the measurement at wavelengths 313, 320, 340, 443 and 550 nm. Panel (b) shows the predicted cloud-corrected irradiance (E_{cloud}) relationship with the measured irradiance at wavelengths 313, 320, 340, 443 and 550 nm.

1.7.3 Light attenuation coefficient

For some sample dates (5 out of 9 for Lac Hebecourt, and 4 out of 7 for Lac Croche), we estimated K_d using empirical equations developed using our own measurements. Relationships were less powerful in the turbid lake (Lac Hébécourt), see Table S1.3.

Table S1.3. Empirical models prediction attenuation coefficient in the three studied lakes.

All lakes

	equation	r^2
K_d313	6.9813 * a_{440} + 9.9312	0.76
K_d320	4.9814 * a_{440} + 8.0963	0.55
K_d340	2.9034 * a_{440} + 7.2646	0.56
K_d443	0.5277 * DOC - 0.7998	0.80
K_d550	0.2136 * DOC - 0.5026	0.92

Non-turbid lakes

	equation	r^2
K_d313	9.1563 * a_{440} + 6.9045	0.86
K_d320	8.3991 * a_{440} + 3.6672	0.88
K_d340	4.5568 * a_{440} + 5.4002	0.94
K_d443	0.9402 * a_{440} + 0.9751	0.93
K_d550	0.1699 * DOC - 0.2562	0.84

1.7.4 Model validation

The photo-mineralization model was validated with in situ measurements of DIC photo-production in the water column of Lac Croche in July 2015. The measurements were performed following methods described in Graneli *et al.*, (1996). Briefly, lake surface water was sampled at 0.5 m depth at the center of the lake and brought back immediately to the lab. Water was immediately filtered-sterilized (Sterivex 0.22µm filters units with polyethersulfone membrane) and poured in fused quartz tubes (d=25mm, length=200mm, volume=95 ml). Quartz tubes were previously cleaned into 10% HCl solute for 24h and rinsed three times with milli-Q water and then oven-dried. The tubes were sealed with previously autoclaved rubber stoppers perforated by two cannulae (also autoclaved) of different length, one reaching the bottom of the tube and the other just below the stopper (Granéli *et al.*, 1996). Stoppers were set to avoid any bubbles and air into the tubes and tubing. Four tubes per depth (2 dark and 2 light) were set horizontally at 0 (just under water), 0.2, 0.7 and 2 m in the center of the lake and at different positions to avoid shading. The tubes were incubated in the lake for 2 days to cumulate enough light to detect DIC accumulation (~18h of sunlight). The dark tubes were wrapped in foil paper. After the incubation, tubes were opened and the water was gently poured to prevent any bubbles into borosilicate vials sealed with rubber septa with PTFE coating for further measurements of DIC on an OI-1010 TIC-TOC Analyzer (OI Analytical, College Station, TX, USA). DIC photo-production was calculated as the difference between the light and dark concentrations after the in situ incubation. We compared measured rates with modeled rates, which were estimated using modeled cloud-corrected irradiance, laboratory light incubations and absorbance, as described in the main manuscript. Results showed reasonable agreements between the modeled volumetric rates and the measured DIC production in Lac Croche (Figure S1.4).

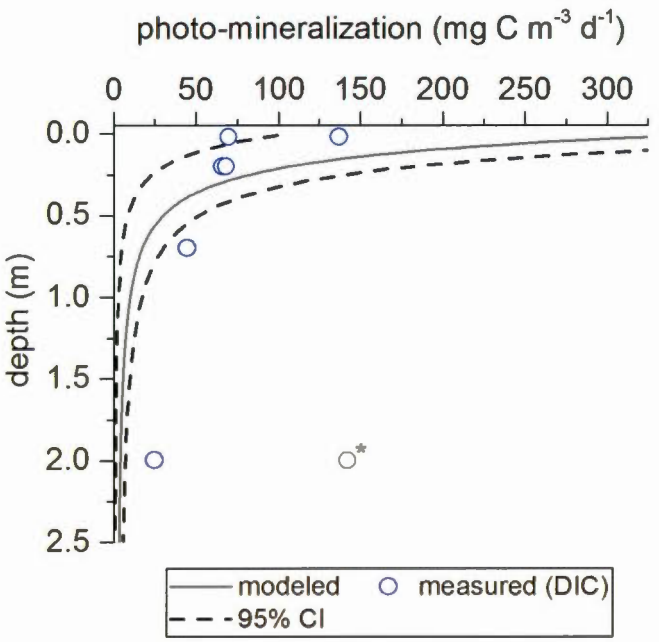

Figure S1.4. Model validation

Model validation showing good agreement between modeled and measured rates of DIC photo-production. (*) One measurement out of 8 however showed unrealistic DIC photo-production at 2 m depth (grey circle), suggesting that some contamination must have happened during the vial preparations.

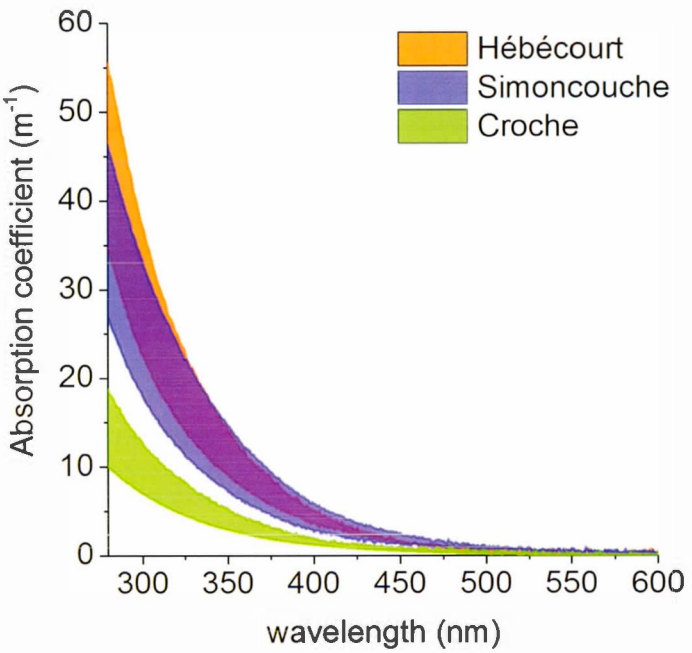

Figure S1.5. Mean absorption coefficient for the three study lakes

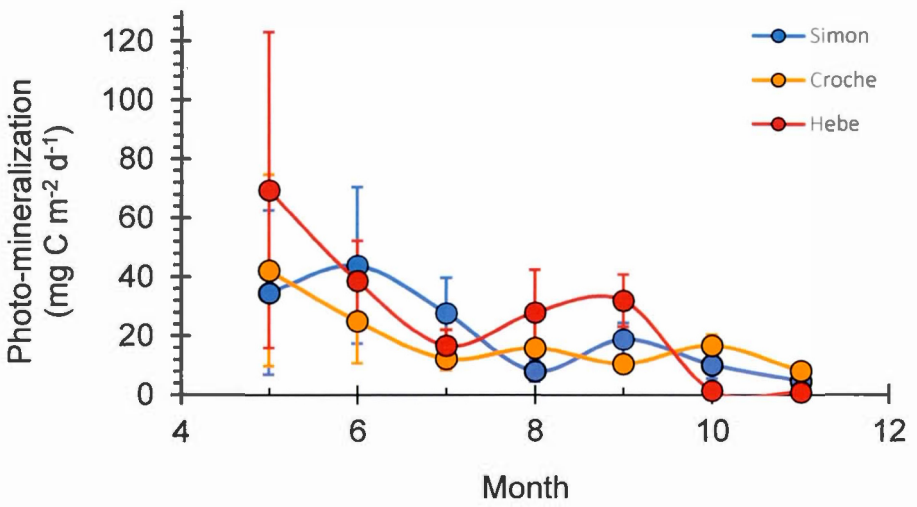

Figure S1.6. Monthly photo-mineralization rates (circles) showing natural spline interpolation (lines) used to integrate the whole year rates.

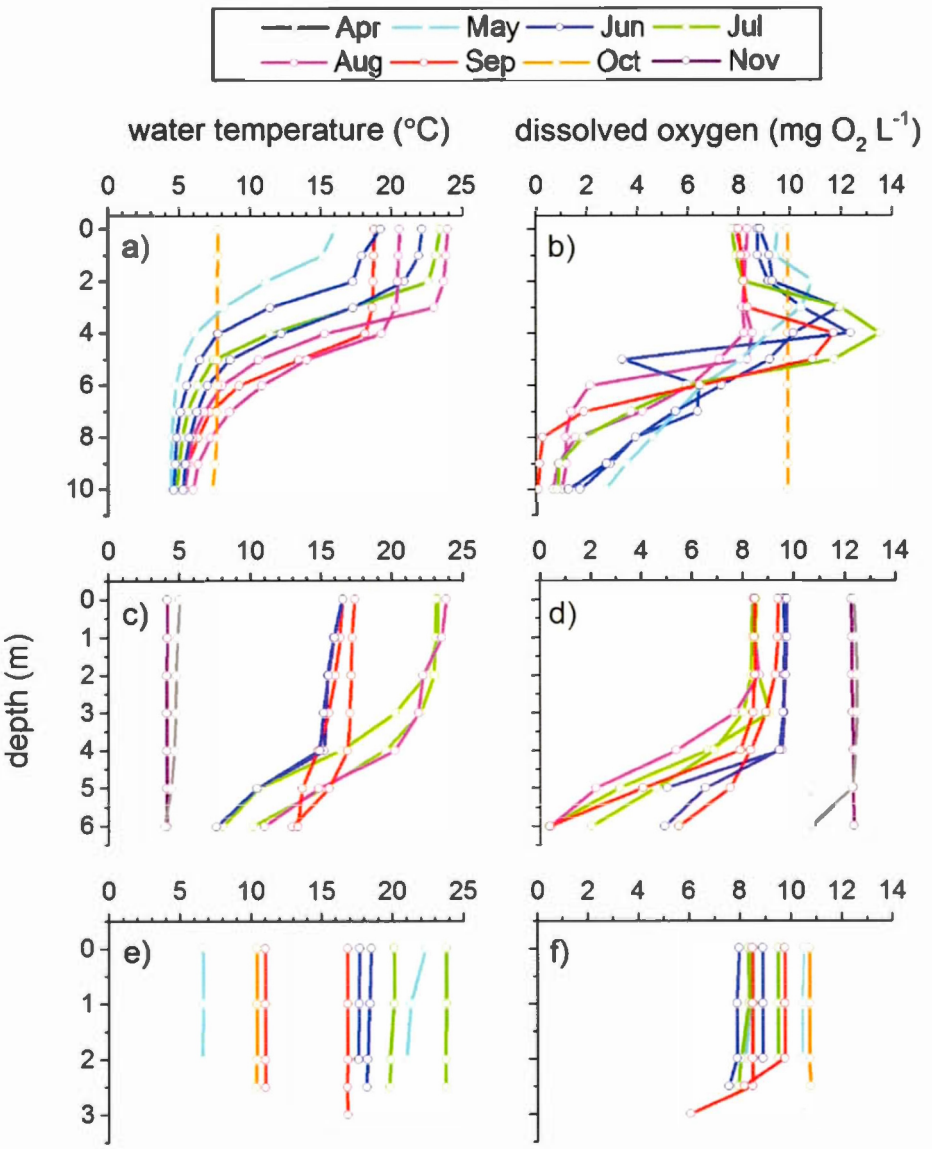

Figure S1.7. Vertical profiles of water temperature and dissolved oxygen

Vertical profiles of water temperature (**a**, **c**, **e**) and dissolved oxygen (**b**, **d**, **f**) for lakes Croche (**a**, **b**), Simoncouche (**c**, **d**) and Hébécourt (**e**, **f**). Color codes represent the time of the year (month).

CHAPITRE II

MODELING ALLOCHTHONOUS DISSOLVED ORGANIC CARBON MINERALIZATION UNDER VARIABLE HYDROLOGIC REGIMES: UNDERSTANDING THE BASELINE PRODUCTION OF CO_2 IN BOREAL LAKES

Dominic Vachon[1], Yves T. Prairie[1], François Guillemette[2] and Paul A. del Giorgio[1]

[1]*Groupe de Recherche Interuniversitaire en Limnologie, Département des sciences biologiques, Université du Québec à Montréal, Montréal, Canada.*

[2]*Department of Earth, Ocean, and Atmospheric Science, Florida State University, Tallahassee, USA.*

In preparation

Keywords: allochthonous DOC, boreal lakes, reactivity continuum

N.B. References cited in this chapter are presented at the end of the thesis.

2.1 ABSTRACT

Here we assess the interaction between hydrology and the reactivity of allochthonous dissolved organic carbon (DOC_{alloch}) in determining the potential of DOC_{alloch} to generate CO_2 through biological and photo-chemical mineralized in boreal lakes. We developed a mechanistic model that explicitly integrates the reactivity continuum concept (RCC) to reconstruct mineralization of DOC_{alloch} within lakes under variable hydrologic conditions, and used empirical measurements of DOC_{alloch} concentrations and reactivity as inputs to this model. The model predicts a steady state lake DOC_{alloch} concentration (L-DOC_{alloch}) and its average overall reactivity ($\overline{K}_{alloch}$), which integrates the distribution of DOC_{alloch} ages within the lake as a function of the DOC_{alloch} loading, the original reactivity of this DOC_{alloch} (K_0) and the lake water residence time (WRT). The modeled DOC_{alloch} mineralization rates and concentrations at steady state were in agreement with expectations based on observed and published values of ambient lake DOC (L-DOC) concentrations and reactivity. Results from this modelling exercise show that the interaction between WRT and K_0 is a key determinant of the ambient concentration and reactivity of lake DOC_{alloch}, which we show represents the bulk of DOC in most of these lakes. The steady state $\overline{K}_{alloch}$ also represents the proportion of CO_2 that can be extracted from DOC_{alloch} during its transit through lakes, and partly explains the patterns in surface water pCO_2 oversaturation that have been observed across gradients of lake size and volume. We estimate that in-lake DOC_{alloch} mineralization could potentially contribute on average 30-40% of the observed surface carbon dioxide partial pressure (pCO_2) across northern lakes. Applying the reactivity continuum framework to in-lake DOC_{alloch} dynamics improves our understanding of DOC_{alloch} transformation and fate along the aquatic network, and results in a predictable mosaic of DOC reactivities and potential CO_2 emissions across lakes of a landscape.

2.2 INTRODUCTION

The dissolved fraction of organic matter is by far the largest organic carbon pool in the water column of lakes (Prairie, 2008), and is mainly derived from the terrestrial environment (Wilkinson *et al.*, 2013). It is increasingly recognized that this terrestrially derived carbon is not only highly photo-chemically reactive (Opsahl et Benner, 1998; Wetzel *et al.*, 1995) but also biologically labile (Ågren *et al.*, 2008; Marin-Spiotta *et al.*, 2014; McCallister et del Giorgio, 2008), thus influencing several key aspects of lake (Cole *et al.*, 2000; Prairie, 2008; Solomon *et al.*, 2015). In particular, the mineralization of DOC_{alloch} establishes a baseline level metabolism (Guillemette *et al.*, 2013; McCallister et del Giorgio, 2008), which may contribute significantly to the widespread CO_2 oversaturation observed across northern lakes (Cole *et al.*, 2007; Tranvik *et al.*, 2009). Although this is an issue of fundamental importance to our understanding of lake function and of the biogeochemical role of lakes in the landscape, a direct mechanistic link between DOC_{alloch} and lake CO_2 has seldom been established.

At the core of this question is our understanding of the fate of DOC_{alloch} when it enters lakes, and in particular its mineralization dynamics. Previous studies have attempted to address this fundamental question using very different approaches: conventional input-output DOC mass balances (e.g., Dillon et Molot 1997; Algesten *et al.*, 2003), combination of isotopes and in vitro incubations (Guillemette *et al.*, 2013; Karlsson *et al.*, 2007; McCallister et del Giorgio, 2008) and modeling (e.g., Cole *et al.*, 2002; Hanson *et al.*, 2011; 2014a; Solomon *et al.*, 2013). These approaches, however, yielded either limited mechanistic insights of DOC_{alloch} mineralization or information that was difficult to scale up to the whole ecosystem. In addition, most studies have focused on the mineralization dynamics of the ambient lake DOC pool (Hanson *et al.*, 2014a; Koehler *et al.*, 2012; Stets *et al.*, 2010), but this ambient lake DOC pool is the net result of various transformation processes, and provides little insight on its own on the mineralization dynamics of the incoming DOC_{alloch}.

To effectively reconstruct the fate of DOC_{alloch}, it is necessary to have information on the amount of DOC that enters lakes from their surrounding basin, and to capture the behaviour of this carbon once it arrives to lakes. Under the simplest scenario, this DOC_{alloch} entering the lake will be degraded at a constant rate determined by some level of initial reactivity. Although DOC degradation has often been modeled as a simple first order process in many previous studies (Hanson *et al.*, 2011; Hanson *et al.*, 2014a; Molot et Dillon, 1997; Stets *et al.*, 2010), there is now ample evidence that this approach does not effectively capture the dynamics of ambient DOC degradation. The molecular complexity of DOC (Kellerman *et al.*, 2014) results in very different degrees of persistence of specific groups of compounds in the environment (Kothawala *et al.*, 2014). Several studies in soil, sediment and aquatic systems have shown that organic C degradation dynamics are better represented by a continuum of reactivity (Boudreau et Ruddick, 1991; Koehler *et al.*, 2012; Vähätalo *et al.*, 2010), wherein the most reactive compounds are degraded first, leaving behind increasingly recalcitrant components (Kalbitz *et al.*, 2003; Wickland *et al.*, 2007). In the context of terrestrial DOC loaded to lakes, this implies that the reactivity of this C will not stay constant, but will rather change as a function of the residence time of this C within the lake. Understanding the dynamics of DOC_{alloch} mineralization in lakes and its potential contribution to surface water CO_2 thus requires the integration of DOC_{alloch} loading to lakes and its reactivity within a reactivity continuum framework that effectively incorporates the temporal dimension associated to the transit of this carbon through lakes.

In this paper we develop a conceptual framework and accompanying mechanistic model where we have explicitly addressed these major challenges, and use this to explore the fate of inflowing DOC_{alloch} into boreal lakes. The model simulates in-lake mineralization of incoming DOC_{alloch} by incorporating the RCC to the biological mineralization of DOC_{alloch} and a first-order model for DOC_{alloch} photo-mineralization. The mechanistic model essentially recreates an empty lake that is filled with stream

water having realistic ranges in DOC_{alloch} concentrations and reactivity, and follows the transformation of this DOC_{alloch} within the residence time of the lake, to a steady state that is characterized by a specific distribution of different age and reactivity classes of this DOC_{alloch}. We used empirical measurements of DOC_{alloch} load, DOC_{alloch} initial reactivity and lake environmental condition as inputs to the model and explore the influence of different combinations of water residence times and DOC_{alloch} initial amounts and reactivities on the mineralization of DOC_{alloch} and the resulting integrated CO_2 production, in a set of boreal lakes in two distinct regions of Québec, Canada.

2.3 METHODS

2.3.1 Conceptual framework

In this conceptual framework, we incorporated both photochemical and biological mineralization of DOC_{alloch} within the receiving lakes, and these components are treated in parallel. The DOC_{alloch} biological reactivity (as an intrinsic property of DOC_{alloch}), is modeled as a continuum (as the RCC; Boudreau et Ruddick, 1991) wherein the mean biological reactivity ($\bar{k}_{bio}$) is described as a function of time (t) spend in the system:

$$\bar{k}_{bio} = \frac{\nu}{\alpha + t} \tag{2.1}$$

where α is the average lifetime of the more reactive compounds and ν is the relative abundance of the most recalcitrant compounds (Boudreau *et al.*, 2008; Koehler *et al.*, 2012; Vähätalo *et al.*, 2010). Applying the RCC to reconstruct biological mineralization of DOC_{alloch} within lakes requires further considerations. For example, the L-DOC_{alloch} pool is constantly replenished in lakes, outflowed from the system, and mineralized, all of which will modify the age distribution of the standing stock of L-DOC_{alloch}. In lakes, as in any reservoir containing a transiting mass, each DOC_{alloch} (or water) molecule has a different age (τ), here defined as the time since the molecule entered the system. Considering that the lake is instantaneously and constantly mixed (like a continuously stirred tank reactor, CSTR), the probability distribution function of ages $\psi(\tau)$ of the DOC_{alloch} (or water) can be defined as:

$$\psi(\tau) = \frac{1}{\tau_a} e^{-\tau/\tau_a} \tag{2.2}$$

where τ is the individual molecule age, and τ_a is the average age of DOC pool, which is tightly linked to WRT (Bolin et Rodhe, 1973; Monsen *et al.*, 2002). New DOC_{alloch},

which continuously enters the lake will be constantly "rejuvenating" the L-DOC_{alloch} pool, and this independently of potential in-lake production of new autochthonous DOC (DOC_{autoch}). According to the RCC, since the biological reactivity of a given pool is a function of time (its own age), the mean biological reactivity of DOC_{alloch} in a lake ($\bar{k}_{bio}$) is the integration of the continuum of all the different reactivities within the pool, weighted by the distribution of the age of the cohorts in the pool:

(2.3) $$\bar{k}_{\mathrm{bio}} = \int \frac{v}{\alpha+\tau} \times \psi(\tau)\mathrm{d}\tau,$$

where, v/α represents the initial reactivity of DOC_{alloch} when it enters the lake (K_0), such that $\frac{v}{\alpha+\tau}$ is the distribution of reactivities as a function of the age of each cohort. The mean overall reactivity of the L-DOC_{alloch} pool ($\bar{K}_{alloch}$) is thus the sum of the biological reactivity, expressed by $\bar{k}_{bio}$ described above, and the photochemical reactivity (k_{photo}), which we conceptualize as a first order decay as a function of mean UV-A irradiance in the water column and thus remain constant.

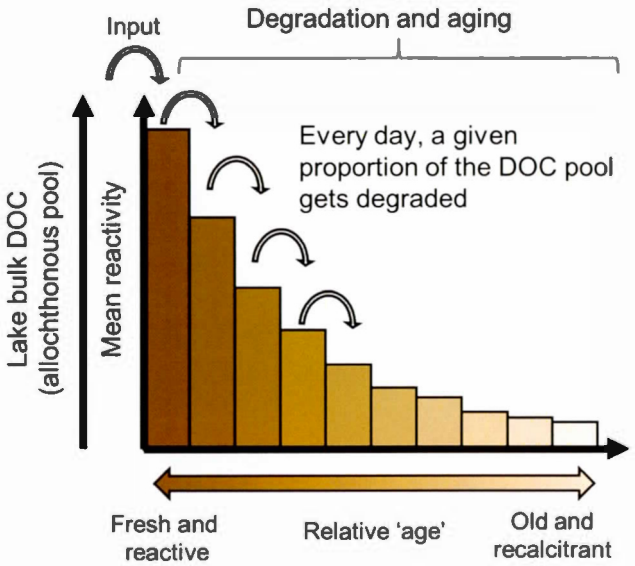

Figure 2.1. Conceptual model of DOC_{alloch} degradation in a lake.

The lake DOC_{alloch} pool consist in multiple sub-pool of DOC_{alloch} having different ages (relative to the day it enters the lake) and reactivity. At each time-step, a new and fresh DOC_{alloch} load enters the lake (''input'') and at the same time, the other sub-pools are being degraded (according to their own reactivity and environmental condition) and are aging (one day older each day). The relative abundance (first Y axis) and its reactivity (second Y axis) are higher for fresher DOC_{alloch} sub-pool and gets lower as the sub-pools are getting degraded (and older).

2.3.2 Mechanistic model of in-lake DOC_{alloch} mineralization

For the modeling purpose, each lake was considered as a single box which is completely and instantaneously mixed, and having an area of $1 m^2$ and depth corresponding to the targeted lake mean depth (targeted lakes are described below). At each time step, a new cohort of DOC_{alloch} of age '0' enters the lake, of which a given proportion will either be mineralized (or flocculated), persist and moved to the next age class (1 day old) or exit the lake (considering the lake to be instantaneously mixed) (Figure 2.1). Note that DOC_{alloch} age is here considered as the relative time (in days) since it has entered the lake, and not the absolute carbon age, which is harder to assess and is not the purpose of the study. The evolving in-lake DOC_{alloch} pool (L-DOC_{alloch}) thus consists of a vector of multiple cohorts of DOC_{alloch} masses of increasing age (starting from 1 day) (Figure 2.1). At each time step, the change in the L-DOC_{alloch} pool change is described as:

(2.4a)

$$\frac{dL - DOC_{alloch}}{dt} = DOC_{alloch\,IN} - BM - PM - floc - DOC_{alloch\,OUT} + A_{DOCalloch}$$

where $DOC_{alloch\,IN}$ is DOC_{alloch} load for the new cohort (Table 2.1; Eq. 2.4b), *BM* is the L-DOC_{alloch} mineralization by bacteria at lake temperature (Table 2.1; Eq. 2.4c), PM is the L-DOC_{alloch} photo-mineralization (Table 2.1; Eq. 2.4d), *floc* is the fixed loss of L-DOC_{alloch} to flocculation (0.0019 d^{-1}; von Wachenfeldt et Tranvik 2008), $DOC_{alloch\,OUT}$ is the L-DOC_{alloch} export to downstream systems (Table 2.1; Eq. 2.4e), and $A_{DOCalloch}$ is a vector manipulation where each cohort moves to the next age class (see Figure 2.1). Note that the model does not account for the bacterial degradation of photo-processed DOC_{alloch}. All the model equations are explained in Table 2.1. Equation 2.4a was numerically solved to reach equilibrium (dL-DOC_{alloch}/dt = 0) using an ordinary differential equation solver ('ode.1D' function using LSODA integration method from

the 'deSolve' package, R Development Core Team, 2008). We ran the model under various scenarios using empirical measurements of quantity and reactivity of DOC_{alloch} from small streams and measured lake characteristics such as WRT, water temperature and UV light conditions, which is detailed in the following sections.

Table 2.1. Equations of DOC_{alloch} mineralization dynamic model in lake

	Main equations	*description*
(2.4b)	$DOC_{IN} = streamDOC \times Q_{IN}$	daily DOC_{alloch} loading into lake
(2.4c)	$BM = lakeDOC \times k_{Bio} \times 1.07^{(T-20)}$	daily DOC_{alloch} biological mineralization with Aaherius correction for temperature (Venkiteswaran *et al.*, 2007)
(2.4d)	$PM = lakeDOC \times k_{Photo} \times mUVA$	daily DOC_{alloch} photo-chemical mineralization
(2.4e)	$DOC_{OUT} = lakeDOC \times Q_{OUT}$	daily DOC_{alloch} leaving the lake
	Other equations	*description*
(2.4f)	$Q_{IN} = Q_{OUT} = lake\ volume/WRT$	daily inflowing (or outflowing) water volume [a]
(2.4g)	$mUVA = iUVA * \frac{(1-e^{(-Kd*z)})}{(Kd*z)}$	mean UV-A irradiance in the water-column [b]

[a] assuming that the lake level is unchanged and the precipitation equals evaporation on the lake, WRT is the lake water retention time

[b] where $iUVA$ is the incident UV-A irradiance just below the surface water (see Supporting Information S2.3), Kd is the UV-A light extinction coefficient and z is lakes mean depth

2.3.3 Stream and Lake Sampling

We have used data previously collected and published for other purposes in the context of the large-scale Industrial Research Chair in Carbon Biogeochemistry in Boreal Aquatic systems (CarBBAS) research program, as both input to the model, and to compare with model outputs. These data include ambient lake and stream CO_2 and DOC concentrations, lake respiration, and more importantly for this study, measurements of biological and photochemical degradation of both stream and lake DOC. We used detailed measurements made in a small and shallow boreal lake in the Chicoutimi region in the province of Québec, Canada (Lac Simoncouche; 48.23°N, 71.25°W) and its two inflowing streams (both having an upstream lake). Further information on the general lake characteristics is detailed in Vachon et del Giorgio (2014). We use additional measurements made in a set of 21 lakes and 7 streams in two different regions: 10 lakes and 4 small streams (Strahler order 1) from the Chicoutimi region (where Lac Simoncouche is located), sampled in 2011. The additional 11 lakes and 3 small streams (Strahler order 1) were sampled in 2010 around the Lac Duparquet Research and Teaching Forest (FERLD), which is located in the Abitibi region in western Québec (48.5°N, 79.4°W). All of these lakes were sampled once in July and the streams were sampled 2-3 times between May and October. The general characteristics of the lakes and streams are presented in Table 2.2, and further lake and watershed features, as well as sampling details and the full data sets can be found in (Campeau *et al.*, 2014; Lapierre et del Giorgio, 2014; Rasilo *et al.*, 2014). In brief, lake surface water pCO_2 (at 0.5 m depth) was measured by pumping water through a gas equilibrator (MiniModule), which was connected in a closed loop to a infra-red CO_2 gas analyzer (EGM-4, PP Systems, Amesbury, MA, USA) (Cole et Prairie, 2009). Lake underwater irradiance was measured using a UV-visible profiler (PUV-2545, Biospherical Instrument Inc., San Diego, USA) at five different wavelengths (313, 320, 340, 443, and 550 nm), and diffuse vertical attenuation coefficients ($K_{d,\lambda}$) were computed for each measured wavelength (λ) (Frenette *et al.*, 2006). Daily UV-A

irradiance (315-400nm; W m^{-2}) was modeled using the Tropospheric Ultraviolet Visible (TUV) model (Madronich et Flocke, 1997) for location and date of the simulation, corrected for cloud, water surface transmittance and cosine (Supporting Information S2.1). Water samples were collected near the surface (0.5 m) at the deepest part of lake or stream and was filtered in situ (0.45 µm) for subsequent DOC concentration and absorbance analyses. Additional unfiltered water was brought back to the lab in a cooler for further water chemistry analyses, pelagic respiration rates, and DOC degradation experiments (see details below). Lake pelagic respiration (R) was estimated from dark incubations of unfiltered water at near in situ temperature in the dark for 48h (Marchand *et al.*, 2009). Briefly, O_2 concentrations were measured every 4 hours using an optode system (Fibox 3, PreSens, Regensburg, Germany), and respiration rates were derived from the linear decreases of O_2 and converted to C unit assuming RQ of 1.2 (Berggren *et al.*, 2012). Total phosphorus (TP) was analyzed spectrophotometrically after persulfate digestion and chlorophyll *a* (chl*a*) concentration was estimated spectrophotometrically following filtration on Whatman (GF/F) filters and hot ethanol (90%) extraction. DOC concentration was measured on an OI-1010 TIC-TOC Analyzer (OI Analytical, College Station, TX, USA) using wet persulfate oxidation. The hydrologic load of Lac Simoncouche was estimated by a water mass balance approach and additional lake hydrologic loads were estimated from bathymetric data and lake discharge derived from digital elevation maps and mean runoff information. Further details are provided in the Supporting Information section (S2.2).

Table 2.2. General characteristic of studied lakes and streams

(mean ± standard deviation)

	Lac Simoncouche		Chicoutimi		Abitibi	
	Lake	Streams	Lake	Stream	Lake	Stream
n streams	1	2	10	4	11	3
n samples	11	18	10	10	12	8
WRT (days)	34	-	111	-	356	-
DOC (mg C L^{-1})	7.0 ± 0.7[a]	6.1 ± 1.1[a]	8.1 ± 2.2	10.7 ± 2.2	15.0 ± 3.1	16.9 ± 7.0
a_{440} (m^{-1})[b]	2.0 ± 0.5	2.0 ± 0.5	5.0 ± 4.7	9.2 ± 10.7	5.8 ± 5.1	6.6 ± 4.8
TP (µg L^{-1})	9.5 ± 2.5	15.2 ± 10.1	11.4 ± 4.3	21.8 ± 23.4	52.8 ± 42.3	23.3 ± 10.4
chla (µg L^{-1})	1.4 ± 0.9	0.8 ± 0.4	2.0 ± 0.6	1.4 ± 1.0	10.3 ± 9.2	0.9 ± 0.5

[a] DOC samples were taken weekly (or biweekly for streams)
[b] absorption coefficient at 440 nm

2.3.4 Determination of initial DOC_{alloch} reactivity (K_0), and ambient lake DOC reactivity (K_L)

We used measurements of DOC biological and photo-chemical reactivity that had been performed in small order streams to approximate the reactivity of terrestrially-derived DOC (DOC_{alloch}) entering lakes, based on dark and light incubations under controlled conditions. To quantify biological degradation, water was filtered (2.7 µm nominal pore-size GF/D Whatman filter) and incubated in 500 ml glass bottles (in replicate) at room temperature (21 ± 1°C) in the dark for 14-18 days. Bottles were sub-sampled every 1 or 2 days to measure DOC concentration. For each lake sample, we calculated the biological reactivity of DOC as the daily DOC loss divided by the initial DOC concentration (k_{bio}; d^{-1}). For stream DOC biological reactivity assessments, we clustered incubation data per region to build three regional reactivity models: 1) the Lac Simoncouche model includes June, July and August stream samples, 2) the Chicoutimi model includes 4 streams sampled in July, and 3) the Abitibi model includes 3 streams sampled in late May, July and November. We modeled stream biological reactivity using the reactivity concept as:

$$\frac{DOC_t}{DOC_0} = \left(\frac{\alpha}{\alpha+t}\right)^{\nu} \quad (2.5)$$

where DOC_t/DOC_0 is the DOC at time t (days) relative to initial concentration in the incubation, α is the average lifetime of the more reactive compounds and ν is the relative abundance of the most recalcitrant compounds (Boudreau et Ruddick, 1991; Koehler *et al.*, 2012; Vähätalo *et al.*, 2010). We added four long-term values (> 1 year) of DOC_t/DOC_0 derived from published studies (Hernes, 2003; Koehler *et al.*, 2012; Vähätalo *et al.*, 2010) (Figure 2.2), in order to extend the time scale of the modeled DOC degradation dynamics of DOC_{alloch}. The additional published time points were reasonably constrained (i.e. the proportion of DOC remaining after 1 year was always between 0.6 and 0.8) and were taken from similar systems (i.e. boreal and temperate

lakes and rivers). The implications of these data addition on our modeling results were accounted for by using the standard error of the fitted parameter (Table 2.3) in the Monte Carlo simulation described below. We estimated the reactivity of ambient lake DOC (K_L, d^{-1}) similarly to stream water reactivity, using dark incubations of lake DOC, except that K_L was estimated as the linear slope of DOC loss (mg C L^{-1} d^{-1}) over 16-18 days, divided by the initial DOC concentration in the incubation (mg C L^{-1}).

For photo-chemical DOC degradation experiments, the same filtered water as the biological experiment was exposed to artificial sunlight in a solar simulator (Q-sun Xe-1, Q-Lab; light intensity of 0.68W m^{-2} at 340 nm) in 40 ml borosilicate vials at controlled temperature (24°C). DOC concentration was measured after 12 and 24 hours of exposure, and DOC_t/DOC_0 was calculated. Cumulative UV-A energy exposure was calculated according to solar simulator irradiance, glass transmittance and incubation time, and is expressed as KJ m^{-2} (see Supporting Information S2.3 for further details on photo-chemical assessments). Photo-chemical DOC_{alloch} mineralization was modeled as a first order decay function of cumulative UV-A energy exposure as:

$$DOC_E/DOC_0 = e^{(-k_{photo}*E_{UVA})}, \quad (2.6)$$

where DOC_E/DOC_0 is the proportion of DOC mineralized, k_{photo} is the photo-chemical mineralization constant, and E_{UVA} is the cumulative UV-A energy exposure. All parameters estimations of stream biological and photo-chemical kinetic models were conducted using nonlinear model curve fitting (R Development Core Team, 2008), and are presented in Table 2.3. All parameters were statistically significant at $p < 0.05$.

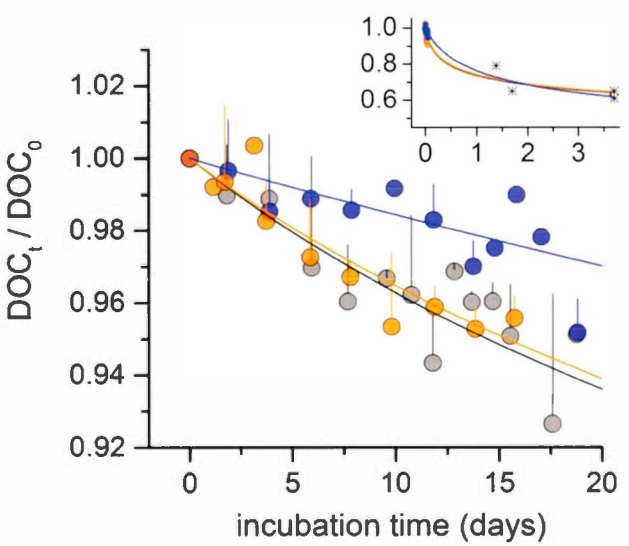

Figure 2.2. Time course of the relative DOC degradation to the initial concentration of stream water

Grey circles are combined data from Lac Simoncouche streams, blue are combined streams data from the Chicoutimi and orange circles are combined streams data Abitibi regions. Insert in panel shows longer term trend in the degradation models showing assumed proportions of remaining DOC (black stars) (see Methods section for further details). Note that the x-axis scale of the insert is in years instead of days. Data were binned by day only for visual purpose, all the fits were performed on unbinned data. All the fitted parameters and initial DOC concentrations are detailed in Table 2.2.

Table 2.3. Initial DOC concentrations and fitted parameters of the streams biological and photo-chemical incubations.

Region or lake	n streams	initial DOC	Biological degradation parameters			Photo-degradation k_{photo} (10^{-5})	
		mg C L^{-1} (mean ± SD)	α[a] (± SE)	v[b] (± SE)	r^2	m^2 KJ^{-1} (± SE)	r^2
Lac Simoncouche	2	6.3 (± 1.7)	24.3 (± 4.4)	0.11 (± 0.01)	0.91	1.69 (± 0.15)	0.74
Chicoutimi	4	8.2 (± 1.2)	115.5 (± 44.9)	0.19 (± 0.03)	0.96	5.70 (± 0.90)	0.52
Abitibi	5	11.1 (± 5.4)	25.9 (± 4.6)	0.11 (± 0.01)	0.96	3.04 (± 0.53)	0.50

[a]Average lifetime of the more reactive compounds (Boudreau et Ruddick, 1991).
[b]Relative preponderance of the more refractory compounds (Boudreau et Ruddick, 1991).

2.3.5 Model simulations

We ran the model under seven different scenarios: five different periods of the year in Lac Simoncouche (spring, summer, late summer with storms, fall and winter under ice), and two other scenarios representing mid-July conditions in a lake having average characteristics from the Chicoutimi and Abitibi regions. For Lac Simoncouche, DOC loads from the two incoming streams accounted for about 70% of the incoming water. For the remaining 30% (although variable among seasons (see Table S2.1 in the Supporting Information section for exact proportion per season), we used DOC_{alloch} concentration and initial reactivity (K_0) from the measured stream waters in Chicoutimi (Table 2.2 and Table 2.3). The environmental conditions used in the different scenarios are summarized in Supporting Information section S2.4. We assessed the potential error in the resulting rates by performing a Monte Carlo simulation (n=99), which accounted for variability in initial DOC concentrations (Table S2.1) and DOC degradability parameters (Table 2.3). We compared the modeled values at equilibrium of L-DOC_{alloch}, $\overline{K}_{alloch}$ and CO_2 production resulting from DOC_{alloch} mineralization with the ambient lake DOC concentration (L-DOC) and reactivity (K_L), surface water pelagic respiration (R) and surface water pCO_2 that had been measured in the set of study lakes.

2.4 RESULTS

2.4.1 Empirical estimates of allochthonous DOC loading and reactivity

In this approach, we assume that the DOC_{alloch} quantity and quality that we measured in small streams (Strahler order 0-1) represent the DOC_{alloch} that is loaded to boreal lakes in the different regions (Laudon *et al.*, 2011). The characteristics of the sampled streams are shown in Table 2.2. For the streams that discharge into Lac Simoncouche, monthly average DOC concentrations ranged from 5.3 mg C L^{-1} in May up to 7.0 mg C L^{-1} in August (when two major storm events occurred). Discharge from these two major stream into Lac Simoncouche accounted for about 70% of the lake total hydrologic load, thus we attributed the remaining 30% as lateral inputs (probably from surface runoff and groundwater). The DOC_{alloch} concentration and reactivity from this portion of the total hydrologic load was considered to be equivalent to the mean stream DOC concentration and reactivity from the Chicoutimi region (Tables 2.2 and 2.3). Integrated over the whole year, and including storm events and spring freshet, we estimate that the total external DOC_{alloch} load was 180.6 g C m^{-2} (lake) yr^{-1} in Lac Simoncouche. The average stream DOC concentration in Abitibi was higher than that in Chicoutimi streams and in the two streams flowing into Lac Simoncouche, yet due to the lower average runoff in Abitibi, the DOC_{alloch} load (39 g C m^{-2} (lake) yr^{-1}) was lower than in Chicoutimi (105 g C m^{-2} (lake) yr^{-1}). The biological reactivity of stream DOC_{alloch} (k_{bio}) had similar behaviour between the Abitibi and Lac Simoncouche streams, and both showed higher reactivity than the Chicoutimi streams DOC_{alloch} (Figure 2.2a). The photo-chemical reactivity of stream DOC_{alloch} (k_{photo}), on the other hand, was higher in the Chicoutimi streams than in the Lac Simoncouche and Abitibi streams (Figure 2.2b). The initial biological reactivity of stream DOC (K_0), computed as v/a, was on average 0.0045 d^{-1}, 0.0016 d^{-1}, and 0.0042 d^{-1} for streams around Lac Simoncouche, Chicoutimi and Abitibi, respectively (Table 2.2).

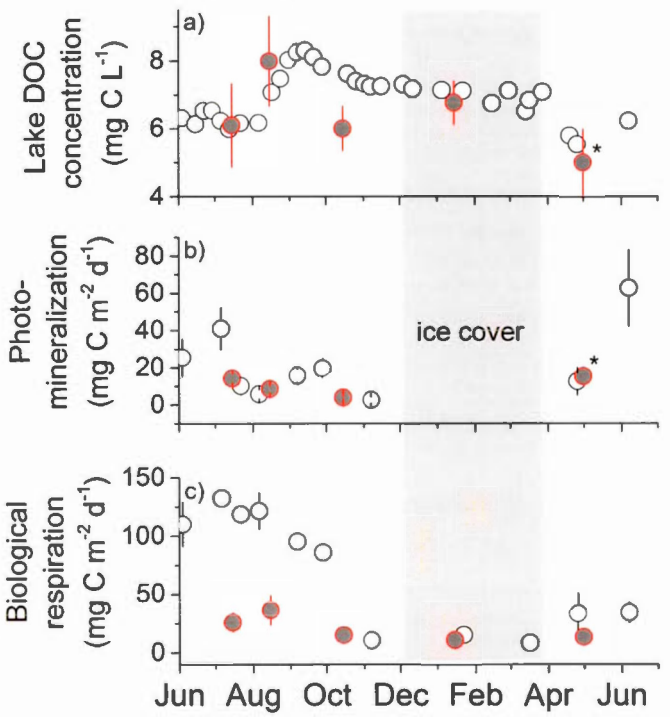

Figure 2.3. Results from the simulations in Lac Simoncouche

(**a**) DOC concentration, (**b**) DOC photo-mineralization and (**c**) water-column total respiration of measured in lake (open circle) and modeled from allochthonous DOC (grey dots) in Lac Simoncouche from June 2011 to July 2012. Asterisks refer to modifications made to the DOC inputs for the spring scenario (further details are provided in the discussion section).

2.4.2 Modeling in-lake DOC_{alloch} dynamics

Our mechanistic model allowed the incoming DOC_{alloch} to be degraded biologically and photo-chemically under realistic lake temperature and UV irradiance conditions, and to establish steady state mineralization rates as well as mean DOC_{alloch} concentrations within the lake water retention time. Table 2.4 shows the results of simulations under the seven different scenarios, in which modeled L-DOC_{alloch} concentrations range from 5 to 8 mg C L^{-1}, mean biological reactivity ($\bar{k}_{bio}$) ranges from 0.0011 to 0.0023 d^{-1}, and L-DOC_{alloch} biological and photo-chemical mineralization range from 0 to 36.6 mg C m^{-2} d^{-1} (Table 2.4). Figure 2.3a shows the resulting modeled equilibrium L-DOC_{alloch} concentrations from June 2011 to July 2012 in Lac Simoncouche, which closely matched the measured L-DOC concentrations. The modeled photo-chemical L-DOC_{alloch} mineralization rates, ranging from 3.9 in fall to 15.3 mg C m^{-2} d^{-1} in spring, also matched the estimated rates of whole-water column photo-mineralization estimated in this same lake (Chapter I; Figure 2.3b). Modeled biological L-DOC_{alloch} mineralization yielded higher rates than photo-chemical processing, ranging from 10.8 mg C m^{-2} d^{-1} in winter and up to 36.6 mg C m^{-2} d^{-1} in summer. Over an annual cycle, biological L-DOC_{alloch} mineralization was relatively constant and consistently lower compared to the measured total pelagic respiration in the lake (Figure 2.3c).

The simulations we carried out for the Abitibi and Chicoutimi lakes resulted in similar L-DOC_{alloch} concentrations and L-DOC_{alloch} mineralization rates (around 40 mg C m^{-2} d^{-1}). The relative contribution of biological and photo-chemical mineralization to total L-DOC_{alloch} degradation was, however, different between the two regions, and the biological L-DOC_{alloch} mineralization was on average more important in Abitibi lakes than in Chicoutimi lakes. Taking all simulations together (Simoncouche, Abitibi and Chicoutimi), the ratio between modeled biological L-DOC_{alloch} mineralization rates and measured water column respiration (R) ranged from 0.1 to 0.7, and was linked to the

measured chl*a* concentration in the surface water (Figure 2.4), such that the proportion of lake water column respiration explained by L-DOC_{alloch} mineralization was higher under low chl*a* situations.

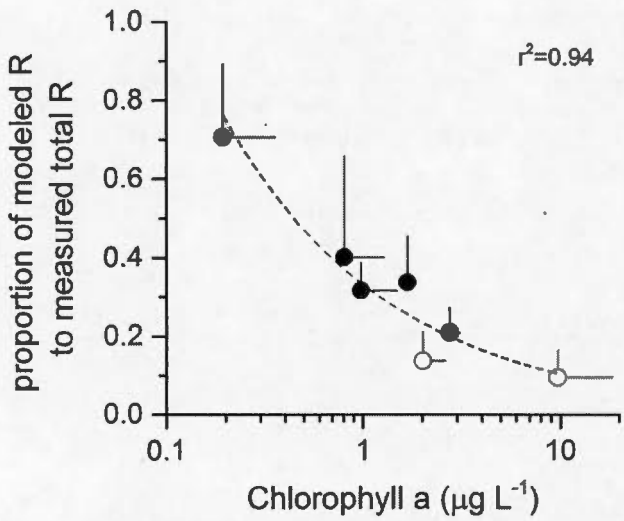

Figure 2.4. Relationship between the proportion of modeled in-lake degradation of allochthonous DOC (modeled R) to measured lake pelagic respiration (Lake R) and lake surface chlorophyll α concentration.

Black dots are from Lac Simoncouche and open circles are from the Chicoutimi and Abitibi regions. Grey dash line represent the log-normal regression line.

Table 2.4. Results from the simulation.

Modeled lake DOC_{alloch} concentration, mean biological degradability ($\bar{k}_{bio}$), DOC_{alloch} biological and photo-chemical mineralization rates at steady state from the simulation under 5 different scenarios

Region/Lake	WRT	Lake DOC_{alloch}	mean biological degradability $\bar{k}$	DOC_{alloch} bacterial respiration	DOC_{alloch} photo-mineralization
	(days)	(mg C L^{-1})	(d^{-1})	(mg C m^{-2} d^{-1})	(mg C m^{-2} d^{-1})
Simoncouche					
spring	14	5.0 ± 1.0	0.0023	13.4 ± 5.1	15.3 ± 4.7
summer	63	6.1 ± 1.2	0.0017	26.3 ± 7.9	13.9 ± 2.7
summer (storm)	20	8.0 ± 1.3	0.0021	36.6 ± 12.3	8.9 ± 1.9
fall	58	6.0 ± 0.6	0.0018	15.3 ± 2.8	3.9 ± 0.6
winter	64	6.8 ± 0.6	0.0016	10.8 ± 6.8	0 ± 0
Chicoutimi	111	7.6 ± 1.5	0.0011	25.4 ± 10.9	13.3 ± 3.3
Abitibi	356	7.6 ± 2.9	0.0011	31.9 ± 13.3	9.9 ± 3.8

2.4.3 Role of water residence time

The resulting L-DOC_{alloch} concentration at the model equilibrium consisted in a distribution of cohorts of different ages, which in turn determines the mean biological reactivity of the residual DOC_{alloch} that persists in the lake ($\bar{k}_{bio}$). Figure 2.5a shows that the modeled $\bar{k}_{bio}$ declines as a function of WRT under fixed environmental conditions and K_0, in both Chicoutimi and Abitibi lakes. For comparative purposes, Figure 2.5a also shows the measured K_L in these lakes. K_L was generally higher than the modeled $\bar{k}_{bio}$, although the former also tended to decline with WRT.

The potential pCO_2 oversaturation baseline driven by the mineralization of L-DOC_{alloch} integrates DOC_{alloch} loading, its reactivity and the air-water gas exchanges, all within the context of lake water retention time. In July and August in Lac Simoncouche, the combined biological and photo-chemical DOC_{alloch} mineralization had the potential to elevate the lake surface water pCO_2 by approximately 440 µatm, once air/water gas exchange is factored in using a wind-based gas exchange coefficient coupled to lake size gas exchange model (Vachon et Prairie, 2013), and monthly averaged wind speeds. The surface water pCO_2 in Chicoutimi and Abitibi lakes driven by the mineralization of L-DOC_{alloch} could potentially average 550-570 µatm assuming a reasonable gas exchange coefficient of 0.5 m d^{-1}. However, this value was not fixed but decreases with lake WRT. In short WRT lakes, the mineralization of L-DOC_{alloch} could potentially sustain a pCO_2 oversaturation baseline of over 1000 µatm in Abitibi lakes and around 600 µatm in Chicoutimi lakes. Increasing WRT and gas exchanges coefficient decrease the potential pCO_2 from L-DOC_{alloch} mineralization, whereas increasing the incoming DOC_{alloch} initial reactivity and loading would increase potential pCO_2. Figure 2.5b also shows the measured pCO_2 in these lakes, which generally exceeded the modeled pCO_2 oversaturation baseline, but which like to the modeled baseline, also tended to decrease with increasing WRT.

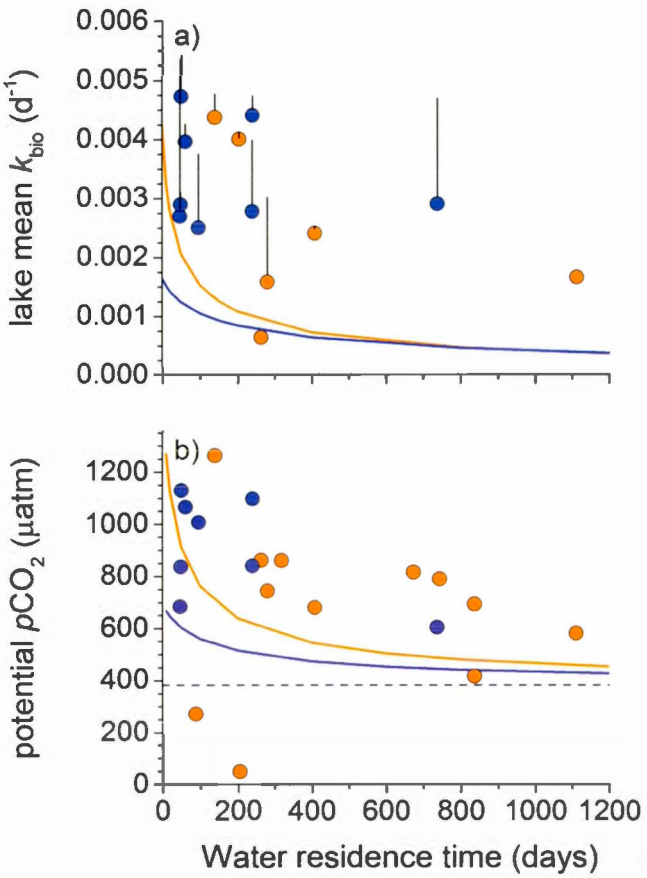

Figure 2.5. Relationships between WRT and mean *k* and pCO_2

Panel (**a**) shows the lake WRT and biological mean decay rate ($\bar{k}$) in Chicoutimi (blue) and Abitibi (orange). Solid lines represent the numerical approximations of the resulting mean degradability (Equation 2.3) from initial reactivity in Chicoutimi (blue line) and Abitibi (orange line). Color dots are short-term (14 days) degradability measurements from lake water. Panel (**b**) is the relationship between lake WRT and lake surface water pCO_2 potentially emerging from the mineralization (bio + photo) of DOC_{alloch} in the lake (solid lines) and measured (color dots).

2.5 DISCUSSION

2.5.1 Mineralization dynamics of L-DOC_{alloch}

The simple mechanistic model that we developed, combined with realistic, empirically determined estimates of stream DOC quantity and quality, was able to effectively reconstruct the concentrations and reactivity of DOC not only in Lac Simoncouche (Figure 2.3a), but also in a broader set of Chicoutimi lakes, where modeled L-DOC_{alloch} accounted for about 95% of the measured L-DOC pool. The close agreement between modeled L-DOC_{alloch} and measured ambient L-DOC concentrations suggests that in most Chicoutimi lakes (including Lac Simoncouche), the bulk DOC is derived from allochthonous sources, presumably of terrestrial origin. These results are in agreement with DOC isotopic evidence (P.A. del Giorgio, pers. comm.) and from other studies in similar systems (Wilkinson *et al.*, 2013) that the bulk of DOC in these northern lakes is of terrestrial origin. In the Abitibi lakes however, the measured L-DOC (averaging 15.0 mg C L^{-1}) was much greater on average than the modeled lake L-DOC_{alloch} (7.6 mg C L^{-1}), suggesting a greater contribution of internal DOC_{autoch} production, most likely a combination of from phytoplankton, periphyton and macrophyte sources. This increased importance of autochthonous DOC sources is coherent with the fact that these Abitibi lakes are on average much more productive than the lakes elsewhere (average TP of 52 and 11 μg L^{-1}, respectively), and also shallower, allowing for increased macrophyte development.

The combination of DOC_{alloch} load, its reactivity and the environmental conditions (irradiance and water temperature) resulted in variable rates of L-DOC_{alloch} photo-chemical and biological mineralization within the modeled lakes. The modeled photo-chemical L-DOC_{alloch} mineralization rates were similar to rates we independently estimated for the water column of Lac Simoncouche (Chapter I), and comparable to those reported for Swedish lakes (Koehler *et al.*, 2014), suggesting that our simple

model of photo-chemical mineralization of L-DOC_{alloch} captured reasonably well water column L-DOC photo-mineralization (Figure 2.3b). The modeled residual biological reactivity of L-DOC_{alloch} (K_L) is comparable to reported rates of ambient lake DOC lability based on completely different approaches, including in vitro incubations and modeling. Standardized to 20°C, our modeled L-DOC_{alloch} biological mineralization rates ranged from 8.3 to 16.4 mg C m^{-3} d^{-1}, which are within the range of reported rates by Jansson *et al.*, (2008) in sub-arctic lakes and Hanson *et al.*, (2014a) in temperate lakes, and in the lower range of values reported by McCalister et del Giorgio (2008) in a set of temperate lakes and Karlsson *et al.*, (2007) in a set of boreal lakes. On the other hand, the modeled rates of DOC_{alloch} biological mineralization were systematically lower than the measured water column respiration in these lakes, especially in summer (Figure 2.3), suggesting that a significant portion of the measured water column respiration (R) was driven by autochthonous DOC sources. Interestingly, we found that regardless of the season or lake, the ratio of modeled DOC_{alloch} biological mineralization to measured R was a function of chl*a* concentrations (Figure 2.4). This suggests a declining contribution of DOC_{alloch} mineralization to lake total respiration with increasing chlorophyll, (and therefore ecosystem primary production), as has been previously shown (Cole *et al.*, 2000; McCallister et del Giorgio, 2008). During less productive seasons (fall and winter), however, modeled DOC_{alloch} biological mineralization closely matched the lake R measurements (Figure 2.3c). This observation also agrees with Karlsson *et al.*, (2007) for unproductive boreal and sub-arctic lakes, where most of the bacterial respiration was supported by DOC_{alloch}. The overall agreement between the measured (or published) values of pelagic respiration and reactivity of ambient DOC, and our modeled L-DOC_{alloch} concentration and residual reactivity suggests that our combination of mechanistic model and realistic initial conditions captures the essence of the L-DOC_{alloch} dynamics in this set of boreal lakes.

2.5.2 Patterns in lake DOC_{alloch} reactivity

Applying the RCC to modeling biological mineralization of DOC_{alloch} in lakes explicitly introduced a time component reflected in the water residence time. In Lac Simoncouche, for example, the modeled $\bar{k}_{bio}$ showed a remarkable temporal variability, being significantly higher during high flow (spring and summer during the storm events), even if the initial DOC reactivity in streams (k_0) was set constant (Table 2.4). The modeled $\bar{k}_{bio}$ was similar for Chicoutimi and Abitibi lakes (0.0011 d^{-1}, Table 2.4), in spite of major differences in both lake and watershed properties, probably resulting from the interplay between the initial reactivity K_0 (higher in Abitibi) combined with WRT (shorter in Chicoutimi). For similar K_0 of the incoming DOC_{alloch}, lakes with longer residence time will have relatively less biologically labile DOC_{alloch} remaining in the bulk DOC pool. An important implication is that the observed DOC reactivity in a lake (K_L) can vary substantially simply as a function of its residence time, even if the nature of the DOC_{alloch} entering these lakes is identical.

The interplay between the reactivity of the DOC_{alloch} entering a lake and WRT that results in variable $\bar{k}_{bio}$ can be examined from a more theoretical perspective. Although Eq. 2.3 cannot be integrated readily, its behaviour can nevertheless be fully examined through the following approximation (exact within 1%, see Supporting Information S2.5 for derivation):

$$\bar{k}_{\mathrm{bio}} = \frac{0.85\,v}{\tau_w}\, ln\left[1 + \frac{\tau_w}{\alpha}\right] \tag{2.7}$$

showing that, for a given ν and α, $\bar{k}_{\mathrm{bio}}$ generally declines with WRT but that the rate of this declines is modulated by the reactivity continuum parameter α. The effect of WRT is stronger in areas where DOC_{alloch} is intrinsically more reactive. Figure 2.5a shows this relationship between WRT and $\bar{k}_{bio}$ (solid lines), adapted to the different initial DOC_{alloch} reactivities of the two regions. In lakes with short WRT, $\bar{k}_{bio}$ is

naturally closer to its initial reactivity (K_0) than in lakes with long WRT lakes. At shorter WRT (< 6 months), the nature of the initial DOC_{alloch} reactivity plays a key role in determining the lake's steady state DOC_{alloch} reactivity, whereas $\bar{k}_{bio}$ tends to converge at longer WRT regardless of the initial reactivity. This influence of WRT on $\bar{k}_{bio}$ thus implies that a wide range in ambient residual DOC_{alloch} reactivity (i.e. K_L) can be generated on the basis of the same initial DOC_{alloch} reactivity (k_0) simply as a function of shifting water residence time across lakes.

The modeled $\bar{k}_{bio}$ only represents the allochthonous portion of bulk DOC in lakes, and perhaps not surprisingly, the measured biological degradability of bulk DOC (K_L) was on average higher than the modeled predictions (Figure 2.5a). The measured K_L integrates both autochthonous and allochthonous DOC, and because the algal-derived DOC tends to be degraded more quickly compared to terrestrially derived DOC (Guillemette *et al.*, 2013), only a small addition of algal material would greatly increase the overall L-DOC reactivity. Nonetheless, the influence of hydrology on the K_L is still noticeable, and this may suggest that it is the allochthonous portion of K_L that may drive this pattern, and that the reactivity of the autochthonous DOC pool may be largely decoupled from the hydrologic regime. This does not mean, however, that the dynamics of autochthonous DOC mineralization does not conform to a RCC. DOC_{autoch} in the lake also develops an age distribution and a residual degradability (Guillemette *et al.*, 2013), but unlike DOC_{alloch}, the input of DOC_{autoch} is modulated by primary production rather than by the hydrologic regime. This adds another layer of complexity to modeling the dynamics of lake DOC that is however outside the scope of this study.

2.5.3 Lake pCO_2 oversaturation baseline

A critical implication of DOC_{alloch} mineralization within lakes is the potential for CO_2 production, which would sustain a persistent baseline of pCO_2 oversaturation. In Lac Simoncouche, the potential pCO_2 in surface waters derived from DOC_{alloch}

mineralization could explain about one third of the observed pCO_2 oversaturation in that lake (Vachon et del Giorgio, 2014). Similarly, the pCO_2 potentially generated by allochthonous DOC mineralization could explain up to about 30% of the observed average pCO_2 oversaturation in Chicoutimi lakes, and up to 40% of the observed average pCO_2 oversaturation in Abitibi lakes, at the lowest reasonable gas exchange coefficient (k_{CO2} = 0.5 m d^{-1}). These results are consistent with McCallister et del Giorgio (2008), who concluded that bacterial respiration of DOC_{alloch} could potentially account for up to 60% of CO_2 effluxes from similar lakes. Modeled pCO_2 oversaturation in our study lakes were systematically lower than the observed surface water pCO_2 in these systems, and this is to be expected, since it has been well established that a variable but significant portion of pCO_2 oversaturation in boreal lakes is also sustained by direct CO_2 input from the catchment (Vachon et del Giorgio, 2014) and from the sediment organic matter mineralization (Gudasz *et al.*, 2010; Kortelainen *et al.*, 2006).

Regardless of other underlying processes adding or removing CO_2 in surfaces of lakes, DOC_{alloch} mineralization in lakes will systematically produce CO_2. This pCO_2 oversaturation baseline will vary as a function of atmospheric gas exchange coefficient but also likely as a function of the hydrological regime (Figure 2.5b). In short WRT lakes, the higher mean DOC_{alloch} reactivity (i.e. $\bar{k}_{bio}$) yields a greater potential for CO_2 production and therefore higher potential pCO_2 (Figure 2.5b). This potential pCO_2 greatly decreases in longer WRT lakes. While this particular pattern can be partially derived from an allometric relationship that exists between lake size and gas exchange coefficient (Read *et al.*, 2012; Vachon et Prairie, 2013), it also suggests that DOC_{alloch} mineralization may be embedded in these lake pCO_2 patterns. Furthermore, even though DOC_{alloch} mineralization in longer WRT lakes is expected to be minimal, it will nevertheless maintain a baseline metabolism that generates CO_2, and this could partly explain the systematic pCO_2 oversaturation that has been observed even in the largest and deepest lakes (Lapierre et del Giorgio, 2012).

2.5.4 DOC_{alloch} mineralization in lakes: a landscape perspective

Whereas our modeling focused on processes at the lake scale, our results have implications at the landscape (or regional) scale. The biogeochemical role of lakes in a landscape depends to a large extent on the fate of DOC_{alloch}, in terms of whether it is mineralized and emitted, buried in sediments or exported to downstream systems. The proportion of the inflowing DOC_{alloch} that is either mineralized or buried in the sediments (pR) can be estimated using a mass balance approach as $p\mathrm{R} = (DOC_{in}-DOC_{out})/DOC_{in}$ (Dillon et Molot, 1997). It is thus the combination of DOC_{alloch} reactivity and the hydrologic residence time that determines the fate of DOC_{alloch} in lakes. By re-arranging the lake DOC_{alloch} mass balance equation (Eq 2.5a) at equilibrium, pR can also be expressed as:

$$p\mathrm{R} = \frac{WRT \times k_{alloch}}{1+WRT \times k_{alloch}}, \tag{2.8}$$

where k_{alloch} is the total DOC_{alloch} loss rate in the lake by biological and photo-chemical mineralization (here also including flocculation). Our estimated pR fit well with the general relationship between WRT and pR reported by Algesten *et al.*, (2004) for Swedish lakes, and by Dillon et Molot (1997) in Canadian boreal lakes (Figure 2.6). Figure 2.6 also shows the theoretical relationships between pR and WRT derived from Equation 8 assuming fixed k_{alloch} values of 0.005 and 0.0005 d^{-1}. Overlaying these theoretical trends to actual lake pR values (our data combined with values derived for the Swedish lakes and other Canadian lakes) shows that at low WRT, pR values seem to converge to the 0.005 d^{-1} line, while longer WRT values tend to converge more to the 0.0005 d^{-1} line (Figure 2.6). This suggests that a k_{alloch} of 0.0005 d^{-1} likely underestimates pR in short WRT lakes, and that a k_{alloch} of 0.005 d^{-1} overestimate pR in long WRT lakes, in agreement with the reactivity continuum concept. By implementing the reactivity continuum WRT solution formulated in Eq. 2.7 into Eq. 2.8, we can further fit a predictive curve on the pR values using a and v parameters

from the reactivity continuum (red line in Figure 2.6). This resulted in a much better fit ($r^2 = 0.80$) than using a best-fit fixed k_{alloch} value (0.00144 ± 0.00015 d^{-1}), black solid line in Figure 2.6, $r^2 = 0.54$). Instead, our modeling approach yielded reactivity continuum parameters a and v of 108.8 ± 49.1 ($p = 0.03$) and 0.62 ± 0.13 ($p < 0.001$), respectively. Interestingly, the fitted parameters allow us to estimate an initial reactivity (k_0) of the DOC_{alloch} that integrates the Canadian and Swedish lakes, which is in the order of 0.0057 d^{-1}. Although we acknowledge that boreal soil DOC reactivity should vary as a function of vegetation type and molecular composition (Marschner et Kalbitz, 2003; Wickland *et al.*, 2007), this fitting exercise also potentially suggest that the reactivity of soil-derived DOC entering boreal lakes may be relatively homogenous compared to the wide range of biological lability of DOC that has been observed across northern lakes. In this regard, there are recent reports that litter lability is relatively less variable in boreal forest and temperate coniferous forest compared to other biomes (Koehler et Tranvik, 2015).

The differences in apparent lake DOC reactivity (i.e. K_L) and in the resulting pCO_2 that we observe across lakes may be can be largely explained the basis of the RCC, and thus be a reflection of the particular spectrum of residence times that characterize different aquatic networks (Weyhenmeyer *et al.*, 2012). In this regards, our results further suggest that this DOC_{alloch}-derived lake pCO_2 baseline could potentially vary at a landscape scale as well, as a function of average regional lake morphometry, hydrology and soil watershed properties. These are hypotheses that have major consequences on our understanding of terrestrial DOC processing in the aquatic systems, and that should thus be explicitly tested in the future. Nevertheless, the use of the RCC in modeling DOC_{alloch} dynamics over a whole landscape is a powerful tool to understand the fate of terrestrially-derived DOC within northern aquatic networks.

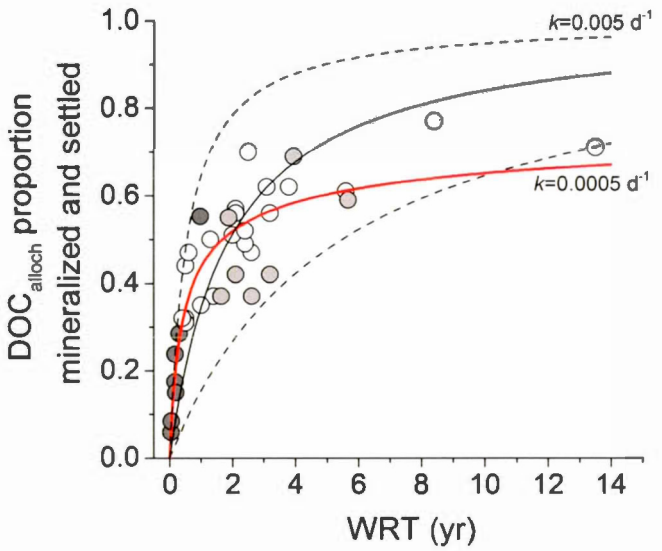

Figure 2.6. Daily propotion of DOC_{alloch} mineralized and settled (pR) in function of lake water residence time (in years).

Dark grey circles is resulting pR derived from our seven simulations (Table 2.4), light grey circles are pR data from Canadian boreal lakes (Dillon et Molot, 1997) and white circles are pR data from Swedish lakes (Algesten *et al.*, 2003). Dashed lines are theoritical trend assuming fixed decay rates (0.005 and 0.0005 d^{-1}). Black solid line is the best fit using a fixed decay constant (k_{alloch} = 0.0014 ± 0.0001 d^{-1} $p < 0.001$, r^2 = 0.54) and red solid line is the best fit using variable k_{alloch} according to the reactivity continuum concept as a function of WRT derived from Eqs 2.3 and 2.7 (a = 108.8 ± 49.1, p = 0.03, v = 0.62 ± 0.13, $p < 0.001$, r^2 = 0.80). Note that the fitted k_{alloch} is intergrating photo- and biological mineralization and flocculation.

2.6 CONCLUSIONS

Evaluating DOC_{alloch} mineralization in lakes necessarily implies the integration of several processes including physical factors such as hydrological regimes in combination with the complexity of intrinsic DOC_{alloch} composition and reactivity in the environment. Our mechanistic model allowed us to constrain the magnitude of DOC_{alloch} mineralization in boreal lakes, but more importantly to evaluate the influence of residence time on the residual reactivity of this within the lake and its potential to sustain a pCO_2 oversaturation baseline in lakes. The implementation of a RCC on the dynamics of DOC_{alloch} degradation at the lake scale yielded insight into the mechanisms determining the fate of incoming DOC_{alloch} to boreal lakes, and the evolution of its mean reactivity within the constraints of the lake water residence time. This insight is particularly important in the context of major current environmental changes, that include not only shifts in hydrology, but also a decadal trend of increasing DOC concentration and color across northern lakes (Roulet et Moore, 2006). It has been hypothesized that this "browning" trend is also accompanied with increases in the reactivity of this C as it enters aquatic networks (Lapierre *et al.*, 2013). Our results suggest that these co-occurring shifts in hydrology, DOC loading and DOC reactivity may have major consequences on the dynamics of DOC_{alloch} mineralization and its resulting fate in boreal lakes, particularly in terms of regional aquatic CO_2 emissions.

2.7 ACKNOWLEDGEMENTS

We would like to thank Annick St-Pierre, Alice Parkes, Audrey Campeau, Mathieu Dumais and Jean-Philippe Desindes for field and laboratory assistance. We also thank Christopher Solomon and Jean-François Lapierre for helpful advices and discussions as well as HSC for continuous unwavering guidance. This project was part of the large-scale research program of the Industrial Research Chair in Carbon Biogeochemistry in Boreal Aquatic Systems (CarBBAS), co-funded by the Natural Sciences and Engineering Research Council of Canada (NSERC) and Hydro-Québec to PDG. NSERC doctoral scholarship and UQAM-FARE scholarship was also attributed to DV.

2.8 SUPPORTING INFORMATION

2.8.1 Determination of the UV-A energy cumulative exposure

For each sample, the UV-A energy (E_{UVA}) cumulative exposure was evaluated by the following equation:

(S2.1) $$E_{UVA} = t \times \int_{\lambda=315}^{\lambda=400} E_{0\lambda} \times (glass\ trans)_{\lambda} ,$$

where E_{UVA} is the total UV-A energy exposed to DOC in the vial (KJ m^{-2}), t is the exposure time (s), $E_{0\lambda}$ is the wavelength-specific energy emitted by the lamp (W m^{-2}), Figure S2.1). $(Glass\ trans)_{\lambda}$ is the wavelength specific fraction of light that reached the water sample (Figure S2.1).

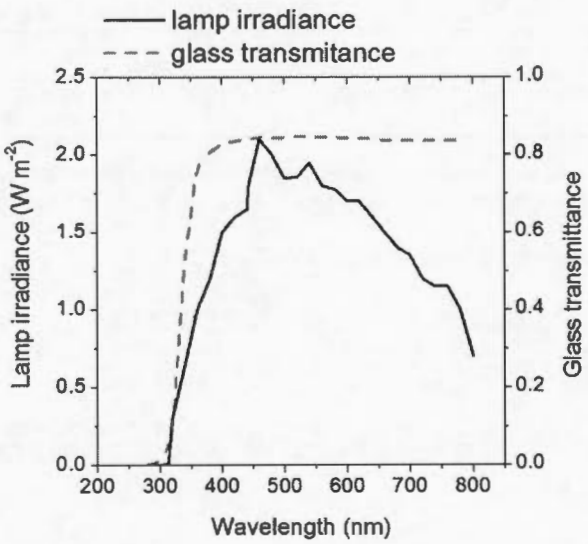

Figure S2.1. Incubation lamp irradiance and incubation tube glass transmittance spectra used in the calculation of energy absorbed by the sample.

2.8.2 Determination of underwater UV-A irradiance

We used modeled direct and diffuse surface downwelling irradiance from the Tropospheric Ultraviolet Visible (TUV) model (Madronich et Flocke, 1997) for each sampling date and location, under clear sky conditions and total ozone content retrieved from OMI-AURA (OMI Science Team, 2012). To convert to daily-integrated just-below-surface downwelling scalar irradiance (*iUVA* ; Eq. 2.6b, Table 2.3), global (direct + diffuse) irradiance from TUV model was corrected for cloud, transmittance at the surface of lake and converted to scalar irradiance by the average underwater cosine following each steps detailed in (Fichot et Miller, 2010). All steps are also described in detail in Chapter I of this thesis. Briefly, cloud radiative fraction for each sampling day and location was retrieved from OMI-AURA (OMI Science Team, 2012) and the correction was based on empirical model from in situ observation of surface irradiance (see Chapter I). The surface water transmittance correction was calculated from Fresnel's law for direct and a fixed value for diffuse (Fichot et Miller, 2010). Further correction for underwater cosine was also calculated following Fichot et Miller (2010).

2.8.3 Solution for integrating Equation 2.3 of the main text

The governing equation integrating the reactivity continuum with the distribution of ages (Eq. 2.3 in the text) has for exact solution:

(S2.2) $$\bar{k} = \int_0^{\infty} \left[\frac{v}{\alpha+t}\right] \frac{e^{-t/\tau_w}}{\tau_w} dt = \frac{Ei\left[\frac{\alpha}{\tau_w}\right]}{\tau_w} e^{\frac{t}{\tau_w}},$$

where *Ei*[ ] stands for the exponential integral, α and ν are the reactivity continuum parameter and τ_w is the lake WRT. Although *Ei*[ ] does not have a general solution, it is bracketed by the following bounds (Abramowitz et Stegun, 1964):

(S2.3) $$\frac{1}{2} e^{-x} ln\left[1+\frac{2}{x}\right] < Ei(x) < e^{-x} ln\left[1+\frac{1}{x}\right].$$

Applying this inequality to Eq. S2.2 yields the following bounds on $\bar{k}$ observed in a lake with a particular WRT (τ_w):

(S2.4) $$\frac{\upsilon}{2\,\tau_w} ln\left[1+\frac{2\,\tau_w}{\alpha}\right] < \bar{k} < \frac{\upsilon}{\tau_w}\, ln\left[1+\frac{\tau_w}{\alpha}\right].$$

Evaluation of these bounds with numerically integrated solutions shows that for our likely values of α, ν, τ_w, $\bar{k}$ is directly proportional to the upper bound (not the case for the lower bound) with an $r^2 > 0.999$ and a proportionality coefficient of 0.85. Thus we arrive at a direct solution for $\bar{k}$ as:

(S2.5) $$\bar{k} = \frac{0.85\,\upsilon}{\tau_w}\, ln\left[1+\frac{\tau_w}{\alpha}\right].$$

. Table S2.1. Input parameters for the different DOCalloch simulations.

Region/Lake	date	sWRR	gWRR	WRT	T	Kd	Z	iUVA	DOCin
Chicoutimi	2010-07-15			110.9	20.3	35.6	3 ± 1.7	1090	10.7 ± 2.1
Abitibi	2011-07-15			355.8	22	30.5	3.5 ± 1.6	1315	16.9 ± 7.0
Simoncouche									
spring	2012-05-01	0.034	0.038		6.5	16.7	2.16	1341	5.3 ± 0.3
summer	2011-07-15	0.011	0.005		23	15.5	2.16	1090	6.8 ± 2.3
summer (storm)	2011-08-15	0.026	0.023		20.5	23.5	2.16	650	7.0 ± 1.7
fall	2011-10-15	0.013	0.003		10.65	21.8	2.16	509	6.5 ± 0.8
winter	2012-01-15	0.01	0.005		3		2.16	0	6.6 ± 0.4

sWRR is the surface water renewal rate, gWRR is the groundwater (lateral) renewal rate, WRT is the lake water retention time (days), T is the mean water temperature (°C), Kd is the UV-A light extinction coefficient (m), z is the lake regional mean (± standard deviation) depth (m), iUVA is the daily incident UV-A irradiance (KJ m^{-2} d^{-1}), DOCin is the mean (± standard deviation) DOC concentration of stream (mg C L^{-1}).

CHAPITRE III

WHOLE-LAKE CO_2 DYNAMICS IN RESPONSE TO STORM EVENTS IN TWO MORPHOLOGICALLY DIFFERENT LAKES

Dominic Vachon and Paul A. del Giorgio

Groupe de Recherche Interuniversitaire en Limnologie (GRIL), Université du Québec à Montréal, Département des Sciences Biologique, C.P. 8888, Succ. Centre-Ville, Montréal, Canada, H3P 3P8.

Published in *Ecosystems* (2014) 17:1338-1353

Authors contributions: Both authors designed the study and wrote the paper. DV performed research and analyzed data.

N.B. References cited in this chapter are presented at the end of the thesis

3.1 ABSTRACT

In lentic systems, hydrology can be dramatically altered after storm events, potentially modifying the carbon budget. In particular, rapid increases in the surface water carbon dioxide partial pressure (pCO_2) have been observed following such events. Several processes may explain these shifts in lake CO_2 dynamics, including vertical mixing, increases in metabolism, and increases in external loading. To evaluate the relative importance of these various processes, we reconstructed the whole-lake daily CO_2 budget by using concurrent estimates of lake metabolism and daily CO_2 mass balance budgets in two lakes with distinct morphometries located in Québec, Canada. We found that storm events caused variable, but significant, changes in whole-lake CO_2 mass. Such events influenced CO_2 dynamics indirectly by inducing shifts in lake metabolism, and directly by importing CO_2 by the inflowing storm waters. Storm intensity (in terms of total amount of precipitation) influences the balance between these two processes, but the final outcome depends on lake morphometry. Our results suggest that when storms are intense enough to drive lake water renewal rate beyond 1% d^{-1}, external CO_2 loadings became the dominant process, overwhelming internal CO_2 production. Lakes with slower hydrological turnover, however, are more susceptible to internal regulation and may simply re-allocate CO_2 from the hypolimnion to the epilimnion following a storm event. Our results further suggest that this tightening of the watershed-lake-atmosphere linkage by climatic events is strongly modulated by lake morphometry. These features should be considered when predicting the impact of future climate change on regional C budgets and emissions.

3.2 INTRODUCTION

The processing of carbon during its transit in inland waters toward the ocean results in substantial carbon emissions to the atmosphere (Cole *et al.*, 2007). The transport of carbon through hydrologic networks includes the passage through multiple lentic ecosystems, where longer water residence time facilitates processing (Algesten *et al.*, 2003; Tranvik *et al.*, 2009). As a result, lakes are generally super-saturated in carbon dioxide (pCO_2) relative to the atmosphere (Cole *et al.*, 1994). The influence of terrestrial environments is undeniable, supplying organic matter for in-lake bacterial degradation (Karlsson *et al.*, 2007; McCallister et del Giorgio, 2008), and by directly exporting CO_2 from soils (Humborg *et al.*, 2010; Maberly *et al.*, 2012). However, the circumstances under which this terrestrial-aquatic linkage determines the role of lakes as reactors for the processing of terrestrial C or conduits of CO_2 are not well defined. This complex linkage is crucial to our understanding of lake CO_2 dynamics, and to our capacity to predict lake carbon fluxes in the context of environmental and climate change (Battin *et al.*, 2009).

The hydrological link between watershed and lake is mediated by surface runoff, which is itself strongly associated to regional precipitation. Annual precipitation patterns have been positively linked to average open-water pCO_2 in boreal lakes (Kelly *et al.*, 2001; Rantakari et Kortelainen, 2005; Roehm *et al.*, 2009). This relationship suggests that movement of various types of carbon from catchments to lakes is enhanced during wetter years (Einola *et al.*, 2011), and especially after storm events (Jones *et al.*, 2009) or intense rain (Ojala *et al.*, 2011), yet the underlying processes are not well understood. Terrestrial carbon export to lakes may be greatly enhanced by precipitation events (Dhillon et Inamdar, 2013; Raymond et Saiers, 2010), and these increased inputs of fresh organic material during stormflow (Buffam *et al.*, 2008; Wilson *et al.*, 2013) may be rapidly degraded within lakes, pushing the ecosystem metabolic balance further into heterotrophy (Klug *et al.*, 2012; Sadro et Melack, 2012; Tsai *et al.*, 2008). Additionally,

hydrological CO_2 inputs may also be important contributors to lake pCO_2 and emissions (Humborg *et al.*, 2010; McDonald *et al.*, 2013; Striegl et Michmerhuizen, 1998), although their linkage to precipitation patterns or storm events is less documented.

Storm events also impact the lake physical structure, which may also influence CO_2 dynamics. When thermal stratification is strong and well established in summer, CO_2 can accumulate in hypolimnia (Houser *et al.*, 2003). Strong winds associated with storm events weaken or disrupt stratification (Jennings *et al.*, 2012; Klug *et al.*, 2012), resulting in the vertical re-allocation of CO_2 from hypolimnion to epilimnion (Åberg *et al.*, 2010), similar to fall mixing events (Kelly *et al.*, 2001; López Bellido *et al.*, 2009; Riera *et al.*, 1999). This event-driven re-allocation of CO_2 may result in increased surface pCO_2 and atmospheric CO_2 fluxes, but contrary to shifts in lake CO_2 driven by external C loading, it does not represent a change in the whole-lake CO_2 mass balance.

Event-driven peaks in terrestrial organic and inorganic C loadings, and event-induced C re-allocation probably all co-occur and contribute to the observed shifts in lake CO_2 fluxes. The relative importance of these processes, and how they vary with lake type and with the nature of the events, is still not well understood. Finer scale studies are thus needed to quantify the impact of storm events on lake CO_2 fluxes, and to understand the underlying processes. This is particularly important in the current context where storm tracks are shifting toward poles (Yin, 2005) and the precipitation intensity is predicted to increase in the next decades, especially in the northern regions (Meehl *et al.*, 2005). In this study, we explore how storm events affect the whole-lake CO_2 mass balance and resulting CO_2 fluxes, and what processes underlie the changes in whole-lake CO_2 mass following those storm events. We additionally explore how lake and watershed morphometries, and storm intensity, influence the contribution of in-lake processes versus external inputs on whole-lake CO_2 dynamics. We focused on three possible pathways leading to increased surface pCO_2 following such

perturbations: (1) CO_2 re-allocation from deep waters during destratification, (2) enhanced organic matter loading and in situ mineralization, and (3) enhanced direct CO_2 loadings from the catchment. In order to differentiate these three pathways, we determined the whole-lake CO_2 mass balance as well as CO_2 fluxes, all on a daily basis during the summer/fall period, using a combination of high-frequency measurements and point sampling. We carried out this study in two lakes with distinct morphometries, in order to explore the influence of lake morphometry in modulating the impact of storm events on lakes CO_2 dynamics, and on the pathways involved.

3.3 METHODS

3.3.1 Study sites and data collection

Both study lakes are situated on the Canadian Shield in the southern Québec, Canada. The general characteristics of the lakes are presented in Table 3.1. Lac Croche (hereafter referred to as the deep lake) is a headwater lake surrounded by a pristine watershed dominated by maple (*Acer saccharum*) and yellow birch (*Betula alleghaniensis*) settled on well-drained Ferro-humic podzols (365 meters altitude, 45.99°N, 74.00°W). Lac Simoncouche (hereafter referred to as the shallow lake) also has a pristine watershed dominated by black spruce (*Picea mariana*) and balsam fir (*Abies balsamea*) settled on podzolic soils (347 meters altitude, 48.23°N, 71.25°W). The lake has two major input streams and several ephemeral streams that only flow after heavy rains. The southern part of the lake had extensive development of aquatic macrophytes (*Brasenia schreberi*) from June to October 2011 (covering up to about 10-15% of total lake area). The study period for both lakes was from July to November 2011. Our study was based on two complementary data sets: a continuous (hourly) and a discrete (weekly or monthly) dataset (see details below). The continuous measurements were taken from an autonomous floating platform, located at the deepest point of each lake, and discrete samples of various limnological parameters were taken from a small boat close to the platform, monthly for the shallow lake and weekly for the deep lake.

Table 3.1. General characteristics of the studied lakes.

Water residence time is the averaged for year 2011 and is calculated as lake volume divided by lake discharge. DOC, Chl*a*, TP, TN and pH were the study period average taken at 0.5m depth at the deepest point of the lakes.

	Croche (east basin)	**Simoncouche**
Charateristics	Mean ± SD	Mean ± SD
Lake area (ha)	6.3	86.1
Watershed area (ha)	88	2633
Volume (m^3)*	380965	1812894
Mean depth (meters)	6.0	2.1
Water Residence Time (days)†	170	50
DOC (mg C L^{-1})*	4.43 ± 0.27	7.28 ± 0.77
Chlorophyll a (µg L^{-1})*	1.17 ± 0.43	1.80 ± 0.84
Total Phosphorus (µg L^{-1})*	3.6 ± 0.9	9.74 ± 2.57
pH*	6.6 ± 0.4	7.7 ± 0.3

*Study period average †Year average

3.3.2 Continuous and discrete lake measurements

Continuous measurements were performed from two different platforms. In the deep lake, the autonomous floating platform was equipped with a weather station (see below), and a variety of underwater sensors, of which here we only report data for CO_2, O_2 and temperature. In brief, surface water pCO_2 was measured at 0.5 m depth using a submerged infra-red CO_2 probe (Vaisala GMP-343, Finland) covered with a diffusion membrane (PTFE) that allowed gas equilibrium without the need to pump air; measurements were taken every hour. Oxygen was also recorded hourly at 0.5 m from an optical sensor, and temperature was recorded at every meter, both deployed in a multi-sensor string (Precision Measurement Engineering, Inc., USA). For the shallow lake, the autonomous platform consisted of subsurface CO_2 and O_2 sensors, and a thermistor chain that extended to the bottom. Surface water pCO_2 was measured hourly at 0.5m depth, by pumping air in a closed re-circulating loop (Tygon tubing) connected to an infra-red sensor (Vaisala GMP343, Finland) situated on the floating platform. Gas exchange between water and pumped air in the loop was carried out in two meters long of gas-permeable silicon tubing (1 mm wall thickness) deployed at 0.5 m depth to allow complete gas equilibrium (Huotari *et al.*, 2009). Oxygen concentration was measured hourly with an optical oxygen logger (Zebra-Tech D-opto, accuracy: 0.02 mg L^{-1}), deployed at a 0.5 m. The thermistor chain consisted of 7 temperature sensors (Onset Hobo Pendant, Accuracy: 0.54°C), deployed under the surface and each meter depth. All gas probes were either manually or factory calibrated prior to deployment and all time-series were visually checked for quality by comparing with manual points measurements.

Lake levels were continuously measured using a pressure probe (Precision Measurement Engineering) in the deep lake, and a level logger (Trutrack, New Zealand), installed near shore in the shallow lake. The shallow lake outflow discharge was calculated on the basis of a stage-discharge curve established from the outflow

water level measurements and point measurements of discharge using an acoustic Doppler velocimeter (Sontek FlowTracker, USA). There are no permanent inflows in the deep lake, and the lake outflow discharge was instrumented with a level logger coupled to an installed V-shape weir, allowing estimates of continuous discharge (Station de biologie des Laurentides, Universite de Montreal).

In addition to the above continuous measurements, we took monthly (in the shallow lake) and weekly (in the deep lake) measurements of CO_2 vertical profiles at each meter depth, by pumping water (using a peristaltic pump) through a diffusion membrane (Liqui-Cel, MiniModule) to allow gases to equilibrate, connected to an infra-red gas analyzer (PP System, EGM-4) (Cole et Prairie, 2009). Vertical profiles also included measurements of dissolved O_2, temperature, pH and conductivity using a multi-parameter probe (Yellow Spring Instrument).

3.3.3 Environmental data

For the shallow lake, hourly wind speed (average of measurements made over 2 minutes at the end of each hour), and barometric pressure were provided by a nearby weather station (Environment Canada) about 12 km north of the lake. Barometric pressure was corrected for the altitude difference between the lake and the station. Precipitation data were collected by another meteorological station (Laboratoire d'Écologie végétale et animale of Université du Québec à Chicoutimi) situated within the lake watershed, about 2 km south of the lake. The barometric pressure and air temperature corresponding to the deep lake were recorded directly on the floating platform, which was equipped with a Vaisala WXT520 weather station. Wind speed (15 minute averages at 1 second sampling rate), and precipitation were obtained from a meteorological station located ~350 meters south of the autonomous platform (Station de biologie des Laurentides, Universite de Montreal).

The lake thermal stability was calculated from continuous water temperature measurements and bathymetric data using Lake Analyzer program (Read *et al.*, 2011). Lake stability is here presented as the Schmidt stability (St, J m^{-2}), which is the aerial amount of energy required to completely mix the lake, and is expressed by the following equation:

(3.1) $$St = \frac{g}{LA}\int_0^{z_{max}}(z - z_v)\rho_z A_z \delta z$$

where g is acceleration due to gravity, LA is the surface area of the lake, z_{max} is the maximum depth of the lake, z is the depth of the lake at any given interval, z_v is the depth to the center volume of the lake, ρ_z is density of water at depth z, and A_z is the area of the lake at depth z.

3.3.4 CO_2 flux calculation

Atmospheric CO_2 fluxes were calculated using Fick's law of gas diffusion expressed by this equation:

(3.2) $$F_{CO2} = k_{CO2} \cdot Kh \cdot (pCO_{2\,water} - pCO_{2\,air})$$

where F_{CO2} is the CO_2 flux across the air-water interface (mg C m^{-2} d^{-1}), k_{CO2} is the gas transfer velocity for CO_2 at a given temperature (m d^{-1}), Kh is the Henry's coefficient (corrected for temperature) and pCO_2 is the CO_2 partial pressure (µatm) in the surface of water and in the atmosphere. We assumed a constant atmospheric pCO_2 of 390 µatm (point onsite measurements ranged from 380 to 400 µatm). The gas exchange coefficient was determined from k_{600} (Jähne *et al.*, 1987), standardized to a Schmidt number of 600 using the following equation:

(3.3) $$k_{CO2} = k_{600}\,(Sc_{CO2}/600)^{-0.67}$$

where Sc_{CO2} is the CO_2 Schmidt number for a given temperature (Wanninkhof, 1992). We used two different models to estimate k_{600}: an exponential wind-based model (Cole et Caraco, 1998):

$$k_{600} = 2.07 + 0.215 \cdot U_{10}^{1.7} \quad (3.4)$$

and a wind-based model that further accounts for lake size (Vachon et Prairie, 2013):

$$k_{600} = 2.51 + 1.48 \cdot U_{10} + 0.39 \cdot U_{10} \cdot \log_{10}\mathrm{LA} \quad (3.5)$$

where k_{600} is in cm h^{-1}, U_{10} in m s^{-1}, LA is the lake area in km^2. CO_2 fluxes were calculated using both models for each hourly interval based on the measurements of ambient pCO_2 and wind speed, and here we report the daily average flux from both models (derived from equations 3.4 and 3.5).

3.3.5 Whole-lake water and CO_2 mass balance calculation

For calculation purposes, each lake was considered as composed of two well-mixed layers, which we here refer to as epilimnion and hypolimnion, the latter comprising the metalimnion as well. We determined the physical separation between the two layers by computing daily values of the upper mixed layer depth (Z_{mix}). We consider the upper mixed layer vertically homogenous in temperature, and we defined Z_{mix} as the depth corresponding to the maximum of the second derivative of the temperature profile with depth (see Supporting Information for further details). The total lake volume was calculated daily using the lake hypsometric curves, and the measured lake level; the volume of epilimnion was calculated using the lake hypsometric curves, the measured lake level and Z_{mix}, and the volume of hypolimnion was calculated as the difference between total and epilimnetic volume.

The total epilimnetic CO_2 mass was calculated using the daily average surface pCO_2 and temperature from the continuous measurements, multiplied by daily epilimnetic

volume. The hypolimnetic CO_2 mass was calculated from data obtained in the manual sampling dates, by multiplying the gas concentration at 1-m intervals from the depth profiles by the volume of the 1-m layer calculated using the lake bathymetry. The total hypolimnetic CO_2 mass was then calculated as the sum of all the layers below the corresponding Z_{mix} for that date. These hypolimnetic masses could be calculated only for the dates in which we sampled, and in order to derive daily hypolimnetic CO_2 masses we had to interpolate between these dates. In the case of the deep lake, there was a strong linear positive relationship between mean hypolimnetic CO_2 concentration and day of the year (see Results section for details), and we used this relationship to estimate the daily hypolimnetic CO_2 mass by combining the predicted CO_2 concentration and the estimated hypolimnetic volume for that day. In the case of the shallow lake, we did not find such consistent hypolimnetic CO_2 concentration increase through time, probably because of the weaker stratification. However, we found a strong linear relationship between the measured total hypolimnetic CO_2 mass and the measured Z_{mix}, and we used this empirical model to predict hypolimnetic CO_2 mass based on the daily measured Z_{mix} (see Results section for details). The whole-lake CO_2 mass was the sum of the epilimnetic and hypolimnetic CO_2 masses; since the epilimnetic mass was calculated from daily measurements we assumed no error in this estimate, so the error associated to the total lake CO_2 mass value was assumed to be equivalent to that of the hypolimnetic mass, which was calculated as the 95% confidence interval from the linear regression models used.

We assessed the whole-lake CO_2 production and import rates (whole-lake CO_2 mass balance, CO_{2mb}), which integrates whole-lake net ecosystem metabolism, including pelagic and benthic environments, photo-oxidation of organic matter and CO_2 inputs from surface or sub-surface waters. Daily areal CO_{2mb} (mg C m^{-2} d^{-1}) was calculated as the sum of atmospheric flux, loss from the lake discharge and daily total CO_2 mass changes, which can be described as:

(3.6) $$CO_{2mb} = F_{CO2} + \Delta CO_{2mass} + CO_{2out}$$

where F_{CO_2} is the CO_2 flux with the atmosphere, ΔCO_{2mass} is the daily change in the lake CO_2 mass and CO_{2out} is the amount of CO_2 exported by the lake output.

3.3.6 Whole–lake metabolism calculations

Estimates of community respiration (R), gross primary production (GPP) and net ecosystem metabolism of the surface layer ($NEM_{epi} = GPP_{epi} - R_{epi}$) were calculated using free-water continuous (hourly) measurements of surface water dissolved oxygen (O_2). Using the diurnal changes in O_2 allowed us to differentiate the potential in-lake (biological) production of CO_2 from the external CO_2 inputs, and therefore their relative contribution to the whole-lake CO_2 mass balance. NEM_{epi} represents the net change in dissolved O_2 over time corrected for gas exchange during that period (Cole *et al.*, 2000):

(3.7) $$NEM_{epi}\ (\text{hourly}) = \Delta O_2\ (\text{hourly}) + D/Z_{mix}$$

where ΔO_2 is the change in O_2 concentration in the epilimnion (mmol m^{-3} h^{-1}), D is the diffusive O_2 flux with the atmosphere (mmol m^{-2} h^{-1}), and Z_{mix} (m) is the depth of the mixed layer at the beginning of this period. We assumed no exchange with hypolimnetic water, and therefore D represents exchange with the atmosphere and were thus determined using equations 3.2 and 3.3, but replacing O_2 for CO_2 in the calculations, and using the average k_{600} resulting from equations 3.4 and 3.5. The daily NEM_{epi} (mmol m^{-3} d^{-1}) is the sum of the hourly NEM from midnight to 23:00. Epilimnetic respiration (R_{epi}) was determined as the net consumption of oxygen during nighttime (R_{epi} = night-time NEM_{epi}) integrated over the period when PAR = 0. Night-time R was assumed to be equal to daytime R, such that GPP_{epi} represents the net O_2 production over the day corrected for these respiration rates ($GPP_{epi} = NEM_{epi}$ (day) + R_{epi}), integrated over the period when PAR > 0. We converted all metabolic rates to C

units to be able to compare the NEM_{epi} with the CO_2 mass balance by assuming RQ and PQ of 1. Night-time O_2 increase were occasionally observed, resulting in positive respiration values (i.e. O_2 production). Because GPP calculation also relies on R values, this bias consequently affects GPP. Nighttime increases in O_2 have also been reported in previous studies (McNair *et al.*, 2013; Tsai *et al.*, 2008), and may result from vertical entrainment of O_2-rich metalimnetic water or transport of O_2-rich waters from the littoral (Hanson *et al.*, 2008). During those days, physically-driven O_2 variability overwhelmed the biological signal, and therefore, those values and their associated NEM were removed from the analysis. This corresponded to approximately 15% and 20% of the total observations for the deep lake and the shallow lake, respectively.

To complete the whole-lake estimates of metabolism, we also calculated the daily hypolimnetic NEM (NEM_{hypo}) using the change in the mean hypolimnetic CO_2 concentration over successive sampling days during the well-stratified periods (Brothers *et al.*, 2012), multiplied by the mean hypolimnetic volume. The whole-lake net metabolic CO_2 production ($NM_{CO2}P$) was then determined as:

$$NM_{CO2}P = (TNEM_{epi} + TNEM_{hypo}) / LA \quad (3.8)$$

where $NM_{CO2}P$ (mg C m^{-2} d^{-1}) is the whole-lake areal metabolic production of CO_2, $TNEM_{epi}$ is the daily NEM_{epi} multiplied by the epilimnetic volume (converted into CO_2 rate; mg C d^{-1}), $TNEM_{hypo}$, is the daily hypolimnetic NEM multiplied by the hypolimnetic volume (mg C d^{-1}), and LA is lake area (m^2).

3.4 RESULTS

3.4.1 Environmental data

The two lakes showed very different patterns in physical structure, especially in terms of thermal stratification. Figure 3.1A-D show the patterns in thermal stratification and Schmidt stability for both lakes. The deep lake was thermally stratified during most of the study period, reaching its highest Schmidt stability of 206.8 J m^{-2} by July 22nd. The Z_{mix} decreased gradually throughout the period, from around 2 m to 10 m, resulting in a hypolimnion that had a maximum thickness of 8 m (Figure 3.1a). The lake completely mixed and became isothermal in November 4 and full ice cover started on December 10, resulting in 28 days of well-mixed water column. The shallow lake developed a weaker stratification (Figure 3.1b), resulting in lower Schmidt stability values (Figure 3.1D). Because of the particular morphometry of this lake (mean lake depth of 2 m), Z_{mix} was closer to the bottom of the lake, and the hypolimnion was often less than 2 m thick. The maximum Schmidt stability (27.9 J m^{-2}) was reached on July 3, the lake mixed completely on October 5, and had full ice cover by November 28, resulting in 43 days of well-mixed water column. During the month of July, the average contribution of hypolimnetic volume to the total lake volume was 68% and 17% for the deep lake and the shallow lake, respectively.

Increases in wind speed and precipitation related to storm events also affected the physical conditions and hydrology of the lakes. Figure 3.1E-J shows averaged daily wind speed, lake discharge and total precipitation. For both lakes, sudden increases of lake discharge always followed precipitation events, although major precipitation events also occurred with little or no corresponding increases in lake discharge, especially in the shallow lake (Figure 3.1G-J). We selected for our subsequent analysis, storm events that were followed by a noticeable and persistent decrease in stability together with an increase of lake discharge, representing a large range in event intensity

(dotted lines with their identification numbers in the light grey area). In addition to discharge changes, events often resulted in decreases in thermal stability, ranging from about 5 to 40% loss from pre-storm value, and some events show peaks in daily average wind speed, up to 5 m s^{-1} in both lakes (events 5, 8, 13 and 15, for example, Figure 3.1E-F).

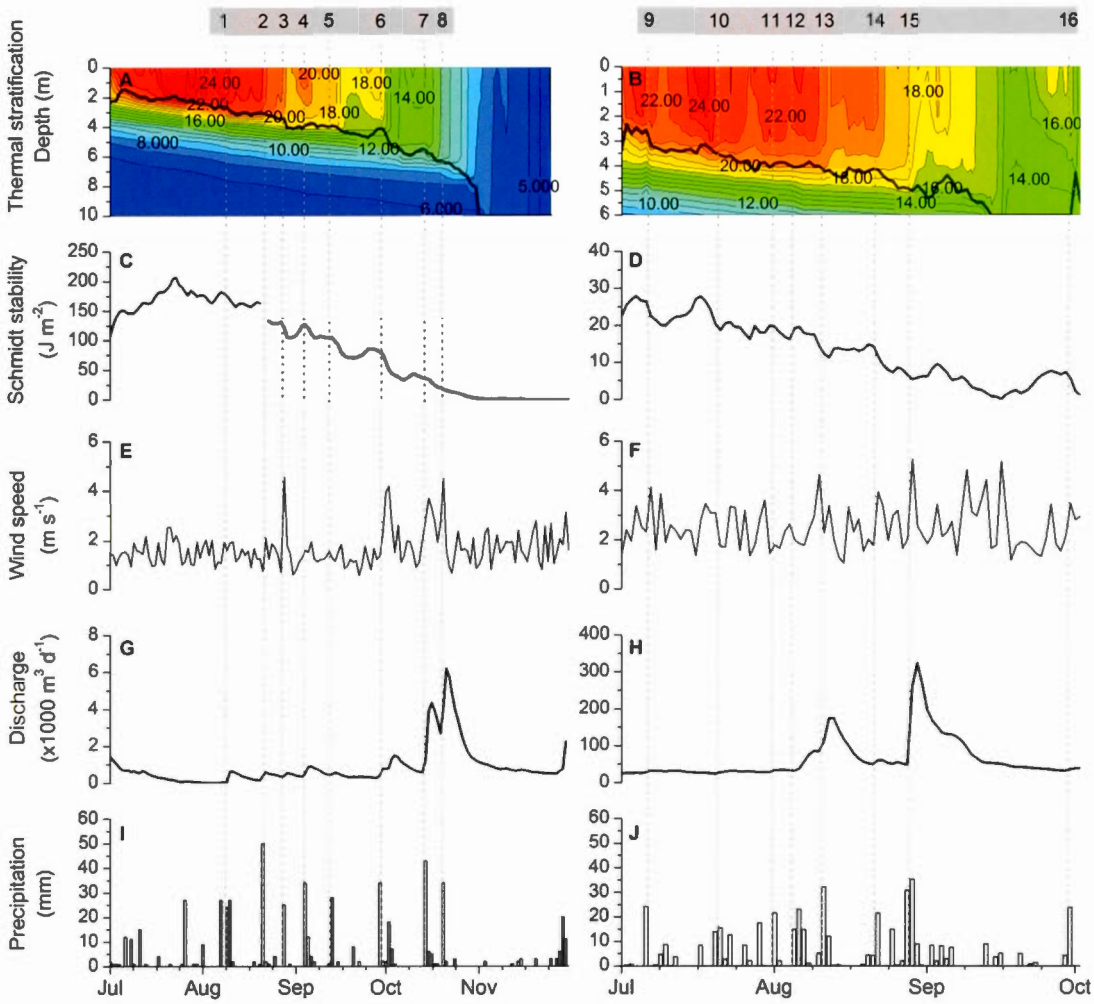

Figure 3.1. Environmental and lakes physical conditions

Storm events disturb patterns in meteorological drivers, which modify the physical condition of lakes. Here is shown the lakes thermal stratification in Celsius (A and B) plot together with the mixed layer depth (dark grey line). Then, the Schmidt stability (C and D), wind speed at 10m (E and F), daily averaged lake discharge (G and H) and daily total precipitation (I and J) for the study period for the deeper lake Croche (left graphs) and the shallower lake Simoncouche (right graphs). Grey dot lines show the selected storm events numbered above in the light grey area. Note the different scales, except for wind speed and precipitation.

3.4.2 Carbon dioxide dynamics

Both lakes showed similar patterns in surface pCO_2 and atmospheric CO_2 flux during the study period, however, the patterns in whole-lake CO_2 mass differed noticeably (Figure 3.2). In both lakes, the period of stronger thermal stratification was characterized relatively stable surface water pCO_2 and atmospheric fluxes, with no directional trend (Figure 3.2A; from July to October and Figure 3.2B; from July to August), followed by a thermally unstable period characterized by much higher and variable pCO_2 values and atmospheric fluxes (Figure 3.2A, from October to December and Figure 3.2B, from mid-August to mid-September). Water/air CO_2 fluxes calculated using the model proposed by Vachon et Prairie (2013) yielded slightly higher CO_2 fluxes than those based on the Cole et Caraco (1998) model (Figure 3.2C-D). In the deep lake, the average surface water pCO_2 (± SD) during the more thermally stable period (July to end of September) was 689 ± 66 µatm, with an average CO_2 flux (± SD) of 88.7 ± 36.8 mg C m^{-2} d^{-1}. In late September, both surface pCO_2 and fluxes drastically increased 1128 ± 202 µatm and 616.2 ± 208.6 mg C m^{-2} d^{-1} (average values from October to December). In the shallow lake, the average pCO_2 (± SD) during the thermally stable period (July) was 634 ± 144 µatm, with an average CO_2 flux (± SD) of 107.8 ± 65.7 mg C m^{-2} d^{-1}. In early August, pCO_2 and fluxes also increased to 1156 ± 215 µatm and 458.1 ± 181.0 mg C m^{-2} d^{-1}, respectively (average values from mid-August to end of September). Those increased values were maintained during events 14 and 15 and decreased in late September (Figure 3.2B and D).

While we observed similar average pCO_2 values in both lakes, our estimates of whole-lake CO_2 mass revealed different patterns. The total CO_2 mass in the deep lake slowly but consistently increased during summer, to then gradually decrease following event 6 (Figure 3.2E). For the shallow lake, whole-lake CO_2 mass stayed relatively constant during July but drastically increased in early August, in parallel to increases in both pCO_2 and CO_2 fluxes following event 13 (Figure 3.2F). Vertical CO_2 mass distribution

patterns were also different between the study lakes. During the more thermally stable period in July, only 10% of the total CO_2 mass in the deep lake was in the epilimnion, contrarily to the shallow lake, where the epilimnion accounted for on average 40% of the whole lake CO_2.

We additionally modeled daily hypolimnion CO_2 masses to derive estimates of daily whole-lake CO_2 mass, that we could use in our whole-lake CO_2 mass balance calculations. For the deep lake, hypolimnetic CO_2 concentration (mg C m^{-3}) linearly increased over time (r^2=0.94, RMSE=0.166, $[CO_2]_{hypo}$ = -2.53 + 23*DOY, $p < 0.001$). Modeled daily hypolimnetic CO_2 mass was calculated as the product of concentration and hypolimnion volume (Figure 3.2A). For the shallow lake, hypolimnetic CO_2 mass (kg C) was linearly related to Z_{mix} (r^2=0.95, RMSE=65.44, hypo CO_{2mass} = 1145 – 181.8*Z_{mix}, p = 0.0053), and was thus modeled using daily Z_{mix} values. In both lakes, modeled whole-lake CO_2 masses agree well with point measurements, falling within the 95% confidence interval limits.

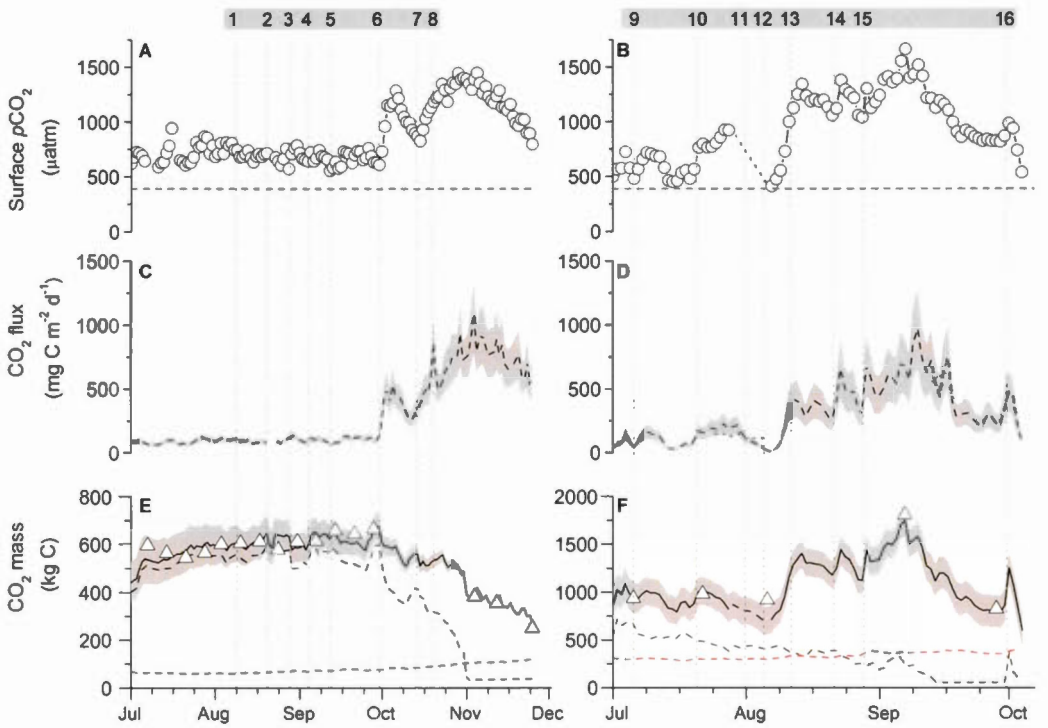

Figure 3.2. Daily averaged surface pCO_2, atmospheric CO_2 fluxes and CO_2 masses.

Although lakes surface CO_2 dynamic may look similar between the two lakes, the whole-lake CO_2 mass dynamics differs remarkably. Here is shown the daily averaged surface pCO_2 (A and B), atmospheric CO_2 fluxes (C and D) and CO_2 masses (E and F) presented with the selected storm events (grey dot lines) for the deeper lake Croche (left graphs) and the shallower lake Simoncouche (right graphs). Daily CO_2 fluxes were estimated with k_{600} derived by two wind-based models; the averaged flux is shown by the dash line surrounded by actual values from both models (grey area, representing Vachon et Prairie (2013) model as the upper limit and Cole et Caraco (1998) model as the lower limit). Daily averaged CO_2 masses are showed as the modeled hypolimnetic CO_2 masses (black dash lines) and total CO_2 masses (black lines). Grey areas correspond to the 95% confidence interval limits of the predicted values by the model. Open triangles are the point measurements of the whole-lake CO_2 masses. Red lines show the pCO_2 and whole-lake CO_2 mass at equilibrium with the atmosphere. Note the different scales for CO_2 masses.

3.4.3 Metabolic rates and carbon dioxide mass balance

Both lakes showed similar ranges in respiration and primary production rates (Figure 3.3), although the values for the deep lake seem to be more variable. The epilimnion of the deep lake was net heterotrophic during the whole study period (mean NEM < 0) with average NEM (±SD) of -45.2 ± 58.9 mg C m^{-3} d^{-1}, average R of -154.0 ± 124.0 mg C m^{-3} d^{-1}, and average GPP of 108.4 ± 110.5 mg C m^{-3} d^{-1}. We observed slight decreases in NEM in late July, during September and early October (Figure 3.3A). The latter (close to event 6) was also coupled with enhanced rates of R and GPP. The epilimnion of the shallow lake was slightly net autotrophic (mean NEM > 0) in July, to then become in near metabolic balance (mean NEM = 0) following event 12 (Figure 3.3B). For the whole study period, average NEM (±SD) was 2.3 ± 50.6 mg C m^{-3} d^{-1}, average respiration was -53.1 ± 84.7 mg C m^{-3} d^{-1} and average GPP was 149.2 ± 85.2 mg C m^{-3} d^{-1}.

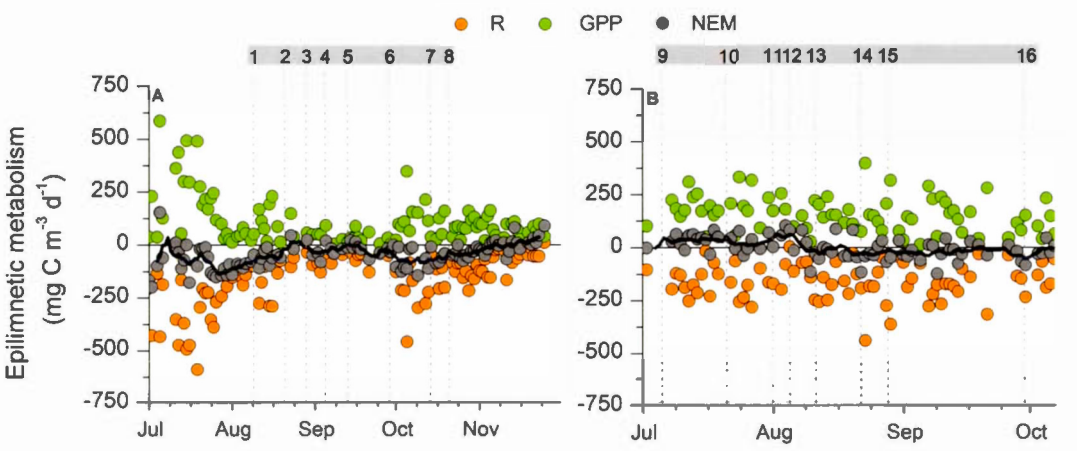

Figure 3.3. Epilimnetic metabolism balance

Epilimnetic metabolism balance is also influenced by meteorological events. Here is shown, for the deeper lake Croche (A) and the shallower lake Simoncouche (B), the volumetric rates of epilimnetic respiration (R, orange dots), gross primary production (GPP, green dots) and net ecosystem metabolism (NEM, dark grey dots) measured with free-water oxygen measurements. Negative rates of NEM represent net heterotrophy, while positive rates represent net autotrophy. Black lines represent the smoothed trend calculated with a 7-days moving average.

The comparison between whole-lake metabolism and CO_2 mass balance ($NM_{CO2}P$ and CO_{2mb}, respectively, expressed in mg C m^{-2} d^{-1}) revealed the influence of rain events on lake CO_2 dynamics (Figure 3.4). Whole-lake $NM_{CO2}P$ have been estimated by adding hypolimnetic estimates of NEM (NEM_{hypo}) during the well-stratified period to epilimnetic rates (NEM_{epi}), which were now expressed as CO_2 rates for comparison purpose. For the deep lake, NEM_{hypo} was 23 mg C m^{-3} d^{-1}, which corresponded to a relatively constant increase in hypolimnetic CO_2 concentration during the well-stratified period (July to October). For the shallow lake, NEM_{hypo} was 50 mg C m^{-3} d^{-1}, based on the observed linear increase in hypolimnetic CO_2 concentration during the well-stratified period (July and early-August only). $NM_{CO2}P$ and CO_{2mb} in the deep lake initially followed the same pattern, including the rapid intensification during early October (Figure 3.4A, events 6-8). However in November following event 8, we observed a disproportionate increase in CO_{2mb} relative to $NM_{CO2}P$ and a decoupling of the two. For the shallow lake, CO_{2mb} was always greater than $NM_{CO2}P$, and the offset between the two abruptly increased in early August and remained high through September. In both lakes, these periods of offset between CO_{2mb} and $NM_{CO2}P$ (in November for the deep lake and August-September in the shallow lake) were preceded by events of rapid increase of the hydrological regime, as reflected in the daily water renewal rate (Figure 3.4C-D).

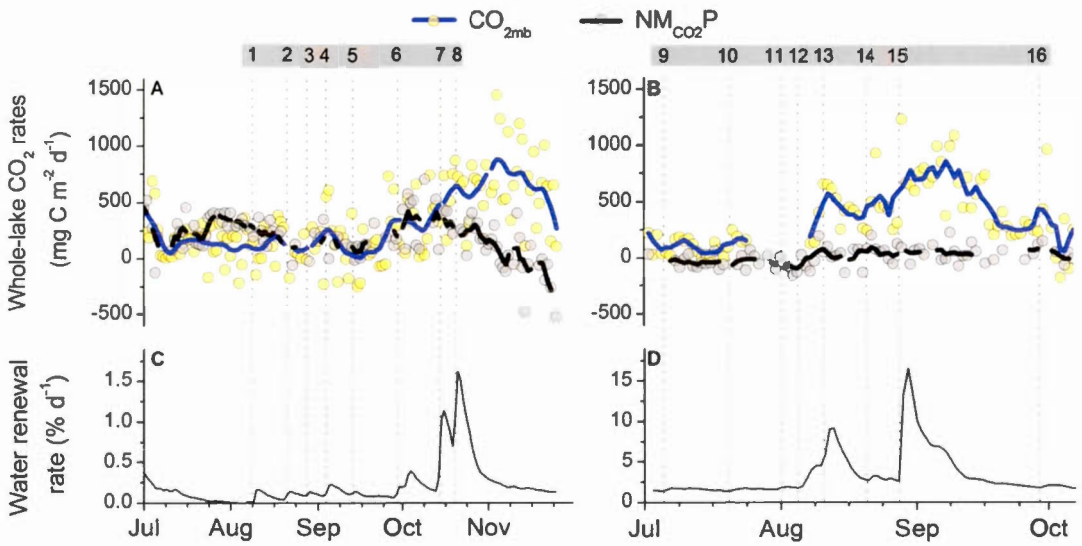

Figure 3.4. Whole-lake net ecosystem metabolism

Storm events impact on lakes CO_2 sources is modulated by hydrology. Here is shown, for the deeper lake Croche (left) and the shallower lake Simoncouche (right), the whole-lake net ecosystem metabolism expressed in areal CO_2 rates (NEM_{lake}, light grey dots) derived from free-water oxygen measurements and daily whole-lake CO_2 production and/or import ($CO_{2\ mb}$, light yellow dots) estimated by mass balance calculations (A and B). Trends are showed using a 5-days moving average for NEM_{lake} (black line) and for $CO_{2\ mb}$ (blue line). For basis of comparison, note here that positive NEM_{lake} rates represent CO_2 production (i.e. net heterotrophy). Lower panel (C and D) show lakes water renewal rates (% d^{-1}). Grey dot lines show the selected storm events. Note the different scales for water renewal rates.

3.5 DISCUSSION

3.5.1 Storm-related patterns in lake CO_2 dynamics

We observed a relatively stable pCO_2 level in both lakes during summer (July), oscillating around 650 µatm. This pCO_2 level is comparable to reported values in temperate and boreal lakes of similar DOC concentrations (Roehm *et al.*, 2009; Sobek *et al.*, 2003), and lake size (Kelly *et al.*, 2001; Roehm *et al.*, 2009). For the deep lake, this period of remarkably stable pCO_2 and fluxes was extended to September, in spite of several major storm events (events 1-5 in Figure 3.2A and C). The absence of major pCO_2 or flux variations could be explained by the strong thermal stratification of the water column (Figure 3.1A), limiting CO_2 entrainment from the hypolimnion, and by the modest hydrological response to the storm events during the period (Figure 3.1G). The whole-lake CO_2 mass, however, slightly but consistently increased during that period (Figure 3.2E), likely due to hypolimnetic CO_2 accumulation driven by hypolimnetic metabolism (Brothers *et al.*, 2012; Den Heyer et Kalff, 1998; Houser *et al.*, 2003). Similarly, in the shallow lake, summer (July) surface pCO_2 and fluxes were relatively stable and reacted only slightly to storm events (Figure 3.2B). This relatively stable gas dynamic in both lakes may also be related to periods of microstratification occurring during the day, which further limit mixing and atmospheric gas exchanges, especially in small sheltered lakes (Read *et al.*, 2012). We experienced technical issues with the pCO_2 probe in the shallow lake in late July and early August (Figure 3.2B, dash line), which, however, did not affect the subsequent analyses since no major storm events occurred during this period, and oxygen-based metabolism was stable throughout this time.

Surface pCO_2 and CO_2 fluxes drastically increased in both lakes towards the end of the summer and the beginning of fall, coinciding with major rain storms (Figures 3.2E-F). The simplest explanation for this shift is increased water column mixing and the

associated mobilization of hypolimnetic CO_2, a pattern that has been well established for northern dimictic lakes (Huotari *et al.*, 2009; Kelly *et al.*, 2001; Riera *et al.*, 1999). Since this hypothesis does not involve any new sources of CO_2 to the lake, it necessarily implies that the increased CO_2 evasion in the fall be matched by an equivalent loss of total CO_2 mass in the lake. Our results, however, suggest that the reallocation of hypolimnetic CO_2 was insufficient to explain the changes in lake pCO_2 and CO_2 fluxes to the atmosphere during this period in either of the lakes. This is particularly evident for the shallow lake, where increasing surface pCO_2 and CO_2 fluxes from early August and throughout the early fall co-occurred with a pattern of increasing whole-lake CO_2 mass (Figure 3.2F). In the deep lake, although increased CO_2 fluxes to the atmosphere in late summer and fall did coincide with a decline in total lake CO_2 mass (Figure 3.2A), our detailed CO_2 mass balance for the period requires the inclusion of other sources in addition to hypolimnetic CO_2. In both cases, our evidence based on the patterns in whole-lake CO_2 mass suggests that storms may play a major role in shaping lake CO_2 budgets, particularly in the late summer and fall periods, coinciding with an overall decline in water retention within the catchment due to reduced plant and tree production and evapotranspiration and enhanced runoff. Lake and watershed morphometry, however appear to modulate the extent of in-lake CO_2 production and external inputs of CO_2 to lakes following rain storms. As we discuss below, we suggest that lakes with large watersheds relative their volume may be more sensitive to storm-induced external C loading and that lakes with relatively smaller watersheds may favor internal C processing.

3.5.2 Responses of lake metabolism to storms

Free-water oxygen measurements from lake surface waters have been widely used to estimate ecosystem metabolism, including community respiration and gross primary production (Hanson *et al.*, 2003; Solomon *et al.*, 2013; Staehr et Sand-Jensen, 2013). This method integrates several ecosystem processes, and the resulting estimates of

NEM incorporate biological oxygen consumption and production, and photochemical oxidation in pelagic waters and, to a certain extent, benthic respiration and primary production in the case of sediments that are in contact with epilimnetic waters (Bogert *et al.*, 2007; Staehr *et al.*, 2011). To remove all the potential physically-driven biases in our estimates, we removed data which corresponded to night-time O_2 increases, as mentioned in the methods section. It is unlikely that this removal step influenced the overall trends we report here, since these data where scattered throughout the time series (Figure 3.3). However, our metabolic measurements still showed large day-to-day variability. This day-to-day variability has been reported before, and has been argued to be driven by biological processes (Solomon *et al.*, 2013; Staehr *et al.*, 2010b). This variability can also be due to unaccounted gas exchange with the hypolimnion, or to atmospheric gas exchange due to thermal mixing mainly during night (Read *et al.*, 2012; Sadro *et al.*, 2011; Staehr *et al.*, 2012), which may not be properly parameterized by current wind-based models (Vachon et Prairie, 2013). Regardless of this large day-to-day variability and the data removal step, our average estimates of respiration and gross primary production rates are comparable to reported values from lakes with similar TP and DOC content (Coloso *et al.*, 2011; Hanson *et al.*, 2003), and we will thus focus on averages and overall trends of metabolism measurements, especially NEM, rather than on the details of day-to-day variability.

Rain storms, through their hydrological effects, have been reported to influence lake metabolism, generally promoting respiration over primary production, resulting in a shift toward heterotrophy (Klug *et al.*, 2012; Sadro et Melack, 2012; Tsai *et al.*, 2008). Our metabolism data however, show that it is not always the case. In the deep lake we observed responses in ecosystem metabolism that may be associated to storm events, although the large day-to-day variability in the measurements makes it difficult to discern the specific effect of each event. We can nevertheless observe a clear response following event 6 (Figure 3.3A), where both R and GPP were enhanced, but the effect on respiration was greater, which resulted in a lowering of negative NEM (i.e. more

CO_2 production). This may suggest that the inputs of labile organic matter resulting from the storm were proportionately greater than nutrient inputs loaded either from surface waters through hydrologic inputs, or brought to the surface from hypolimnetic waters due to wind-driven partial mixing. Similarly, in the shallow lake, despite large day-to-day variability in R and GPP, a clear shift in NEM also occurred after event 12 in early August (Figure 3.3B). After this particular event, NEM shifted from autotrophic to slightly heterotrophic. This shift seemed to have been driven mostly by a decline in primary production, which could have resulted from decreased water transparency due to an increase in organic matter concentration (Klug *et al.*, 2012). During this event there was nevertheless a slight enhancement of R, which may have been due to increases in biological and photo-reactive DOC loading resulting from this event (Figure 3.1H). It is clear from these observations that storm events may influence lake metabolism in different manners, either by remobilizing nutrients by wind-driven mixing, adding new labile or photo-reactive organic matter from hydrologic inputs, or shifting the light climate, and that some of these metabolic shifts may lead to significant increases in in-lake CO_2 production. Interestingly, not all storms resulted in a noticeable shift in ecosystem metabolism, so it is clear that the influence of these events on the functioning of lakes is complex and may be further masked by background variability and measurement uncertainty.

3.5.3 Relative contribution of lake metabolism and external C loading on the CO_2 mass balance

The comparison of the whole-lake CO_2 mass balance (CO_{2mb}) with the estimated whole-lake metabolic production of CO_2 ($NM_{CO2}P$) allows us remove the effect of CO_2 reallocation and to therefore estimate the contribution of in-lake processes to the calculated CO_2 mass changes (Figures 3.4A and B). There is a large day-to-day variability in CO_{2mb}, which reflects in part the large variability in average daily CO_2 fluxes that are used in the calculation, so it is the average trends in time shown in

Figures 3.4A and B that are more relevant in the context of this study. In the case of the deep lake, CO_{2mb} closely followed $NM_{CO2}P$ during all of the summer, suggesting that summer CO_2 dynamics in this lake are largely driven by in lake processes (Figure 3.4A). During this period, the influence of storms on the deep lake CO_2 was mediated mostly by their influence on metabolism, including shifts toward heterotrophy after event 6, as discussed in the previous section. Interestingly, events 7 and 8, which occurred later in the fall, resulted in an almost complete decoupling between $NM_{CO2}P$ and CO_{2mb}, with large increases in CO_{2mb} completely fueled by external inputs of CO_2. This suggests that even if in this particular lake CO_2 dynamics seem to be less coupled with the watershed, large rain storms may be able to load enough external CO_2 to significantly influence the whole-lake CO_2 dynamic. In the shallow lake, $NM_{CO2}P$ and CO_{2mb} were also relatively stable during mid-summer, except that $NM_{CO2}P$ was slightly negative (net autotrophic), but there was a small and relatively constant positive offset of CO_{2mb}, suggesting a constant input of external CO_2 during this period (Figure 3.4 B). Like in the deep lake, however, a large storm (event 13) triggered a strong increase in CO_{2mb}, resulting in a strong divergence between $NM_{CO2}P$ and CO_{2mb}, and a second major storm (event 15) further amplified this offset (Figure 3.4 B), suggesting that these storms led to large increases in the contribution of external CO_2 inputs. These results clearly suggest that storm events may influence lake CO_2 dynamics through shifts in lake metabolism, or through shifts in the magnitude of the CO_2 loading mediated by the hydrological charge generated by the event. This further reflects the influence of the larger watershed area to lake volume ratio, which allows a tighter hydrological connection with terrestrially-produced CO_2.

Concerning the direct CO_2 loading effect, in the deep lake, external CO_2 became dominant following event 8, and post-storm CO_2 loading averaged 324 ± 216 mg C m^{-2} d^{-1} (10-day average after event 8). Likewise, the shallow lake loaded 412 ± 147 mg C m^{-2} d^{-1} after event 13 (which generated a water renewal rate of 9 %), and 700 ± 145 mg C m^{-2} d^{-1} after event 15 (which generated a water renewal rate of 16 %). These CO_2

loads contributed essentially 100% of the atmospheric CO_2 fluxes and of the net CO_2 accumulation in the lake during these same periods. If we assume that lake discharge is roughly equivalent to water input, we can estimate the CO_2 concentration of the inflowing water needed to sustain the observed CO_{2mb} after these events. This calculation shows that event 8, in the deep lake, resulted in inflowing water having a pCO_2 of approximately 6,500 µatm. Events 13 and 15 in the shallow lake resulted in inflowing waters having pCO_2 of approximately 8,500 µatm. These values are intermediate between those reported for boreal and temperate stream pCO_2 (Campeau et del Giorgio, 2014; Sand-Jensen et Staehr, 2011; Teodoru *et al.*, 2009), and those reported for sub-surface soil water pCO_2 in the boreal (Öquist *et al.*, 2009; Worrall *et al.*, 2005) and temperate biome (Elberling et Ladegaard-Pedersen, 2005). Our own measurements of sub-surface water pCO_2 using piezometers in both lake catchments are in the range of 15,000 to 30,000 µatm during the same study period (see Supporting Information for details), which would suggest either dilution of groundwater CO_2 during these large hydrological inputs, or a mix of surface and groundwater CO_2 inputs. Regardless, the inflowing water pCO_2 required to drive the lake CO_2 patterns that we observed is reasonable.

3.5.4 The interaction between storm intensity and lake and watershed morphometry

Our results suggest that rain storm events can potentially decouple lake CO_2 dynamics from lake ecosystem metabolism, presumably when the external inputs of CO_2 driven by the increased hydrologic charge overwhelm internal processes. However, not all storms resulted in such decoupling, which further implies that storm intensity and timing may dictate how the event will influence lake CO_2 dynamics. Because the same storm event may result in different hydrological responses among various lake ecosystems, the intensity of storms can be expressed in terms of the resulting lake water renewal rate (Figure 3.4 C-D), which combines both the amount of precipitation and the lake and watershed morphometry. This metric allows expressing the intensity of

storm events in a comparable scale fort both lakes, which represents the relative volume of water that was replaced daily (% d^{-1}). In the deep lake, water renewal rates during the summer were consistently low, below 0.5% d^{-1} even during storms, which may explain the remarkably stable and internally-regulated CO_2 dynamics during the summer. Events 7 and 8, which triggered the decoupling between CO_{2mb} and $NM_{CO2}P$ in the deep lake (Figure 3.4A), however, were associated to a lake volume replacement exceeding 1% d^{-1}, suggesting a threshold in storm intensity beyond which external CO_2 loadings begin to overwhelm internal processes. In the shallow lake, the mid-summer base flow represents a water renewal rate that systematically exceeded 1% d^{-1} (average mid-summer 1.5% d^{-1}), which is consistent with the small but sustained influence of external CO_2 loading observed in this lake during the period. Major storm events 13 and 15 (Figure 3.4D) generated water renewal rates of up to 15% d^{-1}, further amplifying the external loading signal, which completely dominated the CO_2 dynamics in the lake during the period. The pattern that emerges from combining the results from both lakes is shown graphically in Figure 3.5, where the absolute amounts of external CO_2 inputs (Figure 3.5A), and their contribution to whole-lake CO_2 dynamics (Figure 3.5B) tend to be negligible at water renewal rates < 1% d^{-1}, but dramatically increase beyond renewal rates > 1% d^{-1}. It has been shown that large lakes, having long water residence times, are more likely to be internally-regulated, even after intense precipitations (Ojala *et al.*, 2011; Rantakari et Kortelainen, 2005), and that small and fast water residence lakes are more likely to receive external CO_2 after storm events (Jones *et al.*, 2009). However, the exact threshold over which external CO_2 inputs dominate the CO_2 mass balance is far from being definitive, as other processes such as catchment productivity and lake metabolism may also influence the threshold value beyond hydrology. Moreover, whether the transition from internal to external regulation is a smooth linear function of water renewal rate, or a step change, is a fundamental issue that has yet to be determined. A continuous transition would involve varying hydrological loads that nevertheless have a rather constant CO_2 concentration. A step response, on the other hand, would imply that CO_2 concentrations in the inflowing water actually vary with

the intensity of the hydrologic load, which have been observed in soil and stream water (Öquist *et al.*, 2009). The latter could also happen if increased runoff and subsurface groundwater flows mobilize different pockets of soil CO_2 (Rasilo *et al.*, 2012), or if the storms occur at times when soil CO_2 peaks, for instance when the soil temperature is highest (Pumpanen *et al.*, 2008). Our own observation would support the latter, since our measurements show that subsurface groundwater pCO_2 in these lake catchments peak at the end of the summer (see Supporting Information for details), when the most intense storms tend to occur.

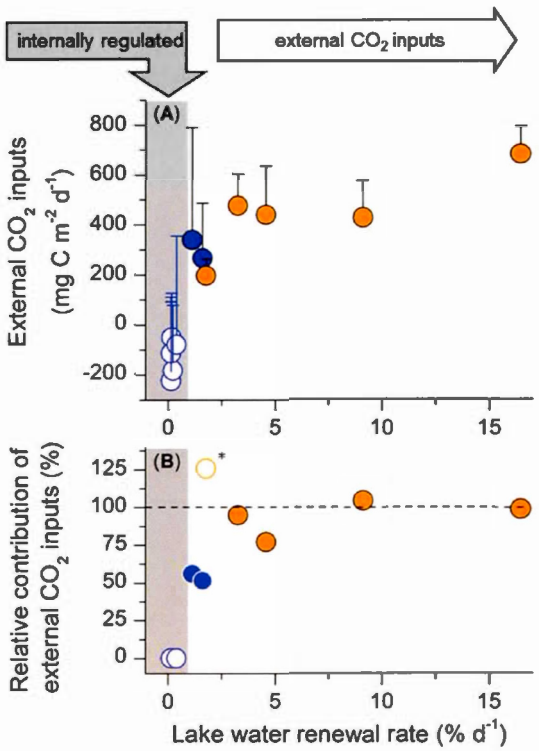

Figure 3.5. External CO_2 inputs in function of lakes water renewal rates

Here is shown the (A) daily external CO_2 inputs per lake meter square (mg C m^{-2} d^{-1}) into the deeper lake Croche (blue circles) and the shallower lake Simoncouche (orange circles) in function of lakes water renewal rates (% d^{-1}). The light grey areas are showing a hydrological threshold of 1 % d^{-1}, suggesting the dominant process following a storm event. External inputs were calculated as the 5-days average following the highest water renewal rate of the selected storms, presented with their standard deviation (positive error bars; negative bars are equivalent magnitude, but not showed). Open circle are events in Croche where the external inputs were considered not significantly different than 0. (B) The relative contribution of external CO_2 inputs to the whole-lake CO_2 dynamic (calculated by a mass balance approach). Open blue circles are Croche contribution which were here considered to be 0. Open orange circle with a star was over the 100% line (dash line) because the lake was net autotrophic, and thus needed more than 100% of CO_2 external inputs to close the CO_2 budget.

The influence of lake and watershed morphometry is such that for an equivalent storm intensity (i.e. total precipitation), lakes with greater watershed area to lake volume ratio (WA:LV) will have a greater potential for volume replacement (Klug *et al.*, 2012), thus resulting in higher lake water renewal rates, and this purely morphometric effect renders lakes with high WA:LV more sensitive to storms than lakes with low WA:LV. Lakes with higher WA:LV ratios are thus more tightly connected to their watersheds, and in the case of our shallow study lake, this is also reflected in higher DOC and TP content (see Table 3.1). Conversely, lakes with low WA:LV, such as our deep lake, function more independently from their watersheds, such that CO_2 dynamics are mostly internally regulated, unless major rain events replace enough water (here showed as a threshold of 1% d^{-1}). This demonstrates that whereas the absolute intensity and frequency of events is important, lake and watershed morphometries are key in modulating the CO_2 response of lakes to these climatic events.

3.6 CONCLUSIONS

Our results show that storms influence lake CO_2 dynamics indirectly through their influence on lake metabolism, and directly via loading of external CO_2. Furthermore, we suggest that the intensity of the storm relative to the lake and watershed morphometry determines the relative importance of these pathways. More generally, we propose that in lakes with water renewal rates < 1% d^{-1}, CO_2 dynamics are largely dominated by internal lake processes. We suggest that when storm events increase lake water renewal over a certain threshold (here tentatively identified as > 1% d^{-1}), external CO_2 loadings may overwhelm internal processes. This external CO_2 may further be related to the timing of storms, which may influence the CO_2 concentration of soil water that is associated to the hydrologic load. As water renewal rate is related to lake and watershed morphometry, these variables also dictate the dominant CO_2 pathways. Here we show that storm events are more likely to induce additional CO_2 in lakes with larger WA:LV. In contrast, lakes with smaller WA:LV will be more susceptible to re-allocation of CO_2, something that will happen regardless at fall turn-over and therefore will not alter the annual C budget. Our study highlights the fact that climatic events leading to increased hydrological flow may greatly enhance the direct catchment-lake-atmosphere connection through increased soil-derived lake CO_2 fluxes. This link, however, is strongly modulated by lake and watershed morphometry, such that the influence of these climatic events on the annual lake CO_2 emissions will differ greatly not only among lake types, but more generally between landscapes that differ in their topography. These properties need to be considered when predicting the impact of future climate change on regional C budgets and emissions.

3.7 ACKNOWLEDGMENTS

We would like to thank Alice Parkes for her dedication to the automated systems, especially in Lac Croche. Mathieu Dumais and Jean-Philippe Desindes for field and laboratory assistance. We also thank Jean-François Lapierre for helpful advice and discussions, Adam Heathcote, Shoji Thottathil and two anonymous reviewers for useful comments on previous versions of the manuscript, and HSC for unwavering guidance. This project was part of the large-scale research program of the Industrial Research Chair in Carbon Biogeochemistry in Boreal Aquatic Systems (CarBBAS), co-funded by the Natural Sciences and Engineering Research Council of Canada (NSERC) and Hydro-Québec to PDG. NSERC doctoral scholarship and UQAM-FARE scholarship was also attributed to DV.

3.8 SUPPORTING INFORMATION

3.8.1 Calculation of the upper mixed layer depth

We determined the physical separation between the two layers by computing daily values of the upper mixed layer depth (Z_{mix}). The upper mixed layer is considered relatively vertically homogenous in temperature, density and gas. As the thermocline is defined as the depth of the maximum change in temperature, we defined Z_{mix} as the maximum change in temperature changes, which is computed as the maximum second derivative of temperature profile. Because temperature measurements are taken at discrete depth intervals, precise mixed layer depths are difficult to acquire. To resolve this issue without having to linearly interpolate between measurements, a temperature profile curve was fit by minimizing the sum of squares to a temperature curve model (Minns et Shuter, 2012) before computing Z_{mix}. The following figure shows an example of temperature profiles in Lake Croche (upper panel) and Lake Simoncouche (lower panel), then the temperature change (first derivative) with the peak representing the thermocline (gray dot line) and a typical definition of the upper mixed layer (0.5C m^{-1}, gray dash line), then the change in temperature change (second derivative) showing 2 peaks. The first one is the upper mixed layer (black dash line). The upper mixed layer depth corresponded remarkably well with the depth at which CO_2 starts to accumulate (last graph to the right).

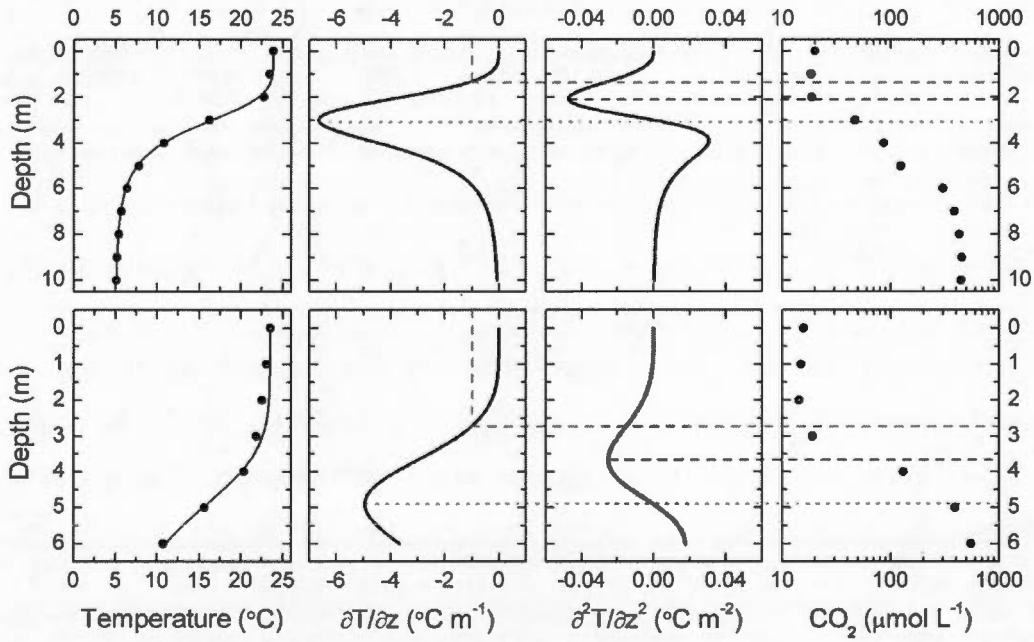

Figure S3.1. Calculation of the upper mixed layer depth

3.8.2 Soil pore water pCO_2 measurements

Point measurements of soil pore-water pCO_2 were taken monthly in both watersheds, at 3 different locations. Piezometers made of plastic tubes (inner diameter of 2.54cm) were placed in the soil at approximately 3-5 meters from the lake shore, to collect soil pore water at about 20 to 30 cm deep, depending on site soil thickness. Piezometers were flushed 24 hours prior to sampling, to discard stagnant waters. When the piezometer is replenished (approx. 24 h after flushing), we gently pumped the water out of the piezometer using a peristaltic pump 10ml into 60ml syringes (3 times) to create a 1:5 air-water ratio, with ambient air of known CO_2 concentration. Syringes were then vigorously shaken for 1min to have a complete equilibrium. Headspaces were injected in an IRGA (EGM-4, PPsystems) and pCO_2 of water was back-calculated. The following figure shows the average soil pore water pCO_2 of the sampled months during the study period in both lakes.

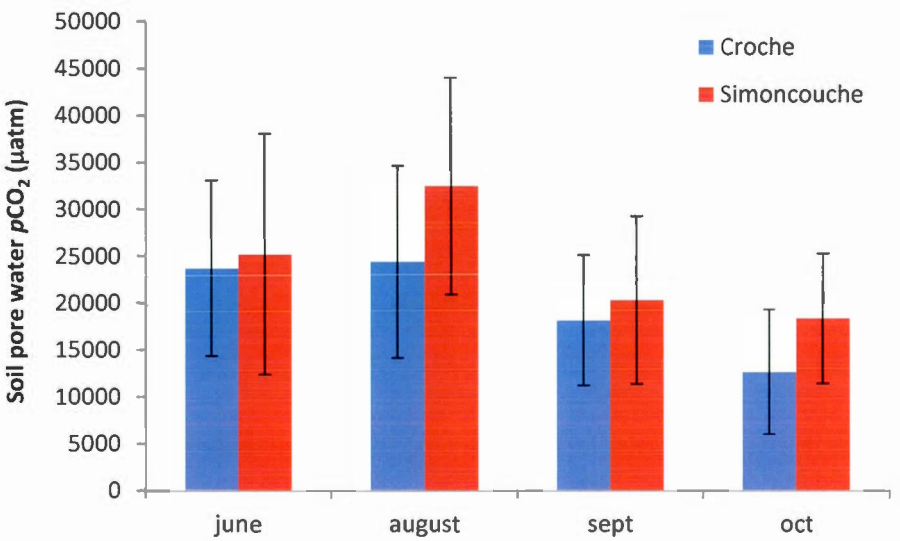

Figure S3.2. pCO_2 measured in soil water

CHAPITRE IV

RECONSTRUCTING THE SEASONAL DYNAMIC OF THE MAJOR PROCESSES SUSTAINING CO_2 EMISSIONS IN NORTHERN LAKES

Dominic Vachon[1,*], Christopher T. Solomon[2] and Paul A. del Giorgio[1]

[1]*Groupe de Recherche Inter-universitaire en Limnologie (GRIL), Département des Sciences Biologiques, Université du Québec à Montréal, Montréal, Canada*

[2]*Groupe de Recherche Inter-universitaire en Limnologie (GRIL), Department of Natural Resource Sciences, McGill University, Ste. Anne de Bellevue, Québec, Canada*

In preparation

Running head: lake seasonal CO_2 dynamics

Key words: northern lake, annual cycle, CO_2 dynamics, seasonality, dissolved organic carbon

N.B. References cited in this chapter are presented at the end of the thesis.

4.1 ABSTRACT

Lake CO_2 emission is an important component of the carbon balance of the northern landscape. Although the seasonal pattern of lake CO_2 concentration and emissions has been well described in the literature, the temporal dynamics of the underlying physical and biological mechanisms sustaining those CO_2 emissions are less understood. Here we reconstruct the major biotic and abiotic processes influencing CO_2 dynamics over an annual cycle in three limnologically different northern lakes, using a combination of empirical measurements and process-based modeling. Our results suggest that the relative importance of each process sustaining CO_2 emissions is not only variable among lakes, but also highly variable among seasons within one lake. Spring CO_2 emissions were largely sustained (between about 50 to 100%) by the release of under ice accumulation, although photo-chemical DOC mineralization and hydrologic CO_2 loading were also relatively important. In summer, due to warmer temperature, pelagic and benthic metabolisms were mainly sustaining CO_2 emissions. In fall, lake CO_2 emissions were generally sustained by hydrologic CO_2 inputs, while hypolimnetic CO_2 accumulation and release also contributed to fall CO_2 emission in the deepest lake. Our results suggest that all the major processes always contributed significantly to CO_2 emissions, but their relative contributions were modulated by the seasonal patterns in climate and hydrology, and also by the morphology and organic carbon inputs among lakes. These lake- and season-specific features modulating the patterns in processes sustaining CO_2 emissions are particularly relevant to achieve more precise regional lake C budgets and to further understand the potential variability of lake CO_2 emissions sensitivity to climate and environmental changes.

4.2 INTRODUCTION

The majority of lakes around the globe emit CO_2 at magnitudes that are significant to the global carbon (C) cycle (Cole *et al.*, 2007; Tranvik *et al.*, 2009). These CO_2 emissions from lakes are particularly important in the northern latitudes landscapes (Raymond *et al.*, 2013), which results from the combination of the widespread CO_2 oversaturation in their surface waters (Cole *et al.*, 1994; Sobek *et al.*, 2005) and the high density of lakes found in the boreal and northern temperate (therein after referred to as northern) regions (Verpoorter *et al.*, 2014). The dynamics of the underlying processes involved in sustaining northern lake CO_2 emissions, however, are still far from being understood and will require to expand the number of finer scale studies of whole lake C budgets (Hanson *et al.*, 2014b). These budget exercises are central to improving our knowledge on lake C cycling over a whole landscape, and our ability to predict future CO_2 emissions under variable environmental changes with less uncertainties.

Lake CO_2 emissions can be sustained by several processes, through which CO_2 is either produced locally or transported from peripheral production sites. In surface waters of northern lakes, many studies have reported rates of community respiration (R) exceeding gross primary production (GPP), which result in negative net ecosystem production (NEP) (Cole *et al.*, 2000; del Giorgio *et al.*, 1997; del Giorgio et Peters, 1994). More negative NEP is usually observed in lakes with higher DOC concentration (Hanson *et al.*, 2004; Prairie *et al.*, 2002), suggesting the bacterial utilization of allochthonous DOC (DOC_{alloch}) exported from the terrestrial environment (del Giorgio *et al.*, 1999; Karlsson *et al.*, 2007; McCallister et del Giorgio, 2008). The magnitude of DOC_{alloch} respiration has been further linked to the DOC_{alloch} load to lakes (Jonsson *et al.*, 2001). Terrestrial organic C inputs to lakes can also be photo-degraded by sunlight and have been shown to be a significant source CO_2 in the surface waters of northern lakes (Cory *et al.*, 2014; Koehler *et al.*, 2014; Chapter I). Unlike the metabolic balance,

however, lake DOC concentrations do not appear to affect areal rates of photo-chemical mineralization (Koehler *et al.*, 2014; Chapter I), albeit some temporal patterns in DOC photo reactivity have been observed (Granéli *et al.*, 1996; Chapter I). Whether it is biologically or photo-chemically mineralized, DOC_{alloch} has a major role in the production of CO_2 in the northern landscape (Lapierre *et al.*, 2013).

Lake CO_2 emissions can also be sustained by the production of CO_2 from peripheral sites, which is then transported to the surface waters of lakes. In particular, CO_2 can be produced in both profundal and littoral sediments (Åberg *et al.*, 2007; Algesten *et al.*, 2005; Gudasz *et al.*, 2010; Kortelainen *et al.*, 2006), which is then transported by diffusion and advection to the lake surface. The relative contributions of pelagic and benthic respiration to lake total CO_2 production have also been suggested to be influenced by the trophic status and DOC content, wherein the contribution of sediment respiration is less important to total lake total respiration in eutrophic and low DOC lakes (Den Heyer et Kalff, 1998; Jonsson *et al.*, 2003). The relative importance of sediment CO_2 production to lake CO_2 emission is also affected by lake morphometry (Åberg *et al.*, 2007; Jonsson *et al.*, 2001; Jonsson *et al.*, 2003; Kelly *et al.*, 2001), being more important in shallow systems. In addition, CO_2 concentrations of boreal streams and groundwater surrounding northern lakes are typically well above atmospheric saturation (Koprivnjak *et al.*, 2010; Öquist *et al.*, 2009). This soil-derived CO_2 can thus be transported to lakes, and potentially contributing significantly to lake surface CO_2 emissions (Kling *et al.*, 1991; Stets *et al.*, 2009; Striegl et Michmerhuizen, 1998). This process is mostly influenced by hydrologic regimes, and thus especially important after rain storm events (Vachon et del Giorgio, 2014).

Most of the abovementioned studies, however, have focused either on individual lakes or on a single process, and typically only during the stratified period in summer. There are only a handful of studies that have addressed the contribution of several key processes across lakes and in time (i.e. Striegl & Michmerhuizen, 1998; Jonsson *et al.*,

2001; Åberg *et al.*, 2007). Not surprisingly, there is a wide diversity of conclusions in the literature concerning the main drivers of lake CO_2 emissions, but these contrasting results are not necessarily mutually exclusive, since they represent fragments and temporal snapshots of the processes underlying CO_2 annual emissions from northern lakes. In fact, all these different pathways may simultaneously sustain CO_2 emissions, albeit their relative contribution to lake CO_2 dynamics should vary between lake types (Lapierre *et al.*, 2015) and seasons within a given lake. In addition, these processes which produce or import CO_2 are overlain by other related processes such as CO_2 export to downstream systems, primary production and carbonate dissolution, all of which remove CO_2 from the surface of lakes. These considerations further add complexity in the assessment of the relative contribution and dynamics of the underlying processes sustaining CO_2 emissions in northern lakes.

The aim of this study is to reconstruct a complete annual cycle of lake CO_2 dynamics, and to quantify the relative contribution of the key underlying abiotic and biotic processes that drive the magnitude and seasonal variability of CO_2 emissions in northern lakes. These major processes include pelagic and sediment respiration, primary production, photochemical DOC mineralization, and the hydrologic input of CO_2. In order to reconstruct these seasonal dynamics, we sampled over an annual cycle three limnologically different northern lakes located in the temperate and boreal regions of Québec, which are representative of lake types that can be found in these northern landscapes. In order to complete our lake CO_2 budgets, we built a simple mechanistic model using our own empirical relationships as a framework to realistically interpolate rates between our measurement points. Because climate conditions (including hydrologic and physical regimes) are highly seasonally variable, we hypothesized that there should be a seasonal succession in the relative contribution of major processes influencing lake CO_2 dynamics. We further hypothesized that the succession patterns must differ between lakes as a function of lake properties (i.e. morphology, trophic status, DOC concentration). This represents the first study to

empirically integrate the main drivers of lake CO_2 along an annual and across major lake types, and thus to recreate the full annual succession of lake CO_2 concentrations and fluxes in these northern landscapes.

4.3 MATERIALS AND METHODS

4.3.1 Study sites and sampling

We targeted three different lakes in the province of Québec (Canada), which were monthly or biweekly sampled during a least one complete year (between 2010 and 2012). The general characteristics of the three lakes are presented in Table 4.1. Lac Croche is a headwater lake surrounded by a pristine watershed dominated by maple (*Acer saccharum*) and yellow birch (*Betula alleghaniensis*) settled on well-drained Ferro-humic podzols (365 meters altitude, 45.99°N, 74.00°W). Lac Simoncouche has a pristine watershed dominated by black spruce (*Picea mariana*) and balsam fir (*Abies balsamea*) settled on podzolic soils (347 meters altitude, 48.23°N, 71.25°W). The lake has two major input streams (each having an upstream lake) and several headwater ephemeral streams that only flow after heavy rains. The southern part of the lake has extensive development of aquatic macrophytes (*Brasenia schreberi*) from June to October (covering up to about 10-15% of total lake area). Lac Hébécourt (273 meters altitude, 48.51°N, 79.38°W) is the shallowest but the largest of the studied lakes and is situated in the Lac Duparquet Research and Teaching Forest (FERLD), a partly managed mix forest dominated by balsam fir (*Abies balsamea*) and white birch (*Betula papyrifera*) settled mainly on glacio-lacustrine clays. The lake has five major stream inputs, four of which are heavily dammed by beavers (*Castor canadensis*).

Table 4.1. Lake general characteristics showing mean values with standard deviation in brackets.

Characteristics	Lac Croche	Lac Simoncouche	Lac Hébécourt
Lake area (ha)	18.1	86.1	775.0
Watershed area (ha)	88	2633	2800
Mean depth (m)	5.1	2.1	2.2
Mean annual air temperature (°C)[a]	2.65	2.57	NA
Ice-free period (days)	202	224	193
Water Residence Time (year)[b]	1.10	0.09	0.48
DOC (mg C L^{-1})[c]	4.6 (±0.5)	6.9 (±0.9)	9.9 (±0.8)
Absorption coefficient at 440nm (m^{-1})[c]	0.8 (±0.2)	1.9 (±0.5)	2.2 (±0.6)
Chlorophyll a (µg L^{-1})[c]	1.4 (±0.7)	1.7 (±0.8)	5.7 (±3.5)
Total phosphorus (µg L^{-1})[c]	4.0 (±1.2)	10.0 (±2.4)	27.6 (±4.7)

[a] measured in 2011
[b] annual average
[c] ice-free season average ± standard deviation
NA = not available for the whole year

4.3.2 Lake, stream and soil water sampling

In each of the three lakes, we performed monthly (weekly in Lac Croche in summer) manual sampling including two sampling points in winter under the ice, in addition to continuous sampling using automated instrumentations (open water season only). For each manual sampling point, a vertical profile (each meter) of temperature, dissolved oxygen, conductivity and pH was performed using a multi parameters probe (Yellow spring instruments, USA). We also performed a vertical profile of pCO_2 by pumping water through a gas equilibration membrane (LiquiCel, Mini module, USA) connected to an infra-red gas analyser (EGM-4, PP systems, Amesbury, USA) (Cole et Prairie, 2009). We calculated PAR extinction coefficient (K_{dPAR}) from the measurements of light in the water column using a PUV profiler (Biospherical Instrument Inc., San Diego, USA) following Frenette *et al.*, (2006). Surface water was sampled (at 0.5m depth at the deepest location of the lake) and brought back to the lab for water chemistry and in vitro incubations. Chlorophyll *a* (chl*a*) samples were analyzed spectrophotometrically following filtration on Whatman (GF/F) filters and hot ethanol (90%) extraction. DOC concentration was measured from 0.45 µm filtered water on an OI-1010 TIC-TOC Analyzer (OI Analytical, College Station, TX, USA) using wet persulfate oxidation. Total phosphorus (TP) was analyzed spectrophotometrically after persulfate digestion.

Each month, we additionally sampled streams flowing into lakes and groundwater from sites close to the lake, for water chemistry, CO_2 concentration and temperature. For groundwater samples, three sets of duplicate piezometers were installed on Lac Croche and Simoncouche catchments and four sets on Lac Hébécourt catchment. Each set consisted of a near-shore piezometer (from 2-5 meters from the shore) and another piezometer farther in the catchment (between 5-10 meters from the lake shore). Piezometers were made of plastic tubes (inner diameter of 2.54 cm) and were placed in the soil at approximately 3-5 meters from the lake shore, to collect soil pore water at

about 20 to 30 cm deep, depending on the soil thickness. Water from each piezometer was collected several times during the year, except in winter. Each time, piezometers were flushed 24 hours prior sampling to discard stagnant waters. When the piezometer was fully replenished (approx. 24 h after flushing), we gently pumped the water out of the piezometer using a peristaltic pump 10 ml into 60 ml syringes (3 replicates) to create a 1:5 air-water ratio, with ambient air of known CO_2 concentration. Syringes were then vigorously shaken for at least 1min to ensure complete equilibrium. Headspace gas were injected in an infra-red gas analyser (EGM-4, PP systems, Amesbury, USA) and pCO_2 of water was back-calculated. Stream water was also sampled each month (including winter). Similar to groundwater, pCO_2 in stream water was measured with the headspace technique, but using a 1:1 ratio.

Automated measurements in Lac Croche and Lac Simoncouche were performed from floating platforms (a detailed description of the platforms is provided in Vachon et del Giorgio, 2014). In brief, hourly measurements of surface water pCO_2 were collected using an infra-red CO_2 probe and dissolved O_2 with optical probes. Water temperature was also hourly measured at each meter from the surface to the lake bottom. No automated dissolved gases measurements were done in Lac Hébécourt, but water temperature was monitored continuously from June to July 2010 using temperature sensors (Onset Hobo Pendant, Accuracy: 0.54° C). We determined the mean CO_2 concentration in the epilimnion ($[CO_2]_{epi}$) by multiplying the daily averaged CO_2 concentration by the epilimnetic volume, determined as the volume over the upper mixed layer depth (Z_{mix}; see Vachon et del Giorgio (2014) for further detail). We also determined the mean CO_2 concentration in the hypolimnion ($[CO_2]_{hypo}$), which is here defined as the volume layer below Z_{mix}. The measurements of CO_2 along the vertical profiles were linearly interpolated between each depth, and the CO_2 concentration at each 0.01m stratum was multiplied by the volume of the corresponding stratum derived from lake bathymetric data. The sum of CO_2 mass in the strata below Z_{mix} was then divided by the hypolimnetic volume to derive a mean CO_2 concentration for the

hypolimnion. Epilimnetic and hypolimnetic volumes were calculated using the hypsographic curves for each lake.

4.3.3 Process rate measurements and empirical models

To reconstruct the CO_2 dynamics and underlying processes for each lake, we first combined monthly measurements conducted in these same systems that have been previously reported: pelagic respiration and depth-integrated estimates of photo-chemical mineralization (Chapter I) as well as daily estimates of GPP (Vachon et del Giorgio, 2014). We additionally measured sediment CO_2 fluxes and estimated hydrologic CO_2 inputs from the catchment, had not been determined in our previous studies and are thus original to this study. We then developed empirical models from these measurements and use previously published relationships to be able to interpolate rates throughout the year. Empirical relationships were finally implemented into a simple process-based model, which is further described below.

Pelagic respiration was measured using in vitro dark incubations, as described in Chapter I. Briefly, unfiltered lake water was incubated at near in situ temperature and O_2 was measured using an optode system (Fibox 3, PreSens, Regensburg, Germany) (Marchand *et al.*, 2009), except for Lac Croche samples and all winter samples, where O_2 was measured using a dual-inlet mass spectrometer (Guillemette et del Giorgio, 2011). Daily rates of O_2 consumption were converted to CO_2 production using a RQ of 1. An empirical relationship predicting pelagic respiration (PR_z) using measurements from all lakes together was built based on water temperature and DOC concentration (Chapter I). In this study, we used this empirical model (accounting for parameter uncertainties) to predict daily epilimnion and hypolimnion respiration rates from linear interpolation of monthly measured DOC concentrations and daily measurements of volume-weighted averaged water temperature (Table 4.2).

Table 4.2. Empirical models and measured parameters used in the models.

Input variables are mean water temperature in the epilimnion or hypolimnion (Tz), mean wind speed at 10m height (U_{10}), incident daily PAR ($iPAR$), lake area (A_{lake}), upper mixed layer depth (Z_{mix}) and dissolved organic carbon concentration ([DOC]). We assumed a 0.92 factor for surface water reflectance in the E_m equation (Kalff, 2002). LC is for Lac Croche, LS is for Lac Simoncouche and LH is for Lac hébécourt.

	symbol	units	Equation or value	source
Empirical models				
volumetric pelagic respiration[a]	PRz	$mg\ C\ m^{-3}\ d^{-1}$	$10^{(-0.19(\pm0.27)\ +\ 0.05(\pm0.01)Tz\ +\ 1.1(\pm0.27)\ \log10[DOC])}$	Chapter I
standardized gas transfer velocity[b]	k_{600}	$cm\ h^{-1}$	$2.51(\pm0.99) + 1.48(\pm0.34) \times U_{10} + 0.4(\pm0.08) \times U_{10} \times \log_{10}A_{lake}$	Vachon et. Prairie, (2013)
Sediment respiration	SR	$mg\ C\ m^{-2}\ d^{-1}$	$10^{(0.036\ (\pm\ 0.002)\times Tz + 1.635\ (\pm0.023)}$	Gudasz *et al.*, (2010)
Other equations and parameters				
gas transfer velocity for CO_2	k_{CO2}	$m\ d^{-1}$	$k_{600} \times (SC_{CO2}/600)^{-0.67} \times (24/1000)$	Jahnee (1987)
Schmidt number	SC_{CO2}		$1800.6 - 120.1*Tz + 3.7818*Tz^2 - 0.047608*Tz^3$	Wanninkhof, (1992)
Mean water column PAR	E_m	$mol\ m^{-2}\ d^{-1}$	$0.92 \times iPAR \times \frac{(1-e^{(-Kd\times Zmix)})}{(Kd\times Zmix)}$	measured
PAR extinction coefficient	Kd	m^{-1}	$0.10\ (\pm0.05) \times [DOC]^{1.22(\pm0.22)}$	modeled
Light specific GPP (*see* Eq. 4.1)	$iota$	$mg\ C\ mol^{-1}\ m^{-1}$	25.4 (± 9.2) in LS, 23.8 (± 11.9) in LC and 31 in LH	measured
proportion of surface water to total water inflow	α		0.9 (± 0.1) for LH, 0.67 (± 0.17) for LS and 0.05 (± 0.01) for LC	measured
surface water [CO_2]	CO_2sw	$mg\ C\ m^{-3}$	1.73 (± 0.88) for LH and 0.77 (± 0.37) for LS	measured
groundwater [CO_2]	CO_2gw	$mg\ C\ m^{-3}$	19.3 (± 2.0) for LH, 10.4 (± 1.7) for LS and 9.1 (± 1.7) for LC	measured

Depth-integrated DOC photo-mineralization was assessed in the three lakes using a combination of filtered water exposure to artificial sunlight at constant temperature (Q-sun, Xe1, Xenon test chamber), in situ measurements of light extinction coefficient, and irradiance modeling (corrected for cloud cover, reflectance and cosine), as described in detail in Chapter I of this thesis. In this study, we used and report the daily rates from interpolation (normal spline interpolation) of monthly depth-integrated photo-chemical DOC mineralization reported in Chapter I, assuming no error around the values.

Gross primary production was assessed using free water O_2 diel curve technique (Vachon et del Giorgio, 2014). Briefly, the changes in surface water O_2 over time can be assumed to be driven by gas exchange with the atmosphere, respiration and primary production. GPP can be calculated as $GPP = \Delta O_2 + R - (D/Z_{mix})$, where GPP is the sum of changes in O_2 concentration in the surface water (ΔO_2) and respiration rates (R) (from night time O_2 decrease), minus the gas exchange rate with the atmosphere (D) (corrected for Z_{mix}). GPP rates were converted into C rates (mg C m^{-3} d^{-1}) assuming a quotient of 1. For the daily interpolation throughout the year, we normalized the 7-days averaged estimates for Lac Simoncouche and Lac Croche by the 7-days averaged light (PAR) available in the upper mix layer to calculate a light corrected GPP parameter (*iota*) specific for each lake (Table 4.2), and described as:

$$iota\ (\text{mg C mol}^{-1}\ \text{m}^{-1}) = \frac{GPP(\text{mg C m}^{-3}\ d^{-1})}{E_m(\text{mol m}^{-2}\ d^{-1})} \quad (4.1)$$

where *iota* is the CO_2 uptake (mg C m^{-3} d^{-1}) per PAR available in the upper mixed layer (mol photons m^{-2} d^{-1}), *GPP* is the 7-days averaged GPP and E_m is the corresponding 7-days averaged PAR light in the upper mixed layer (Table 4.2). E_m was estimated from incident PAR and extinction coefficient (K_{dPAR}; Table 4.2). Daily K_{dPAR} was modeled as a function of DOC concentration (the empirical relationship details are in the Supporting Information). *iota* value from Lac Croche was lower than Lac

Simoncouche, although Lac Croche values were more variable (Table 4.2). Because we had technical problems with the O_2 probe in Lac Hebecourt, *iota* value was extrapolated based on TP concentrations (see Supporting Information for details).

To complete the reconstruction of lake CO_2 dynamics, we additionally estimated sediments CO_2 fluxes and estimated hydrologic CO_2 inputs from the catchment. We used the temperature-dependant model from Gudasz *et al.*, (2010) to generate daily sediment CO_2 fluxes (accounting for parameter uncertainties; see Table 4.2) as a function of water temperature (assuming that sediment temperature is identical to the overlaying water). Sediment CO_2 fluxes from sediment cores incubations were in good agreements with the published empirical model using boreal lake sediment respiration and water temperature (Gudasz *et al.*, 2010) (details in the Supporting Information).

To assess the hydrologic CO_2 import from the catchment, we measured stream and groundwater CO_2 concentrations and combined these measurements with the hydrologic budget from each lake. For each lake, stream water CO_2 and groundwater CO_2 concentrations were considered constant through time. Daily hydrological CO_2 inputs were estimated as the sum of surface water CO_2 loading (stream $[CO_2]$ x stream water input) and groundwater CO_2 loading (groundwater $[CO_2]$ x groundwater discharge). Calculations of the water mass balances and attribution of surface and groundwater discharges for each lake in detailed in Supporting Information.

4.3.4 Process-based model

In order to have daily interpolations of the measured and estimated rates of the major processes influencing CO_2 dynamics in a coherent manner, we developed a simple process-based model, which was mainly driven by empirical relationships built mostly from our own measurements (either presented in the study or reported from previous work). For the modeling exercise, each lake was considered as two well-mixed compartments corresponding to the epilimnion and hypolimnion (the latter comprising the metalimnion as well), and each compartment having its own CO_2 pool (CO_{2epi} and CO_{2hypo}). The governing equations of the process-based model are described in Table 4.3 and the associated empirical relationships and measured fixed parameters are presented in Table 4.2. The model predicts CO_2 mass in epilimnion and hypolimnion based on the inputs of CO_2 (*PR*, *PM*, *SR* and CO_{2in}), the losses of CO_2 (*GPP*, *aFlux* and CO_{2out}), and the exchange between epi- and hypolimnion (*vFlux*) (Table 4.3). Molecular diffusion between layers was assumed to be negligible, however, we modeled CO_2 mass transport (turbulent mixing) between layers when Z_{mix} changed depth (analogous to thermocline erosion). When Z_{mix} increased, hypolimnetic volume decreased, thus transferring its CO_2 mass to the surface layer. Similarly, if Z_{mix} decreased, hypolimnetic volume increased and gained CO_2 mass from the epilimnion (Table 4.3). We acknowledge that chemical re-equilibration of the carbonate system can remove CO_2 for example via carbonate dissolution, or sometimes produce CO_2 if the system receives acids or additional carbonate that is being precipitated. These chemical processes can significantly influence CO_2 dynamics in high alkalinity systems (Cole et Prairie, 2009), however, because our lakes have low alkalinity (< 0.7 meq L^{-1}), we assume that chemical re-equilibration of the carbonate system is negligible compared to the other biological and physical processes.

Table 4.3. Differential and intermediate equations

Q_{in} is derived from Eq. S4.1, V_{epi} is the epilimnetic volume, V_{hypo} is the hypolimnetic volume, A_{lake} is the lake area, A_{epi} is the epilimnetic sediments area, A_{hypo} is the hypolimnetic sediments area, $dVol$ is the volume of water transferred between the two compartments where positive values are transfers from hypolimnion to epilimnion. Other parameters are described in Table 4.2. All rates are in $g\ C\ d^{-1}$

differential equation	*symbol*	*equation*
epilimnetic CO_2 mass	$\frac{dCO_{2epi}}{dt}$	$CO_{2in} + PR + PM + sFlux + vFlux - GPP - aFlux - CO_{2out}$
hypolimnetic CO_2 mass	$\frac{dCO_{2hypo}}{dt}$	$PR + SR - vFlux$
intermediate equations		
CO_2 input	CO_{2in}	$\alpha \times Q_{in} \times [CO_{2sw}] + (1-\alpha) \times Q_{in} \times [CO_{2gw}]$
respiration rates	PR	$PR_z \times V_{epi}(or\ V_{hypo})/1000$
photo-mineralization	PM	$aPM \times A_{lake}/1000$
sediment flux	$sFlux$	$SR \times A_{epi}(or\ A_{hypo})$
vertical CO_2 mass transport	$vFlux$	*if* Z_{mix} *increases:* $vFlux = dVol \times [CO_{2hypo}]$ *if* Z_{mix} *decreases:* $vFlux = dVol \times [CO_{2epi}]$
gross primary production	GPP	$iota \times E_m \times V_{epi}/1000$
air-water flux	$aFlux$	$k_{CO2} \times ([CO_{2epi}] - CO_{2Atm}) \times A_{lake}$
CO_2 output	CO_{2out}	$Q_{out} \times [CO_{2epi}]$

Modeled rates of each process with associated uncertainties were estimated as a function of their respective input variables (Table 4.2), organized in a set of timeseries. We set up input time-series data from the measurements made in all the lakes for at least an annual cycle (usually equivalent to more than 400 consecutive days), which includes epilimnetic and hypolimnetic water temperature, Z_{mix} data, lakes and layers volumes, Q_{in}, Q_{out}, wind speed, PAR, DOC and Chla (see Supporting Information for meteorological time series). Some input time series were however incomplete (i.e. monthly or weekly measurements; e.g. DOC and chl*a* concentrations) and were thus linearly interpolated. We then ran the model using these time series of data inputs. We also determined the ice cover length for each lake from in situ observation and we assumed no gas exchange with the atmosphere and no GPP when lakes were covered with ice. The model ran for each lake (at least a complete year) with 999 iterations, wherein each iteration a random selection of parameters was made from normal distribution determined from the mean and standard deviation values (or error in the case of regression parameters; Table 4.2) along with a Monte Carlo simulation. As a result, the estimates of each process rate and of CO_2 concentration were associated with an uncertainty distribution around there mean. It is important to note that mean modeled values of CO_2 completely emerged from the empirical models (having their own parameters), and thus no parametrization routines were performed. We however validate the use of the process-based model by calculation the fit (coefficient of determination, R^2) between predicted CO_2 concentrations by the model and measured ambient CO_2 concentrations:

$$R^2 = 1 - \left(\frac{SS_{res}}{SS_{tot}}\right) \tag{4.3}$$

where SS_{tot} is the total sum of squares and SS_{res} is the residual sum of squares.

Process rates will be presented as absolute daily rate (mg C m^{-2} d^{-1}), seasonal-averaged (mg C m^{-2} d^{-1}) and annual (g C m^{-2} y^{-1}). We calculated mean seasonal rates of the major

processes, by clustering rates by season (spring, summer, fall and winter). The spring period was considered as the 20-day period after ice melt, which usually corresponds to the time needed to the lake to stratify thermally. Summer was considered as the thermally stratified period, fall was considered as the period where lake water column is completely mixed (about 50 days), and winter is considered as the ice covered period. Relative contribution (%) of process producing (or importing) CO_2 is calculated as the absolute rate of the process divided by the sum of the four major process (PR, SR, PM and CO_{2in}). We further calculated seasonal and annual lake net ecosystem metabolism (NEM) as: PR+SR-GPP.

4.4 RESULTS

4.4.1 Lake CO_2 concentration dynamics

Measured CO_2 concentration in the surface water followed a consistent temporal pattern in all lakes, with relatively low (but over the atmospheric concentration) and constant levels of around 0.23-0.32 mg C L^{-1} (pCO_2 of about 520-630 µatm) throughout the summer (Figure 4.1). There were also significant CO_2 accumulations during winter in all lakes and in the bottom layers of stratified lakes (i.e. Croche and Simoncouche), reaching water-column averaged CO_2 concentrations of around 3.5-4.5 mg C L^{-1} (Figure 4.1). Additionally, high values of surface water CO_2 concentrations (values ranging between under ice and summer values) were also measured in spring, right after ice melt. Measured surface water CO_2 concentrations also increased episodically during the open water season, particularly in Lac Simoncouche in July and August, and in Lac Croche towards the end of September (Figure 4.1). During those short-lasted events, the measured surface water CO_2 concentration nearly doubled compared to the average summer level, and reached almost 1 mg C L^{-1} (pCO_2 of about 1500 µatm).

The CO_2 concentrations measured in the two streams flowing into Lac Simoncouche varied between 0.30 and 1.77 mg C L^{-1}. In the streams flowing into Lac Hébécourt, measured CO_2 concentrations varied between 0.1 mg C L^{-1} in summer and 15.5 mg C L^{-1} in winter. The average (±SD) CO_2 in streams used in the model was 0.76 (± 0.37) and 1.73 (± 0.88) mg C L^{-1} for Simoncouche and Hébécourt, respectively. Note that winter stream CO_2 in winter for Lac Hébécourt were excluded from the average because of the extreme variability caused by ice cover. The measured CO_2 concentrations in the groundwater were generally higher than stream concentrations, and varied between 2.6 and 80.2 mg C L^{-1}. The averaged measured groundwater CO_2 concentration was higher in the Lac Hébécourt catchment, averaging 19.3 mg C L^{-1},

compared to Lac Simoncouche (10.4 mg C L^{-1}) and Lac Croche (9.1 mg C L^{-1}; Table 4.2).

Our process-based model, which integrates the empirical relationships discussed above and measured lake physical conditions, was able to recreate reasonably well the observed patterns in surface and bottom layer CO_2 concentrations in all lakes (Figure 4.1). In particular, the model effectively predicted not only the average CO_2 in each of the lakes, but also key events in the annual cycle, such as the large increases in surface CO_2 concentrations linked to storms events (i.e. October-November in Lac Croche and August-September in Lac Simoncouche). The model predictions for winter, however, were less precise for all lakes (Figure 4.1). Overall, however, the model consistently yielded fits over r^2 of 0.60, except in the hypolimnion of Lac Croche.

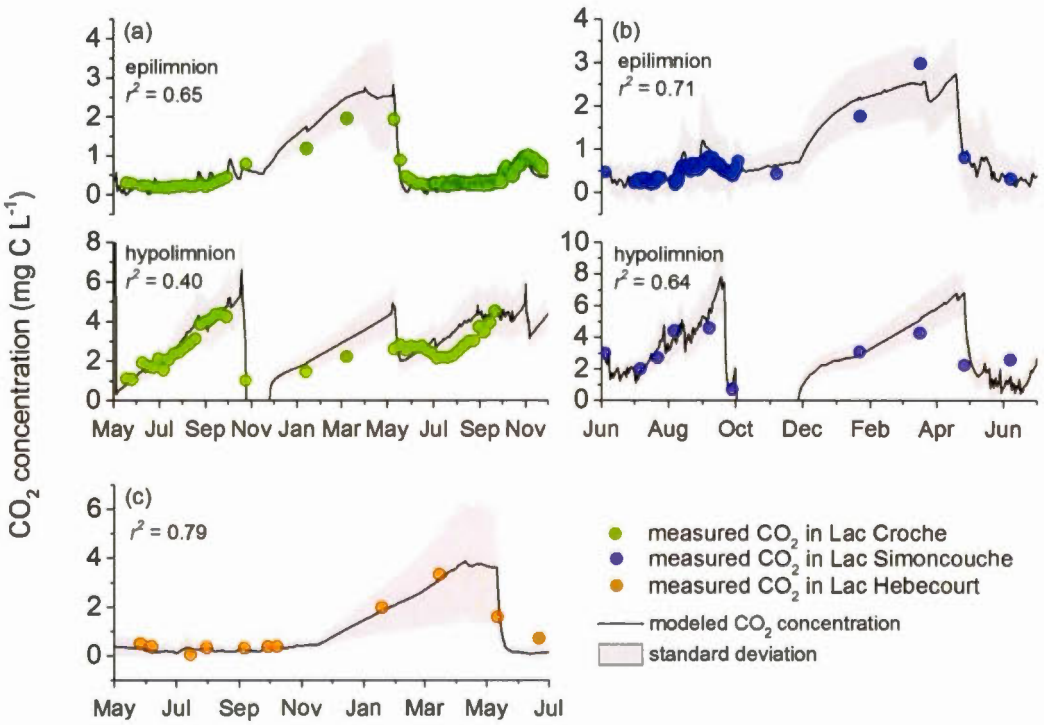

Figure 4.1. Surface and bottom CO_2 concentrations

Measured and modeled surface and bottom CO_2 concentrations in Lac Croche (a), Lac Simoncouche (b) and Lac Hébécourt (c). In each graph, colored circles are the measured CO_2 concentrations and the solid black line is the simulated concentration (with standard deviation resulting from the MC simulation in light grey area).

4.4.2 Reconstructing the sources of CO_2 in northern lakes

Using a series of measurements and empirical models within a mechanistic model framework, we were able to reconstruct the dynamics of the major underlying processes influencing CO_2 concentrations and fluxes with the atmosphere. Figure 4.2 shows daily rates of gross primary production, pelagic and sediment respiration, photo-chemical CO_2 production, and hydrologic CO_2 inputs for each lake. At the whole lake scale, sediment and pelagic respiration areal rates were comparable (accounting for differences in morphometry), both showing summer production up to around 200 mg C m^{-2} d^{-1} in Lac Croche, 100-300 mg C m^{-2} d^{-1} in Lac Simoncouche and up to 300-500 mg C m^{-2} d^{-1} in more productive Lac Hébécourt. At low water temperatures (in winter, early spring and late fall), the pelagic and sediment respiration rates were both low, oscillating around 20 and 80 mg C m^{-2} d^{-1} in all lakes. These low temperature respiration rates were comparable to the highest photo-chemical DOC mineralization rates, which were found in spring, right after ice melt (Figure 4.2). In summer, however, photo-mineralization rates were much lower, around 10-20 mg C m^{-2} d^{-1}, which is comparable to winter under ice pelagic respiration of a shallow lake (for example, average pelagic respiration under ice was 15.7 mg C m^{-2} d^{-1} in Lac Simoncouche).

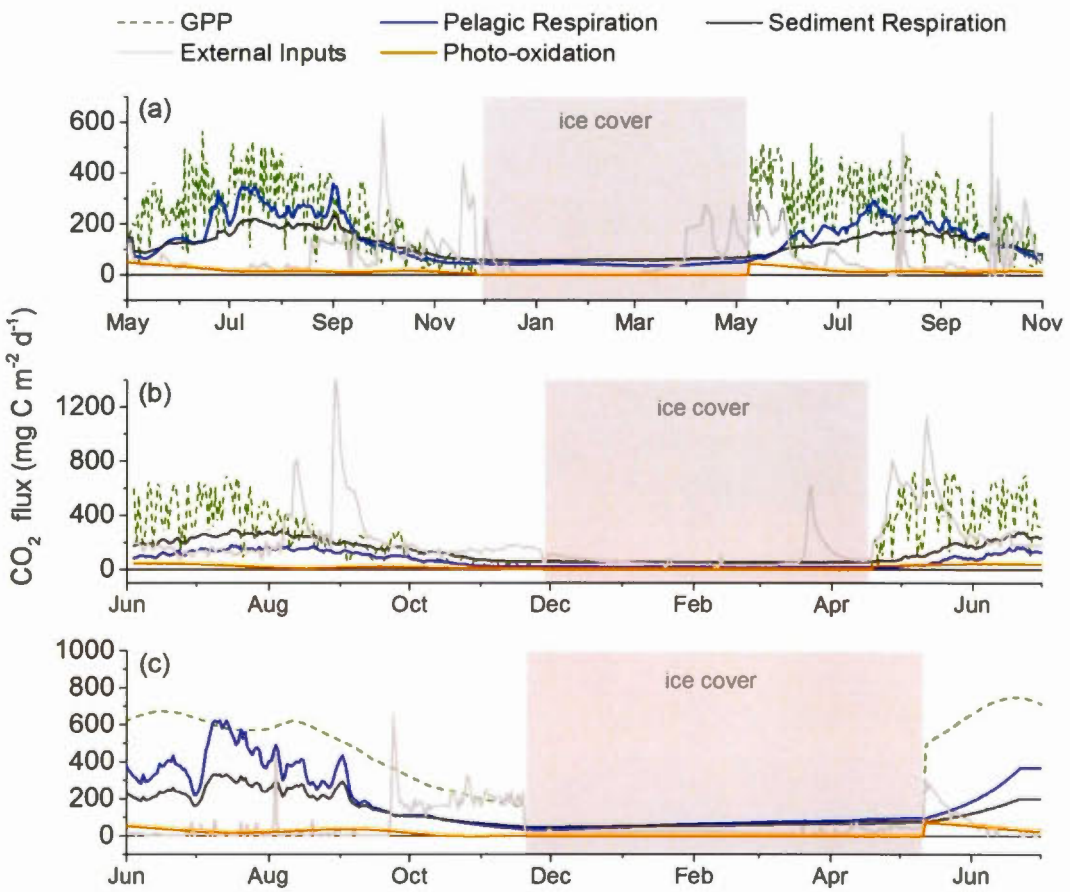

Figure 4.2. Temporal dynamics of the major processes producing CO_2

Daily rates (mg C m^{-2} d^{-1}) of the major processes affecting CO_2 fluxes with the atmosphere over an annual cycle. The presented processes are gross primary production (green) pelagic respiration (blue), photo-chemical DOC mineralization (orange), sediment respiration (dark grey), and hydrologic CO_2 inputs from the catchments (light grey) in (**a**) Lac Croche, (**b**) Lac Simoncouche (**c**) and Lac Hébécourt. Note that gross primary production (GPP) is presented as a positive value for presentation purpose only. GPP is actually removing CO_2 from the water.

Table 4.4. Average seasonal CO_2 fluxes

Average seasonal CO_2 fluxes, where fCO_2 is the lake CO_2 flux to the atmosphere, ΔCO_2 is the mean daily change in whole-lake CO_2 mass, *PR* is the whole water column pelagic respiration, *PM* is the photo-chemical DOC mineralization, *SR* is the sediment respiration, CO_{2in} is the hydrologic CO_2 inputs, CO_{2out} is the CO_2 export at the lake exit and *GPP* is the gross primary production. NEM is the net ecosystem metabolism, which is the sum of *PR*, *SR* and *GPP*. All rates are presented in mg C-CO_2 m^{-2} (lake) d^{-1} for seasonal and g C-CO_2 m^{-2} (lake) y^{-1} for annual. Shaded area identifies the processes adding CO_2 to the lake.

	fCO_2	ΔCO_2	*PR*	*PM*	*SR*	CO_{2in}	CO_{2out}	*GPP*	*NEM*
Spring									
Croche	-646.2	-651.5	72.7	38.5	80.6	215.9	-30.0	-383.1	-229.8
Simoncouche	-364.5	-198.2	21.1	26.7	74.2	491.8	-114.4	-333.1	-237.8
Hébécourt	-463.9	-594.6	131.8	60.5	94.2	160.2	-32.4	-545.0	-319.0
Summer									
Croche	-101.9	+17.7	190.5	16.7	144.5	53.5	-0.9	-284.7	50.3
Simoncouche	-255.1	+0.9	127.4	23.4	218.0	256.2	-44.0	-325.0	20.4
Hébécourt	-58.1	+4.4	339.3	28.6	223.9	30.7	0.0*	-559.9	3.3
Fall									
Croche	-300.6	-122.8	77.1	12.4	92.4	100.8	-5.2	-99.8	68.3
Simoncouche	-195.1	-3.5	36.7	7.5	87.0	139.5	-23.1	-56.0	100.6
Hébécourt	-88.6	+15.4	71.0	1.4	76.1	182.5	-9.8	-217.2	-70.1
Winter									
Croche	0.0	+106.6	42.7	0.0	60.4	50.9	-47.4	0.0	103.0
Simoncouche	0.0	+32.5	15.7	0.0	53.7	73.3	-110.3	0.0	69.4
Hébécourt	0.0	+122.9	64.6	0.0	58.3	21.4	-76.2	0.0	122.9
Annual									
Croche	-43.2	-1.5	36.8	3.6	34.9	24.4	-8.7	-49.3	22.4
Simoncouche	-55.5	+0.7	21.7	4.7	44.1	71.5	-26.5	-60.6	5.2
Hébécourt	-21.4	+0.6	59.4	4.9	43.5	20.0	-14.1	-91.6	11.2

*zero CO_{2out} flux is due to the temporary presence of a beaver dam at the lake exit

Hydrologic CO_2 inputs were by far the most variable flux in all lakes, showing episodic events of extreme CO_2 fluxes from the catchment to the surface water of lakes. These rapid and intense bursts of hydrologic CO_2 inputs sometimes represented up to 6 fold the inputs of CO_2 through in situ respiration rates (Figure 4.2). The general pattern in hydrologic CO_2 inputs was similar across the three lakes, characterized by large fluxes in spring, starting at or before ice melt, and lasting for several weeks thereafter. Similarly, in late summer and fall, increases in precipitation often resulted in large pulses in external CO_2 loading. Lac Simoncouche was particularly affected by intense and brief hydrologic CO_2 inputs, especially in late summer when two important rain storms occurred, resulting in daily fluxes up to 800 and 1200 mg C m^{-2} d^{-1} after rain storms. Lac Simoncouche also showed a higher baseline level of constant hydrologic CO_2 inputs of about 150-200 mg C m^{-2} d^{-1}, which is comparable in magnitude to pelagic and sediment respiration during summer (Figure 4.2). In Lac Croche and Lac Hébécourt, this baseline level was lower at around 10-30 mg C m^{-2} d^{-1}, more comparable to photo-mineralization fluxes.

Lake CO_2 emission is the resulting balance between processes that produce CO_2 and remove CO_2 in the water column. Table 4.4 presents the mean seasonal rates and fluxes and its complementary Figure 4.3 shows the relative contribution of the major processes producing (or importing) CO_2. All lakes showed greater CO_2 fluxes to the atmosphere in spring, ranging from 364.5 to 598.4 mg C m^{-2} d^{-1}. During this period, the major process sustaining CO_2 emissions was the release of accumulated CO_2 under the ice during winter, which accounted for 50 to 100% of the spring emissions (ΔCO_2; Table 4.4). Beside this release of under-ice accumulated CO_2, spring CO_2 emissions were also largely sustained by hydrologic CO_2 inputs, especially in Lac Simoncouche (Table 4.4) where this process contributed up to 80% of the lake total CO_2 production (Figure 4.3). The contribution of hydrologic CO_2 inputs was lower in Lac Croche and Lac Hébécourt, but were still substantial (between 36-56%; Figure 4.3). GPP rates were larger than the sum of *PR* and *SR* (negative NEM) in spring, implying that net

metabolism resulted in a removal CO_2 from the surface water (Table 4.4). In summer, all lakes were largely influenced by pelagic and sediment respiration, contributing to between 50-90% of the lake total CO_2 production. In Lac Simoncouche, summer hydrologic CO_2 inputs were also significant, sustaining slightly more than 40% of the lake total CO_2 production (Figure 4.3). In all lakes, the sum of PR and SR was larger than GPP (positive NEM; Table 4.4). In fall, the higher CO_2 emissions observed in Lac Croche were partly due to the release of hypolimnetic CO_2 accumulated during the summer stratification, which was not the case Lac Simoncouche and Lac Hébécourt (Table 4.4). Hydrologic CO_2 inputs were higher in all lakes in fall, contributing around 40-55% of the total lake CO_2 production (Figure 4.3). Respiration rates (PR and SR) in fall were also significant, and together larger than GPP (positive NEM), except in Lac Hébécourt (Table 4.4). In winter, all the major processes except for photo-mineralization contributed roughly equally.

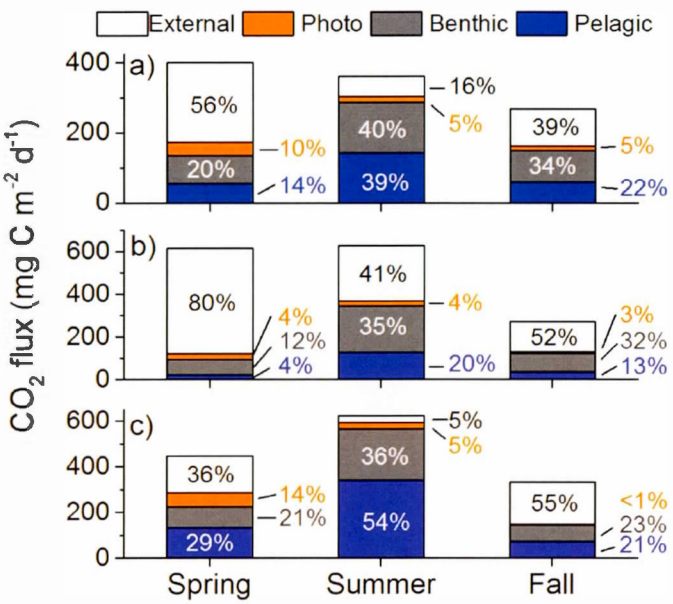

Figure 4.3. Relative contribution of the major processes

Relative contributions of the major processes producing (or importing) CO_2 to the three studied lakes, and clustered by season in (**a**) Lac Croche, (**b**) Lac Simoncouche and (**c**) Lac Hébécourt. White bars represent the external CO_2 inputs, orange bars represent the photo-mineralization, grey bars represent sediment respiration and blue bars represent pelagic respiration.

Over an annual cycle, all lakes showed to be net source of CO_2 to the atmosphere, with CO_2 emissions between 21.4 to 55.5 g C m^{-2} yr^{-1} (Table 4.4). Lac Croche showed a net CO_2 production of 43.7 g C m^{-2} yr^{-1}, of which 58% derived from hydrologic CO_2 inputs, 30% from net ecosystem metabolism, and 8% from photo-mineralization (Figure 4.4). Lac Simoncouche showed greater net CO_2 production of 82.0 g C m^{-2} yr^{-1}, derived from hydrologic CO_2 inputs (87%), net ecosystem metabolism (6%) and photo-mineralization (6%) (Figure 4.4). In Lac Hébécourt, net CO_2 production was 36.1 g C m^{-2} y^{-1}, of which 55% derived from hydrologic CO_2 inputs, 31% from net ecosystem metabolism, and 13% from photo-mineralization (Figure 4.4).

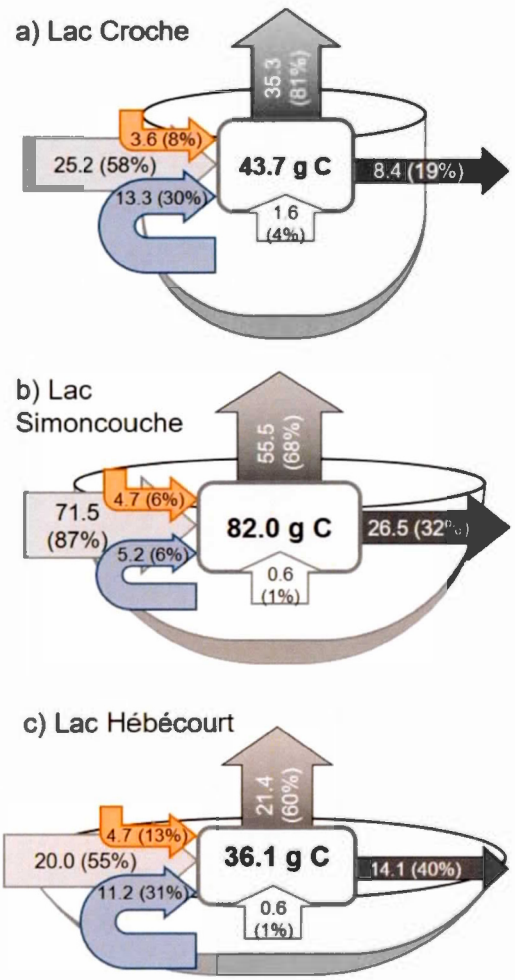

Figure 4.4. Annual CO_2 budget in the study lakes

Annual CO_2 budget in **a)** Lac Croche, **b)** Lac Simoncouche and **c)** Lac Hébécourt. The central white square in each lake is the total lake CO_2 production (g C m^{-2} y^{-1}) as the sum of photo-mineralization (orange arrow), net ecosystem metabolism (blue arrow), hydrologic CO_2 inputs (light grey arrow) and change in CO_2 mass (small arrow below the central square). Outputs of CO_2 as emission to the atmosphere (grey arrow facing up) and outflow (dark grey arrow). All inputs (black font) and output (white font) rates are in g C m^{-2} y^{-1} with their proportion to total lake CO_2 production in brackets. Rates are also showed in Table 4.4.

4.5 DISCUSSION

The temporal dynamics of dissolved CO_2 concentration and emissions in lakes result from the complex interplay of the several biotic and abiotic processes and temporal succession of their relative importance. Studies that are restricted to a specific period or a single process only yield a snapshot picture that is unlikely to represent the entire lake and annual cycle and will thus miss fundamental functioning of the ecosystem. Taking point measurements over the course of a year certainly leads to improved C budgets (Ducharme-Riel *et al.*, 2015; Finlay *et al.*, 2015), but there are still major uncertainties in the interpolation between measurements, especially in terms of episodic events that may nevertheless be critical to the annual budget (Jennings *et al.*, 2012; Vachon et del Giorgio, 2014). The increasing use of automated sensors, allowing high frequency sampling of key lake properties, has substantially improved the temporal coverage of lake CO_2 dynamics and other complementary data (Huotari *et al.*, 2009; Vachon et del Giorgio, 2014). These approaches, however, provide only limited information on the underlying mechanisms that generate and remove CO_2 in the surface of lakes, and therefore little insight on the drivers of the observed magnitude and seasonal variability of lake CO_2. In this regard, mechanistic modeling of lake carbon cycle has clear advantages (Cardille *et al.*, 2007; Hanson *et al.*, 2004; Hanson *et al.*, 2014a), yet results of this approach must interpreted with caution, especially when measured data are limited, numerous underlying assumptions are made or when parameters choice is performed in unrealistic manners. Here we have attempted to overcome some of these limitations by using a combination of high-frequency measurements of lake CO_2 masses and fluxes, with multiple measurements of process rates, interpolated in time and integrated at the lake scale using a simple modeling approach to ensure coherence between the different fluxes. Although we use an extensive set of field measurements and laboratory incubations providing monthly rates of the major processes, we still had to make several assumptions and simplify processes. Even though, we succeeded in recreating the overall magnitude and the main

features of the annual CO_2 budget of three northern lakes, something that has never before been reported at this level of detail.

4.5.1 Seasonal dynamic of processes producing CO_2 in lakes

Reconstructing the CO_2 dynamic within a common framework in three different lakes allowed us to compare the magnitude and relative contribution of the major processes involved in lake CO_2 dynamics over an annual cycle. We first focused on four major processes producing or importing CO_2 to the surface of lakes: pelagic respiration, benthic respiration, external CO_2 inputs and photo-chemical CO_2 production. We found that all four processes systematically contributed in sustaining CO_2 oversaturation and annual emissions in all three lakes, although the relative importance of each process did vary along the seasons. Among the different lakes, the relative contribution of the CO_2 production processes thus followed a consistent seasonal pattern, which may be induced by the roughly similar pattern in temperature, irradiance and precipitation that these northern lakes experienced. During the warm period of summer, pelagic and benthic respiration rates were the highest and were both the dominant processes producing CO_2 (Figure 4.2). In spring and fall, however, when the water column was colder, the relative contribution of pelagic and sediment respiration decreased substantially in all lakes. During those periods, the relative importance of photo-chemical CO_2 production (Chapter I) and hydrologic CO_2 inputs thus increased. In spring, the substantial hydrologic CO_2 inputs during the freshets was the dominant process (Figure 4.2), and similarly in fall, higher precipitation and storms event may have contributed to increased CO_2 loading to lakes (Vachon et del Giorgio, 2014). We suggest that this general seasonal pattern, wherein hydrologic CO_2 inputs dominate in spring/fall and respiration in summer, is likely synchronized by comparable climatic patterns in temperature and precipitations among the study lakes (Vogt *et al.*, 2011).

The common pattern observed in the relative contribution of each process among the lakes was however modulated DOC content, hydrologic regime and morphometry, which were specific to each lake. These lake properties thus tend to promote specific pathways, particularly respiration and hydrologic CO_2 inputs. In short WRT lakes, Lac Simoncouche in particular, each season was largely influenced by hydrologic CO_2 inputs compared to the other lakes (Figure 4.3), which consistently contributed over 40% of the total lake CO_2 production over the whole open-water season. The net hydrologic annual CO_2 input (CO_2in – CO_2out) in Lac Simoncouche was similar to a short water residence time north temperate lake (Lake Shingobee; 48 g C m^{-2} yr^{-1}; Stets *et al.*, 2009). In comparison, longer WRT lakes showed smaller net hydrologic CO_2 inputs (15.7 and 5.9 for Lac Croche and Lac Hébécourt, respectively), in agreement with long WRT lake William (3.7 g C m^{-2} yr^{-1}; Stets *et al.*, 2009). Consequently, the relative importance of internal processes may be greater in longer WRT lakes. For example, Lac Hébécourt CO_2 production was predominately dominated by pelagic and sediment respirations, which together always contributed over 40% of the lake total CO_2 production throughout the annual cycle. In relatively deeper lakes (e.g. in Lac Croche), as the whole water column contribution to DOC biological mineralization, respirations contribution can also be relatively more important to the whole lake total CO_2 production, especially in summer. This suggests that in long WRT lakes (in which here are also either deeper or have higher DOC concentration) the CO_2 dynamics would be more internally regulated. Lake depth, WRT or DOC concentration did not seem to influence photo-chemical CO_2 production, as all lakes showed similar photo-chemical CO_2 production rates on an annual basis (Table 4.4, Figure 4.4). Its relative contribution however was greater in shallow lakes and smaller contribution in high DOC or deeper lakes, which is even more important when we only look at the water-column production (Chapter I). Overall, our results suggest that ecosystem properties like DOC content, hydrologic regime and lake morphometry clearly influence the predominant process supplying CO_2 to the lakes, which properties have already been linked to lake CO_2

dynamics and emissions (Ducharme-Riel *et al.*, 2015; Kankaala *et al.*, 2013; Stets *et al.*, 2009).

4.5.2 Patterns in CO_2 emissions from northern lakes

The observed CO_2 fluxes with the atmosphere result from the balance of all the physical, chemical and biological processes which simultaneously remove and add CO_2 to the lakes. Since multiple processes are involved, it is thus difficult to attribute the CO_2 emission to a single process. Rather, there are different combinations of processes and events resulting in CO_2 emissions that are more likely to happen in certain type of lake or season. For example, even if CO_2 production by the various processes described above are minimized, intense CO_2 emissions can be observed resulting from the decrease of the lake CO_2 mass. This is what is happening after ice melt, when the accumulation and release of CO_2 during winter under the ice greatly contributed to spring CO_2 emissions, a pattern widely observed in boreal lakes (Ducharme-Riel *et al.*, 2015; Karlsson *et al.*, 2013; Striegl *et al.*, 2001). During this short period, all three lakes consistently showed peaks in CO_2 emissions, of which 50 to 100% were explained by the release of CO_2 accumulated under the winter ice (reflected in the negative values of ΔCO_2 in Table 4.4). Similarly, Lac Croche showed significant CO_2 accumulation during summer (mean ΔCO_2 of 15.8 mg C m^{-2} d^{-1}), and this CO_2 was released in fall during the turnover thus contributing significantly to fall CO_2 emissions. There is evidence that this pattern of accumulation and release are more pronounced in deeper lakes (Ducharme-Riel *et al.*, 2015), which is here the case for Lac Croche, and thus influences the seasonal CO_2 emission pattern in those systems.

Besides this accumulation and release process which creates period of high CO_2 emissions, it is the balance between production (or import) and consumption (or export) that dictates the magnitude of pCO_2 oversaturation in the surface of lakes, and thus fluxes with the atmosphere. Lake pCO_2 oversaturation is influenced by the balance

between respiration and primary productivity (P/R ratio; del Giorgio *et al.*, 1999). At first sight, however, GPP was always larger than PR (Table 4.4), which would suggest net removal of CO_2. This apparent net ecosystem autotrophy may however be influenced by the approach used to derive the estimates of GPP and its spatial integration. The GPP estimates were based on free-water O_2 measurements in the center of the lake (Vachon et del Giorgio, 2014), and this method integrated pelagic primary production by phytoplankton and, to a certain extent, macrophytes and periphyton production in the littoral zones (Bogert *et al.*, 2007; Vadeboncoeur *et al.*, 2008). Moreover, autochthonous organic carbon from primary production is usually mineralized in sediments. Therefore, to properly evaluate the net metabolism balance at the whole lake scale, we must integrate the benthic and pelagic processes together. Including *SR* and *PR* usually resulted in P/R ratios < 1, and thus positive NEM (i.e. net CO_2 production) in all the lakes, except in spring, where NEM was transiently removing surface water CO_2. Net ecosystem production (i.e. net CO_2 removal) is usually observed in spring and summer season in eutrophic temperate lakes, mainly due to phytoplankton blooms (Laas *et al.*, 2012; Staehr *et al.*, 2010a). In oligo-mesotrophic lakes, however, we suggest that the combination of constrained respiration by cold temperature and enhanced GPP by the high surface water CO_2 availability (from under ice accumulation and hydrologic inputs) and high irradiance may have caused these negative NEM (net CO_2 consumption) rates in spring. Positive NEM was likely to be more prevalent in fall and winter (Table 4.4), probably because of the reduced (or the absence of) primary production.

The positive NEM further suggests that lakes have to mineralize significant amount of allochthonous DOC (DOC_{alloch}) by biological respiration in both pelagic and benthic environments, in addition if the photo-mineralized DOC_{alloch}. Annual rates of DOC_{alloch} mineralization, estimated as the sum of NEM and PM, were 16.9 g C m^{-2} y^{-1} for Lac Croche, 9.9 g C m^{-2} y^{-1} for Lac Simoncouche, and 16.1 g C m^{-2} y^{-1} for Lac Hébécourt. In long water residence time (WRT) lakes (like Lac Hébécourt and Lac Croche), a

greater proportion of the incoming DOC_{alloch} has been mineralized, while in Lac Simoncouche (which has a shorter WRT), a smaller proportion of DOC_{alloch} was mineralized. This pattern was also found in others boreal lakes in Canada (Dillon et Molot, 1997) and Sweden (Algesten *et al.*, 2003), and suggest that the transit time of DOC_{alloch} is an important factor of its in-lake mineralization.

4.5.3 Implications on current and future lake CO_2 budgets

Northern landscape temperature and precipitation are projected to increase in the next decades (IPCC, 2013), accompanied with potential increase in DOC loading to lakes (Monteith *et al.*, 2007). Results from this study imply that CO_2 emissions sensitivity to these environmental changes may be lake- and season-specific. We estimated the potential response in lakes annual CO_2 emissions by performing a sensitivity analysis and increasing hydrologic regime, DOC and surface water temperature. Not surprisingly, the exercise first revealed that short WRT lakes (Lac Simoncouche) CO_2 emissions are more sensitive to increase in hydrology compared to the long WRT lakes (Lac Croche and Lac Hébécourt). Furthermore, increases in DOC increased respiration and reduced GPP, resulting in enhanced CO_2 emissions especially in summer in Lac Hébécourt. This agrees with recent studies suggesting that increase DOC_{alloch} loading may sustain net heterotrophy in lakes (Solomon *et al.*, 2015; Zwart *et al.*, 2015). Increasing temperature, however, may have variable impact on lakes CO_2 emissions (e.g. Finlay *et al.*, 2015). Our analysis showed that increasing surface water temperature increased CO_2 emissions in all lakes and especially in summer, but was more pronounced in the long WRT, where internal processes are relatively more important. Assessing the impact of such changes on the northern lakes C cycle is challenging (Benoy *et al.*, 2007; Solomon *et al.*, 2015), and this simple sensitivity analysis exercise is not a direct assessment of environmental impacts on lake C budget. It however gives valuable insights on the different responses induced by seasons and

lake types, which should be considered in current and future lake C budgets and environmental changes impact assessments.

In conclusion, our study showed that regardless the type of lake, all the processes we investigated contributed significantly to lakes CO_2 dynamics with variable magnitudes and relative contributions. A common seasonal pattern characterized by the dominance of hydrologic inputs in spring/fall and metabolism in summer was observed in all lakes, although it seemed that this pattern was further modulated by lakes DOC concentration, WRT and morphometry. As a result, studies looking at a constrained period/season or lake type may potentially over- or under-estimate a given process, which may mislead the role of lakes in regional and global C cycles. Our results further suggest a potential differential responses and sensitivities of lakes to environmental changes depending on seasons and lake types. This highlights the needs for more comprehensive lake C models which would account for seasonality and lake properties in order to predict future impact of environmental changes on northern lakes CO_2 emissions with less uncertainties.

4.6 ACKNOWLEDGEMENTS

We would like to thank Alice Parkes, Annick St-Pierre, Mathieu Dumais and Jean-Philippe Desindes for field and laboratory assistance and Jacob Zwart and Stuart Jones for early versions of the process-based model. This project was part of the large-scale research program of the Industrial Research Chair in Carbon Biogeochemistry in Boreal Aquatic Systems (CarBBAS), co-funded by the Natural Sciences and Engineering Research Council of Canada (NSERC) and Hydro-Québec to PDG. NSERC doctoral scholarship and UQAM-FARE scholarship was also attributed to DV.

4.7 SUPPORTING INFORMATION

4.7.1 Meteorological data used in the process-based model

Meteorological data were collected from various stations around each lake, and also from the lake autonomous measuring platforms. For Lac Simoncouche, hourly wind speed, photosynthetic active radiation (PAR), air temperature and precipitation data were provided by a nearby weather station on the shore of the lake (Laboratoire d'Écologie végétale et animale of Université du Québec à Chicoutimi). Lac Croche air temperature were recorded directly on the floating platform, which was equipped with a Vaisala WXT520 weather station. Other weather data (wind speed, PAR and precipitation) were obtained from a meteorological station located c.a. 350 meters south of the autonomous platform (Station de biologie des Laurentides, Université de Montréal). For Lac Hébécourt, wind speed, air temperature and precipitation data were collected from a weather station deployed from May to October on the lake watershed (Danielle Charron, pers. comm. Université du Québec à Montréal). (1) PAR in Lac Hebecourt was not available. Estimated PAR from modeled radiation calculated in Chapter I. Relationship between measured PAR and modeled radiation (400-600) in Lac Croche (r^2=0.87) and Lac Simoncouche (r^2 =0.73).

The temporal patterns in daily averaged air temperature were similar on the three study sites, although wind speed was generally higher over Lac Hébécourt, compared to the other lakes (Figure S4.1). In winter, all lakes were completely covered with ice reaching approximately one meter of thickness, although the duration of ice cover was variable between sites. Lac Croche was covered with ice from 2010-11-26 to 2011-05-08 for a total of 163 days of full ice cover, Lac Hébécourt from 2010-11-20 to 2011-05-11 for a total of 172 days, and Lac Simoncouche from 2011-11-29 to 2012-04-18 for a total of 141 days. Hydrologic regimes also varied substantially between sites. The entire volume of Lac Simoncouche was renewed almost every two months, whereas

Lac Croche and Lac Hébécourt had water renewal times of more than a year in summer. The lake hydrographs are presented in Figure S4.1A. Spring freshets and late summer storm events increased significantly the lake discharges, particularly in Lac Simoncouche, where major storm events occurred in August and increased the lake discharge on a magnitude comparable to the spring freshet (Vachon et del Giorgio, 2014).

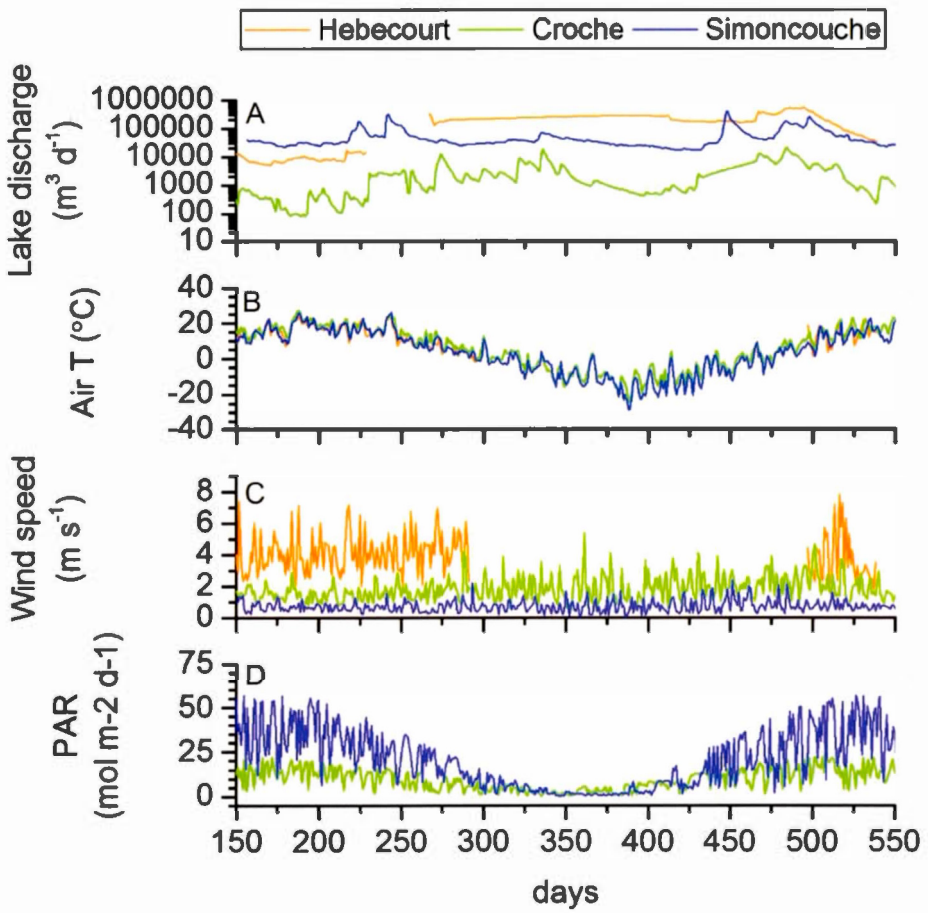

Figure S4.1. Temporal variation of the meteorological data

Daily averaged lake discharge (A), daily averaged air temperature (B), daily averaged wind speed at 10 m (C) and daily photosynthetic active radiation for an annual cycle. Days are consecutive days since 2010 in Lac Hébécourt (day 1 is January 1st 2010 and day 366 is January 1st 2011) and 2011 in Croche and Simoncouche (day 1 is January 1st 2011 and day 366 is January 1st 2012).

4.7.2 Lake water mass balance and groundwater inputs parametrization

We estimated the daily hydraulic loads to each lake (Q_{in}, which is the sum of surface water and sub-surface/groundwater) by calculating the lake water mass balance, described as:

(S4.1) $$Q_{in} = Q_{out} + E - P + \Delta vol$$

where Q_{out} is the lake water discharge through the lake exit, E is the evaporation from the lake surface, P is the precipitation falling directly on the lake surface and Δvol is the lake volume changes. Daily lake volume was estimated from the measurements of lake level combined with the lake bathymetry. Lake levels were continuously (hourly) measured using a pressure probe at the lake bottom (Precision Measurement Engineering, Inc. USA) in Lac Croche, and a level logger (Trutrack, New Zealand), installed near shore in Lac Hébécourt and Lac Simoncouche. The daily discharge from the outlet (Q_{out}) of Lac Simoncouche and Lac Hébécourt, and from the inlet streams (2 in Simoncouche and 5 in Hébécourt) were calculated on the basis of a stage-discharge curve established from stream level measurements and point measurements (each month) of discharge using an acoustic Doppler velocimeter (Sontek FlowTracker, San Diego, USA). For Lac Croche, the lake discharge was continuously monitored with a V-shape weir (Station de biologie des Laurentides, Université de Montréal). Monthly evaporation (E) from the lake surface was estimated with the Jensen-Haise method (Rosenberry *et al.*, 2007) using the 22-year averaged monthly air temperature and total insulation data obtained from the Surface meteorological and Solar Energy (SSE) web portal supported by the NASA LaRC POWER Project (https://eosweb.larc.nasa.gov/project/sse/sse_table).

The proportion of groundwater and stream to the total CO_2 loading were evaluated by a factor (α), which describes the proportion (0-1) of total hydrologic inputs due to stream water (0 being all groundwater and 1 being all stream water inputs). Each lake

α value was calculated as the annual averaged stream water inputs (m3 d-1) divided by the annual averaged total water load, and was also considered constant through time.

Because there are no permanent surface streams in Lac Croche, α value was set to zero. In Lac Hébécourt, the extensive influence of beaver dams in inlet streams resulted in poor stage-discharge curve fits, and in extremely variable and unrealistic α values. We evaluated based on digital elevation maps (GIS) that the area drained by the measured surface inflows was 75%. We assumed that about 25% of inflowing water came from the lateral sub-surface and deep groundwater and set the alfa value to 0.75 (Table 4.2). Lac Simoncouche, the watershed area drained by measured surface inflow was 69.5% of the total watershed area of Lac Simoncouche, which is close to the yearly averaged alfa value of 0.67 (Table 4.2). Surface water and sub-surface water CO_2 inputs to each lake were thus a function of Q_{in}, α and CO_2 concentrations measured in the streams or in groundwater (Table 4.2).

In winter, however, modeled CO_2 was generally exceeding measured CO2 concentration. We thus manually set the water inflow to adjust the fit between modeled CO_2 and measured CO_2. In all lake, the inflow had to be greatly diminished, by 10% to 50% of the measured inflow from the water mass balance. These imbalances can be due to overestimation of the other fluxes (like benthic and pelagic respiration), some gas permeability of ice or lower CO_2 concentration in ground and surface waters during winter.

4.7.3 Empirical relationship between DOC and Kd_{PAR}

We used measurements of PAR and DOC in an empirical relationship to predict daily PAR using linearly-interpolated daily DOC concentrations

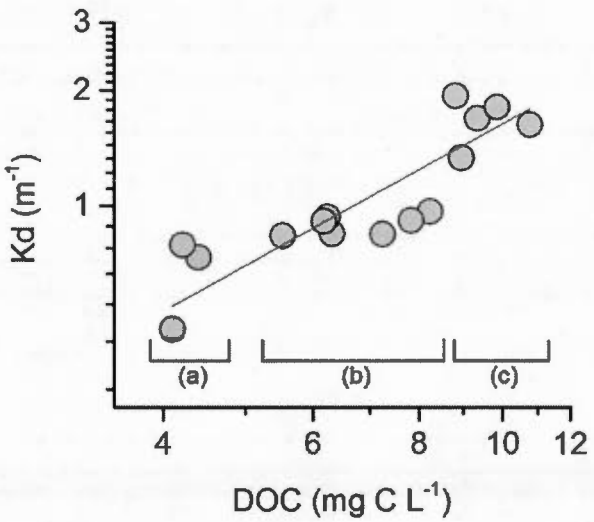

Figure S4.2. Relationship between measured DOC concentration and measured light extinction coefficient for PAR

Lac Croche (a), Lac Simoncouche (b) and Lac Hébécourt (c). $Kd_{PAR} = 0.10 (\pm 0.05) * DOC^{1.22 (\pm 0.22)}$, $R^2=0.72$, n=15). Parameters are showed with standard error.

4.7.4 Agreement between published and measured relationship between temperature and sediments CO_2 production

Sediment CO_2 flux was assessed in sediment cores following *in situ* incubations (Åberg *et al.*, 2007; Den Heyer et Kalff, 1998). Lakes were cored at least 3 times in the summer and once in the winter with a gravity corer, at their deepest zone. In each sampling date, three replicates sediment cores were incubated at the bottom of the lakes for at least 24 hours. Each core consisted of a transparent polycarbonate tube that was half-filled with undisturbed sediments and overlaying water without air, and sealed with rubber stoppers and Parafilm to avoid gas exchanges. Measurements of overlaying water CO_2 concentration using the headspace technique with an infra-red gas analyzer (EMG-4, PP-System, USA) were made before and after the incubation and CO_2 production rates (mg C m^{-2} d^{-1}) were estimated.

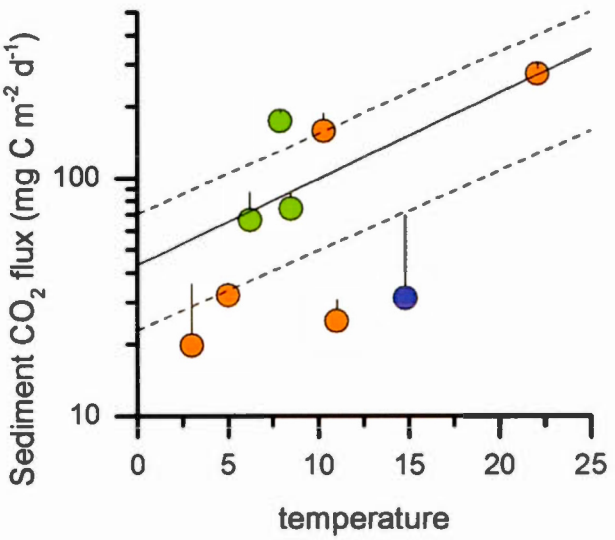

Figure S4.3. Relationship between measured sediment CO_2 fluxes from core incubations with mean incubation temperature.

Solid line is the general model by Gudasz *et al.,* (2010) and the dash lines are the models reported from two lakes with different DOC loading (Gudasz *et al.*, 2010).

CONCLUSIONS GÉNÉRALES

5.1.1 Objectifs et résultats généraux

Le but de cette thèse était d'explorer les différents aspects de la dynamique temporelle des processus qui régulent les concentrations et les émissions de CO_2 des lacs boréaux, en examinant les interactions entre les variations climatiques saisonnières et certaines propriétés clés spécifiques à chaque lac. Les lacs boréaux et tempérés sont étroitement connectés avec le milieu terrestre environnant, favorisant ainsi les échanges de matière et d'énergie. Il est connu que cette connexion est fortement impliquée dans le phénomène de sursaturation en CO_2 à la surface des lacs, cependant, la compréhension des mécanismes sous-jacents qui relient le carbone d'origine terrestre aux émissions de CO_2 vers l'atmosphère comporte toujours certaines lacunes. Jusqu'à présent, les diverses sources potentielles de CO_2 dans les lacs boréaux sont relativement bien connues de manière individuelle et fixe dans le temps, mais la compréhension des dynamiques temporelles des principaux mécanismes qui produisent et enlèvent du CO_2 à la surface des lacs dans un contexte commun demeure incomplète. Ces informations sont essentielles, non seulement pour parvenir vers de meilleures estimations régionales des émissions de CO_2 provenant des lacs boréaux, mais aussi pour prédire avec moins d'incertitudes les futures émissions en considérant les changements potentiels du climat et de l'environnement boréal.

Dans une région boréale donnée, les grandes variations climatiques dues aux saisons que subissent les différents lacs résultent en certaines tendances similaires dans la dynamique des mécanismes de régulation du CO_2. Ainsi, un modèle saisonnier cohérent dans l'ensemble des lacs étudiés a été observé, décrivant une dominance de contribution de la respiration totale (benthique et pélagique) dans la production totale de CO_2 des lacs durant l'été (chapitres I et IV), tandis qu'au printemps et à l'automne,

ce sont plutôt les apports hydrologiques en CO_2 qui était relativement plus importants (chapitre IV). De plus, les évènements épisodiques caractérisés par d'intenses précipitations ont aussi causé une augmentation de l'importance des apports hydrologiques en CO_2 (chapitre III).

Le climat n'est cependant pas le seul responsable de la variabilité saisonnière observée, mais agit plutôt de concert avec certaines caractéristiques clés des lacs boréaux, notamment la réactivité de la matière organique. Ainsi, la combinaison de la variation des propriétés intrinsèques du COD et des conditions environnementales occasionne des périodes d'intense transformation du COD dans la colonne d'eau des lacs boréaux. Au printemps par exemple, la grande disponibilité du COD photo-réactif et des radiations solaires engendre des taux de photo-minéralisation du COD comparable à la respiration totale dans la colonne d'eau (chapitre I). De façon similaire, l'évaluation de la minéralisation du COD allochtone dans les lacs nécessite l'intégration de la complexité de la réactivité du COD combiné aux facteurs physiques et environnementaux. Ainsi, la variabilité temporelle et spatiale de la dégradabilité biologique du COD allochtone a été explorée en incorporant le concept de continuum de réactivité avec les variations de régime hydrologique (chapitre II). Il a été montré que le temps de résidence des molécules de COD module la dégradabilité restante observé dans les lacs boréaux et influence donc sa minéralisation et la production de CO_2. Ainsi, une proportion importante de la production de CO_2 dans la colonne d'eau est alimentée par la minéralisation du COD allochtone (chapitre II). En somme, la compréhension de la variabilité temporelle de la réactivité du COD (chapitres I et II) combinée aux conditions environnementales favorable est primordiale, car ces dynamiques ont le potentiel d'occasionner des périodes de transformation intense du COD, significatives dans le cycle annuel du C des lacs tempérés et boréaux.

Outre ces tendances générales gouvernées par le climat et la qualité de la matière organique, l'importance relative et la dominance de certains processus sont par contre

spécifiques à chaque lac et modulées par ses caractéristiques locales, comme la forme du bassin et le régime hydrologique. Par exemple, les lacs plus profonds permettent l'accumulation de CO_2 pendant l'été, ce qui affecte les émissions automnales, mais aussi, leur volume important de la zone pélagique favorise une contribution plus importante de la respiration pélagique (Chapitre IV). De plus, la combinaison de la configuration topographique et les caractéristiques du bassin versant et du lac déterminent en partie le régime hydrologique de chaque lac. Ainsi, pour une même intensité de précipitation, les lacs ayant un grand bassin versant par rapport à son volume auront plus tendance à recevoir du CO_2 directement du milieu terrestre suite à une tempête (Chapitre III). Les variations du régime hydrologique modulent les apports directs en CO_2 (Chapitre III et IV), mais aussi la dynamique de réactivité biologique et photochimique du COD terrestre (Chapitres I et II). Les lacs ayant un long temps de séjour favorisent aussi la dégradation du COD dans la colonne d'eau (Chapitres II et III), mais ont aussi moins d'apport hydrologique de CO_2 externe (Chapitres II et IV). Le régime hydrologique des lacs est donc une variable clé dans la compréhension du rôle des lacs boréaux dans le paysage. De plus, les effets des évènements climatiques sur la transformation et le transport du C seront aussi grandement influencés par la morphométrie des écosystèmes. En somme, il a été démontré que tous les processus de production de CO_2 contribuent à la sursaturation en CO_2 des lacs tempérés et boréaux et montrent tous une saisonnalité marquée. Ce sont finalement ces successions temporelles des processus physiques, chimiques et biologiques qui sculptent ainsi les tendances temporelles des émissions de CO_2.

5.1.2 Implications des résultats et contributions

La principale contribution de cette thèse est d'avoir placé dans un cadre commun les différents procédés qui influencent la dynamique du CO_2 et des émissions des lacs boréaux et ce, sur une année complète. Dans toute étude scientifique, le choix de l'approche et des méthodes adaptées à la question que l'on se pose est crucial à

l'interprétation et aux implications des résultats obtenus. Par exemple, jusqu'à quel point une mesure est représentative du lac entier et quelle période celle-ci intègre-t-elle ? Est-ce qu'une incubation en laboratoire est représentative de ce qui se passe réellement dans le lac ? Ainsi, chaque méthode et approche possède plusieurs avantages, mais aussi, certaines lacunes qu'il est essentiel de prendre en compte lors de l'interprétation des résultats. Dans cette thèse, la combinaison de différentes approches était donc essentielle conformément aux questions posées. La combinaison de mesures in situ répétées dans le temps, d'incubations in situ et en laboratoire avec des exercices de modélisations procure ainsi une résolution incomparable de la dynamique des processus de production de CO_2. De rares études, sinon aucune, ont combiné le suivi des divers processus avec autant de détails sur une année complète.

Les résultats issus de cette thèse approfondissent donc grandement non seulement notre compréhension générale de la dynamique temporelle du CO_2 dans les lacs boréaux, mais plus particulièrement, la dynamique des processus sous-jacents qui soutiennent les émissions de CO_2. La combinaison de différentes approches a permis d'explorer les différents aspects des mécanismes de production de CO_2 comme les rôles de la réactivité du COD, des régimes hydrologiques ainsi que de la morphométrie des lacs. De plus, l'exploration de ces processus sur une année complète a permis de capturer ensemble les tendances de réactivité du COD, ainsi que les variations des conditions environnementales, mettant en lumière des périodes inattendues de transformation du COD. La compréhension de la dynamique de transformation du COD terrestre et sa destinée est essentielle pour affiner notre conception et notre compréhension du rôle des écosystèmes aquatiques dans le paysage boréal.

Dans les régions nordiques, les conséquences des changements environnementaux sur les émissions de CO_2 provenant des lacs sont plus qu'incertaines et ont un potentiel réel d'avoir un impact considérable sur le cycle global du C. Les résultats issus de cette thèse sont hautement pertinents dans le contexte de changements environnementaux,

incluant les changements de régime hydrologique et l'augmentation des concentrations de COD (c.-à-d. le phénomène de « brunification » des systèmes aquatiques). Ils impliquent que chaque type de lac et chaque saison aura une sensibilité spécifique aux changements climatiques. Certains lacs ou saisons seront plus sensibles aux hausses de température, tandis que d'autres seront plus sensibles aux changements hydrologiques. Cette thèse procure aussi une compréhension plus approfondie sur la dynamique de minéralisation biologique et photochimique du COD, qui est d'autant plus importante dans le contexte des tendances globales d'augmentation des concentrations de COD (et possiblement des changements dans sa réactivité) observées dans les écosystèmes aquatiques. Toutes ces considérations peuvent donc engendrer des modifications majeures au cycle aquatique du C et aux émissions de CO_2 vers l'atmosphère, qui influenceront grandement les futurs exercices de bilan de C dans le paysage boréal. Par conséquent, les tendances saisonnières qui ont été explorées dans cette thèse devraient donc être incorporées dans les futurs schémas conceptuels et modèles de fonctionnement des lacs boréaux et tempérés.

RÉFERENCES

Aarnos, H., Ylöstalo, P. et Vähätalo, A. V. 2012. Seasonal phototransformation of dissolved organic matter to ammonium, dissolved inorganic carbon, and labile substrates supporting bacterial biomass across the Baltic Sea. *Journal of Geophysical Research*, 117 (G1), G01004. DOI: 10.1029/2010JG001633.

Åberg, J., Jansson, M. et Jonsson, A. 2010. Importance of water temperature and thermal stratification dynamics for temporal variation of surface water CO_2 in a boreal lake. *Journal of Geophysical Research*, 115 (G2), G02024. DOI: 10.1029/2009JG001085.

Åberg, J., Jansson, M., Karlsson, J., Nääs, K.-J. et Jonsson, A. 2007. Pelagic and benthic net production of dissolved inorganic carbon in an unproductive subarctic lake. *Freshwater Biology*, 52 (3), 549-560. DOI: 10.1111/j.1365-2427.2007.01725.x.

Abramowitz, M. et Stegun, I.A. 1964. *Handbook of Mathematical Functions With Formulas, Graphs, and Mathematical Tables*. Dover. New York.

Ågren, A., Berggren, M., Laudon, H. et Jansson, M. 2008. Terrestrial export of highly bioavailable carbon from small boreal catchments in spring floods. *Freshwater Biology*, 53 (5), 964-972. DOI: 10.1111/j.1365-2427.2008.01955.x.

Algesten, G., Sobek, S., Bergström, A.-K., Ågren, A., Tranvik, L.J. et Jansson, M. 2003. Role of lakes for organic carbon cycling in the boreal zone. *Global Change Biology*, 10 (1), 141-147. DOI: 10.1046/j.1529-8817.2003.00721.x.

Algesten, G., Sobek, S., Bergström, A.-K., Jonsson, A., Tranvik, L.J. et Jansson, M. 2005. Contribution of sediment respiration to summer CO_2 emission from low productive boreal and subarctic lakes. *Microbial ecology*, 50 (4), 529-35. DOI: 10.1007/s00248-005-5007-x.

Andersson, E. et Kumblad, L. 2006. A carbon budget for an oligotrophic clearwater lake in mid-Sweden. *Aquatic Sciences*, 68 (1), 52-64. DOI: 10.1007/s00027-005-0807-0.

Anesio, A., Granéli, W., Aiken, G.R., Kieber, D.J. et Mopper, K. 2005. Effect of humic substance photodegradation on bacterial growth and respiration in lake

water. *Applied and environmental microbiology*, 71 (10), 6267-6275. DOI: 10.1128/AEM.71.10.6267.

Anesio, A., Tranvik, L., Granéli, W. et Building, E. 1999. Production of inorganic carbon from aquatic macrophytes by solar radiation. *Ecology*, 80 (6), 1852-1859.

Baskerville, G.L. 1974. Use of Logarithmic Regression in the Estimation of Plant Biomass: Reply. *Canadian Journal of Forest Research*, 4 (1), 149-149. DOI: 10.1139/x74-024.

Battin, T.J., Luyssaert, S., Kaplan, L.A., Aufdenkampe, A.K., Richter, A. et Tranvik, L.J. 2009. The boundless carbon cycle. *Nature Geoscience*, 2 (9), 598-600. DOI: 10.1038/ngeo618.

Benoy, G., Cash, K., McCauley, E. et Wrona, F. 2007. Carbon dynamics in lakes of the boreal forest under a changing climate. *Environmental Reviews*, 15 (NA), 175-189. DOI: 10.1139/A07-006.

Berggren, M., Lapierre, J.-F. et del Giorgio, P.A. 2012. Magnitude and regulation of bacterioplankton respiratory quotient across freshwater environmental gradients. *The ISME journal*, 6 (5), 984-93. DOI: 10.1038/ismej.2011.157.

Bertilsson, S., Stepanauskas, R., Cuadros-Hansson, R., Granéli, W., Wikner, J. et Tranvik, L. 1999. Photochemically induced changes in bioavailable carbon and nitrogen pools in a boreal watershed. *Aquatic Microbial Ecology*, 19, 47-56.

Bogert, M.C. Van De, Carpenter, S.R., Cole, J.J., Pace, M.L., Van de Bogert, M.C., Van DeBogert, M.C., Carpenter, S.R., et al. 2007. Assessing pelagic and benthic metabolism using free water measurements. *Limnology And Oceanography Methods*, 5, 145-155.

Bolin, B. et Rodhe, H. 1973. A note on the concepts of age distribution and transit time in natural reservoirs. *Tellus*, 1 (258).

Boudreau, B. et Ruddick, B. 1991. On a reactive continuum representation of organic matter diagenesis. *American Journal of Science*, 291 (May), 507-538.

Boudreau, B.P., Arnosti, C., Jørgensen, B.B. et Canfield, D.E. 2008. Comment on « Physical model for the decay and preservation of marine organic carbon ». *Science (New York, N.Y.)*, 319 (5870), 1616; author reply 1616. DOI: 10.1126/science.1148589.

Brothers, S.M., Prairie, Y.T. et del Giorgio, P.A. 2012. Benthic and pelagic sources of carbon dioxide in boreal lakes and a young reservoir (Eastmain-1) in eastern Canada. *Global Biogeochemical Cycles*, 26 (1). DOI: 10.1029/2011GB004074.

Buffam, I., Galloway, J.N., Blum, L.K. et Mcglathery, K.J. 2008. A stormflow / baseflow comparison of dissolved organic matter concentrations and bioavailability in an Appalachian stream. *Biogeochemistry*, 53 (3), 269-306.

Campeau, A. et del Giorgio, P.A. 2014. Patterns in CH_4 and CO_2 concentrations across boreal rivers: Major drivers and implications for fluvial greenhouse emissions under climate change scenarios. *Global change biology*, 20 (4), 1075-1088. DOI: 10.1111/gcb.12479.

Campeau, A., Lapierre, J.-F., Vachon, D. et del Giorgio, P.A. 2014. Regional contribution of CO_2 and CH_4 fluxes from the fluvial network in a lowland boreal landscape of Québec. *Global Biogeochemical Cycles*. DOI: 10.1002/2013GB004685.

Cardille, J.A., Carpenter, S.R., Coe, M.T., Foley, J.A., Hanson, P.C., Turner, M.G. et Vano, J.A. 2007. Carbon and water cycling in lake-rich landscapes: Landscape connections, lake hydrology, and biogeochemistry. *Journal of Geophysical Research*, 112 (G2), G02031. DOI: 10.1029/2006JG000200.

Cole, J.J. et Caraco, N.F. 1998. Atmospheric exchange of carbon dioxide in a low-wind oligotrophic lake measured by the addition of SF_6. *Limnology and Oceanography*, 43 (4), 647-656.

Cole, J.J., Caraco, N.F., Kling, G.W. et Kratz, T.K. 1994. Carbon dioxide supersaturation in the surface waters of lakes. *Science*, 265, 1568-1570.

Cole, J.J., Carpenter, S.R., Kitchell, J.F. et Pace, M.L. 2002. Pathways of organic carbon utilization in small lakes: Results from a whole-lake 13C addition and coupled model. *Limnology and oceanography*, 47 (6), 1664-1675.

Cole, J.J., Pace, M.L., Carpenter, S.R. et Kitchell, J.F. 2000. Persistence of net heterotrophy in lakes during nutrient addition and food web manipulations. *Limnology and Oceanography*, 45 (8), 1718-1730. DOI: 10.4319/lo.2000.45.8.1718.

Cole, J.J. et Prairie, Y.T. 2009. Dissolved CO_2. Dans *Encyclopedia of Inland Waters*, sous la dir. de Gene E. Likens, vol. 2, p. 30-34. Oxford : Elsevier.

Cole, J.J., Prairie, Y.T., Caraco, N.F., McDowell, W.H., Tranvik, L.J., Striegl, R.G., Duarte, C.M., et al. 2007. Plumbing the Global Carbon Cycle: Integrating Inland Waters into the Terrestrial Carbon Budget. *Ecosystems*, 10 (1), 172-185. DOI: 10.1007/s10021-006-9013-8.

Coloso, J.J., Cole, J.J. et Pace, M.L. 2011. Difficulty in Discerning Drivers of Lake Ecosystem Metabolism with High-Frequency Data. *Ecosystems*, 14 (6), 935-948. DOI: 10.1007/s10021-011-9455-5.

Cory, R.M., Ward, C.P., Crump, B.C. et Kling, G.W. 2014. Sunlight controls water column processing of carbon in arctic fresh waters. *Science*, 345 (6199), 925-928. DOI: 10.1126/science.1253119.

Dhillon, G.S. et Inamdar, S. 2013. Extreme storms and changes in particulate and dissolved organic carbon in runoff: Entering uncharted waters? *Geophysical Research Letters*, 40 (April). DOI: 10.1002/grl.50306.

Dillon, P. et Molot, L. 1997. Dissolved organic and inorganic carbon mass balances in central Ontario lakes. *Biogeochemistry* (1991), 29-42.

Downing, J.A., Cole, J.J., Duarte, C.M., Middelburg, J.J., Melack, J.M., Prairie, Y.T., Kortelainen, P., Striegl, R.G., McDowell, W.H. et Tranvik, L.J. 2012. Global abundance and size distribution of streams and rivers. *Inland Waters*, 2 (4), 229-236. DOI: 10.5268/IW-2.4.502.

Downing, J.A., Prairie, Y.T., Cole, J.J., Duarte, C.M., Tranvik, L.J., Striegl, R.G., McDowell, W.H., Kortelainen, P., Caraco, N.F. et Melack, J.M. 2006. The global abundance and size distribution of lakes, ponds, and impoundments. *Limnology and Oceanography*, 51 (5), 2388-2397. DOI: 10.4319/lo.2006.51.5.2388.

Dubois, K., Carignan, R. et Veizer, J. 2009. Can pelagic net heterotrophy account for carbon fluxes from eastern Canadian lakes? *Applied Geochemistry*, 24 (5), 988-998. DOI: 10.1016/j.apgeochem.2009.03.001.

Ducharme-Riel, V., Vachon, D., del Giorgio, P.A. et Prairie, Y.T. 2015. The relative contribution of winter under-ice and summer hypolimnetic CO_2 accumulation to the annual CO_2 emissions from northern lakes. *Ecosystems*, 18 (4), 547-559. DOI: 10.1007/s10021-015-9846-0.

Einola, E., Rantakari, M., Kankaala, P., Kortelainen, P., Ojala, A., Pajunen, H., Mäkelä, S. et Arvola, L. 2011. Carbon pools and fluxes in a chain of five boreal

lakes: A dry and wet year comparison. *Journal of Geophysical Research*, 116 (G3), G03009. DOI: 10.1029/2010JG001636.

Elberling, B. et Ladegaard-Pedersen, P. 2005. Subsurface CO_2 Dynamics in Temperate Beech and Spruce Forest Stands. *Biogeochemistry*, 75 (3), 479-506. DOI: 10.1007/s10533-005-3690-9.

Ferland, M.-E., del Giorgio, P.A., Teodoru, C.R. et Prairie, Y.T. 2012. Long-term C accumulation and total C stocks in boreal lakes in northern Québec. *Global Biogeochemical Cycles*, 26 (4). DOI: 10.1029/2011GB004241.

Ferland, M.-E., Prairie, Y.T., Teodoru, C. et del Giorgio, P.A. 2014. Linking organic carbon sedimentation, burial efficiency, and long-term accumulation in boreal lakes. *Journal of Geophysical Research: Biogeosciences*, 119 (5), 836-847. DOI: 10.1002/2013JG002345.Received.

Fichot, C.G. et Miller, W.L. 2010. An approach to quantify depth-resolved marine photochemical fluxes using remote sensing: Application to carbon monoxide (CO) photoproduction. *Remote Sensing of Environment*, 114 (7), 1363-1377. DOI: 10.1016/j.rse.2010.01.019.

Finlay, K., Vogt, R.J., Bogard, M.J., Wissel, B., Tutolo, B.M., Simpson, G.L. et Leavitt, P.R. 2015. Decrease in CO_2 efflux from northern hardwater lakes with increasing atmospheric warming. *Nature*, 8. DOI: 10.1038/nature14172.

Frenette, J.-J., Arts, M.T., Morin, J., Gratton, D. et Martin, C. 2006. Hydrodynamic control of the underwater light climate in fluvial Lac Saint-Pierre. *Limnology and Oceanography*, 51 (6), 2632-2645. DOI: 10.4319/lo.2006.51.6.2632.

del Giorgio, P., Cole, J. et Cimbleris, A. 1997. Respiration rates in bacteria exceed phytoplankton production in unproductive aquatic systems. *Nature*, 385, 148-151.

del Giorgio, P.A., Cole, J.J., Caraco, N.F. et Peters, R.H. 1999. Linking Planktonic Biomass and Metabolism to Net Gas Fluxes in Northern Temperate Lakes. *Ecology*, 80 (4), 1422. DOI: 10.2307/177085.

del Giorgio, P.A. et Peters, R.H. 1994. Patterns in planktonic P: R ratios in lakes: Influence of lake trophy and dissolved organic carbon. *Limnology and Oceanography*, 39 (4), 772-787.

den Heyer, C. et Kalff, J. 1998. Organic matter mineralization rates in sediments: A

within-and among-lake study. *Limnology and oceanography*, 43 (4), 695-705.

Gonsior, M., Schmitt-Kopplin, P. et Bastviken, D. 2013. Depth-dependent molecular composition and photo-reactivity of dissolved organic matter in a boreal lake under winter and summer conditions. *Biogeosciences*, 10 (11), 6945-6956. DOI: 10.5194/bg-10-6945-2013.

Granéli, W., Lindell, M., Faria, B. De et Esteves, F. de A. 1998. Photoproduction of dissolved inorganic carbon in temperate and tropical lakes–dependence on wavelength band and dissolved organic carbon concentration. *Biogeochemistry*, 43 (2), 175-195.

Granéli, W., Lindell, M. et Tranvik, L. 1996. Photo-oxidative production of dissolved inorganic carbon in lakes of different humic content. *Limnology and Oceanography*, 41 (4), 698-706.

Groeneveld, M.M., Tranvik, L.J. et Koehler, B. 2015. Photochemical mineralisation in a humic boreal lake: temporal variability and contribution to carbon dioxide production. *Biogeosciences Discussions*, 12 (20), 17125-17152. DOI: 10.5194/bgd-12-17125-2015.

Gudasz, C., Bastviken, D., Premke, K., Steger, K. et Tranvik, L.J. 2012. Constrained microbial processing of allochthonous organic carbon in boreal lake sediments. *Limnology and Oceanography*, 57 (1), 163-175. DOI: 10.4319/lo.2012.57.1.0163.

Gudasz, C., Bastviken, D., Steger, K., Premke, K., Sobek, S. et Tranvik, L.J. 2010. Temperature-controlled organic carbon mineralization in lake sediments. *Nature*, 466 (7305), 478-81. DOI: 10.1038/nature09186.

Guillemette, F. et del Giorgio, P.A. 2011. Reconstructing the various facets of dissolved organic carbon bioavailability in freshwater ecosystems. *Limnology and Oceanography*, 56 (2), 734-748. DOI: 10.4319/lo.2011.56.2.0734.

Guillemette, F., McCallister, S.L., del Giorgio, P.A., McCallister, L.S. et del Giorgio, P.A. 2013. Differentiating the degradation dynamics of algal and terrestrial carbon within complex natural dissolved organic carbon in temperate lakes. *Journal of Geophysical Research: Biogeosciences*, 118, n/a-n/a. DOI: 10.1002/jgrg.20077.

Hanson, P., Bade, D., Carpenter, S.R. et Kratz, T.K. 2003. Lake metabolism: Relationships with dissolved organic carbon and phosphorus. *Limnology and*

Oceanography, 48 (3), 1112-1119.

Hanson, P., Buffam, I., Rusak, J., Stanley, E. et Watras, C. 2014a. Quantifying lake allochthonous organic carbon budgets using a simple equilibrium model. *Limnology and Oceanography*, 59 (1), 167-181. DOI: 10.4319/lo.2014.59.01.0167.

Hanson, P., Carpenter, S. et Kimura, N. 2008. Evaluation of metabolism models for free-water dissolved oxygen methods in lakes. *Limnology and Oceanography* (1956), 454-465.

Hanson, P.C., Hamilton, D.P., Stanley, E.H., Preston, N., Langman, O.C., Kara, E.L. et Emily, L. 2011. Fate of allochthonous dissolved organic carbon in lakes: a quantitative approach. *PloS one*, 6 (7), e21884. DOI: 10.1371/journal.pone.0021884.

Hanson, P.C., Pace, M.L., Carpenter, S.R., Cole, J.J. et Stanley, E.H. 2014b. Integrating Landscape Carbon Cycling : Research Needs for Resolving Organic Carbon Budgets of Lakes. *Ecosystems*. DOI: 10.1007/s10021-014-9826-9.

Hanson, P.C., Pollard, A.I., Bade, D.L., Predick, K., Carpenter, S.R. et Foley, J.A. 2004. A model of carbon evasion and sedimentation in temperate lakes. *Global Change Biology*, 10, 1285-1298. DOI: 10.1111/j.1365-2486.2004.00805.x.

Hernes, P.J. 2003. Photochemical and microbial degradation of dissolved lignin phenols: Implications for the fate of terrigenous dissolved organic matter in marine environments. *Journal of Geophysical Research*, 108 (C9), 3291. DOI: 10.1029/2002JC001421.

Houser, J., Bade, D., Cole, J. et Pace, M. 2003. The dual influences of dissolved organic carbon on hypolimnetic metabolism: organic substrate and photosynthetic reduction. *Biogeochemistry* (3), 247-269.

Hu, C.M., Muller-Karger, F.E. et Zepp, R.G. 2002. Absorbance, absorption coefficient, and apparent quantum yield: A comment on common ambiguity in the use of these optical concepts. *Limnology and Oceanography*, 47 (4), 1261-1267.

Humborg, C., Mörth, C.-M., Sundbom, M., Borg, H., Blenckner, T., Giesler, R. et Ittekkot, V. 2010. CO_2 supersaturation along the aquatic conduit in Swedish watersheds as constrained by terrestrial respiration, aquatic respiration and weathering. *Global Change Biology*, 16 (7), 1966-1978. DOI: 10.1111/j.1365-

2486.2009.02092.x.

Huotari, J., Ojala, A., Peltomaa, E., Pumpanen, J., Hari, P. et Vesala, T. 2009. Temporal variations in surface water CO_2 concentration in a boreal humic lake based on high-frequency measurements. *Boreal environment research*, 14 (april), 48-60.

IPCC. 2013. *Climate Change 2013: The Physical Science Basis. Contribution of Working Group I to the Fifth Assessment Report of the Intergovernmental Panel on Climate Change*. Sous la dir. de. T.F. Stocker, D. Qin, G.-K. Plattner, M. Tignor, S.K. Allen, J. Boschung, A. Nauels, Y. Xia, V. Bex, et P.M. Midgley. *Intergovernmental Panel on Climate Change, Working Group I Contribution to the IPCC Fifth Assessment Report (AR5)(Cambridge Univ Press, New York)*. Cambridge, United Kingdom and New York, NY, USA : Cambridge University Press.

Jähne, B., Münnich, K.O., Bösinger, R., Dutzi, A., Huber, W. et Libner, P. 1987. On the parameters influencing air-water gas exchange. *Journal of Geophysical Research: Oceans*, 92 (C2), 1937-1949. DOI: 10.1029/JC092iC02p01937.

Jansson, M., Hickler, T., Jonsson, A. et Karlsson, J. 2008. Links between Terrestrial Primary Production and Bacterial Production and Respiration in Lakes in a Climate Gradient in Subarctic Sweden. *Ecosystems*, 11 (3), 367-376. DOI: 10.1007/s10021-008-9127-2.

Jennings, E., Jones, S., Arvola, L., Staehr, P.A., Gaiser, E., Weathers, K.C., Weyhenmeyer, G. a., Chiu, C.-Y. et de Eyto, E. 2012. Effects of weather-related episodic events in lakes: an analysis based on high-frequency data. *Freshwater Biology*, 57, 589-601. DOI: 10.1111/j.1365-2427.2011.02729.x.

Johannessen, S.C. et Miller, W.L. 2001. Quantum yield for the photochemical production of dissolved inorganic carbon in seawater. *Marine Chemistry*, 76 (4), 271-283. DOI: 10.1016/S0304-4203(01)00067-6.

Jones, J.B., Stanley, E.H. et Mulholland, P.J. 2003. Long-term decline in carbon dioxide supersaturation in rivers across the contiguous United States. *Geophysical Research Letters*, 30 (10), 1495.

Jones, S.E., Kratz, T.K., Chiu, C.-Y. et McMahon, K.D. 2009. Influence of typhoons on annual CO_2 flux from a subtropical, humic lake. *Global Change Biology*, 15 (1), 243-254. DOI: 10.1111/j.1365-2486.2008.01723.x.

Jonsson, A., Karlsson, J. et Jansson, M. 2003. Sources of Carbon Dioxide Supersaturation in Clearwater and Humic Lakes in Northern Sweden. *Ecosystems*, 6 (3), 224-235. DOI: 10.1007/s10021-002-0200-y.

Jonsson, A., Meili, M., Bergström, A. et Jansson, M. 2001. Whole-lake mineralization of allochthonous and autochthonous organic carbon in a large humic lake(Oertraesket, N. Sweden). *Limnology and Oceanography*, 46 (7), 1691-1700.

Kalbitz, K., Schmerwitz, J., Schwesig, D. et Matzner, E. 2003. Biodegradation of soil-derived dissolved organic matter as related to its properties. *Geoderma*, 113 (3-4), 273-291. DOI: 10.1016/S0016-7061(02)00365-8.

Kalff, J. 2002. *Limnology: inland water ecosystems*. Prentice H. Upper Saddle River, NJ.

Kankaala, P., Huotari, J., Tulonen, T. et Ojala, A. 2013. Lake-size dependent physical forcing of carbon dioxide and methane effluxes from lakes in a boreal landscape. *Limnology and Oceanography*, 58 (6), 1915-1930. DOI: 10.4319/lo.2013.58.6.1915.

Karlsson, J., Giesler, R., Persson, J. et Lundin, E. 2013. High emission of carbon dioxide and methane during ice thaw in high latitude lakes. *Geophysical Research Letters*, 40 (January). DOI: 10.1002/grl.50152.

Karlsson, J., Jansson, M. et Jonsson, A. 2007. Respiration of allochthonous organic carbon in unproductive forest lakes determined by the Keeling plot method. *Limnology and Oceanography*, 52 (2), 603-608. DOI: 10.4319/lo.2007.52.2.0603.

Kellerman, A.M., Dittmar, T., Kothawala, D.N. et Tranvik, L.J. 2014. Chemodiversity of dissolved organic matter in lakes driven by climate and hydrology. *Nature communications*, 5 (May), 3804. DOI: 10.1038/ncomms4804.

Kelly, C.A., Fee, E., Ramlal, P.S., Rudd, J.W.M., Hesslein, R.H., Anema, C. et Schindler, E.U. 2001. Natural variability of carbon dioxide and net epilimnetic production in the surface waters of boreal lakes of different sizes. *Limnology and Oceanography*, 46 (5), 1054-1064. DOI: 10.4319/lo.2001.46.5.1054.

Kling, G., Kipphut, G. et Miller, M. 1991. Arctic lakes and streams as gas conduits to the atmosphere: Implications for tundra carbon budgets. *Science*, 251 (4991), 298-301.

Klug, J.L., Richardson, D.C., Ewing, H. a, Hargreaves, B.R., Samal, N.R., Vachon, D., Pierson, D.C., *et al.* 2012. Ecosystem effects of a tropical cyclone on a network of lakes in northeastern North America. *Environmental science & technology*, 46 (21), 11693-701. DOI: 10.1021/es302063v.

Koehler, B., Landelius, T., Weyhenmeyer, G.A., Machida, N. et Tranvik, L.J. 2014. Sunlight-induced carbon dioxide emissions from inland waters. *Global Biogeochemical Cycles*, 28, 696-711. DOI: 10.1002/2014GB004850.

Koehler, B. et Tranvik, L.J. 2015. Reactivity continuum modeling of leaf, root and wood decomposition across biomes. *Journal of Geophysical Research: Biogeosciences*, n/a-n/a. DOI: 10.1002/2015JG002908.

Koehler, B., von Wachenfeldt, E., Kothawala, D. et Tranvik, L.J. 2012. Reactivity continuum of dissolved organic carbon decomposition in lake water. *Journal of Geophysical Research*, 117 (G1), G01024. DOI: 10.1029/2011JG001793.

Koprivnjak, J.-F., Dillon, P.J. et Molot, L.A. 2010. Importance of CO_2 evasion from small boreal streams. *Global Biogeochemical Cycles*, 24 (4). DOI: 10.1029/2009GB003723.

Kortelainen, P., Rantakari, M., Huttunen, J.T., Mattsson, T., Alm, J., Juutinen, S., Larmola, T., Silvola, J. et Martikainen, P.J. 2006. Sediment respiration and lake trophic state are important predictors of large CO_2 evasion from small boreal lakes. *Global Change Biology*, 12 (8), 1554-1567. DOI: 10.1111/j.1365-2486.2006.01167.x.

Kothawala, D.N., Stedmon, C.A., Müller, R.A., Weyhenmeyer, G.A., Köhler, S.J. et Tranvik, L.J. 2014. Controls of dissolved organic matter quality: Evidence from a large-scale boreal lake survey. *Global Change Biology*, 20, 1101-1114. DOI: 10.1111/gcb.12488.

Laas, A., Nõges, P., Kõiv, T. et Nõges, T. 2012. High-frequency metabolism study in a large and shallow temperate lake reveals seasonal switching between net autotrophy and net heterotrophy. *Hydrobiologia*, 694 (1), 57-74. DOI: 10.1007/s10750-012-1131-z.

Lapierre, J.-F. et Frenette, J.-J. 2009. Effects of macrophytes and terrestrial inputs on fluorescent dissolved organic matter in a large river system. *Aquatic Sciences*, 71 (1), 15-24. DOI: 10.1007/s00027-009-9133-2.

Lapierre, J.-F. et del Giorgio, P.A. 2012. Geographical and environmental drivers of

regional differences in the lake pCO_2 versus DOC relationship across northern landscapes. *Journal of Geophysical Research*, 117 (G3), G03015. DOI: 10.1029/2012JG001945.

Lapierre, J.-F. et del Giorgio, P.A. 2014. Partial coupling and differential regulation of biologically and photochemically labile dissolved organic carbon across boreal aquatic networks. *Biogeosciences*, 11 (20), 5969-5985. DOI: 10.5194/bg-11-5969-2014.

Lapierre, J.-F., Guillemette, F., Berggren, M. et del Giorgio, P.A. 2013. Increases in terrestrially derived carbon stimulate organic carbon processing and CO_2 emissions in boreal aquatic ecosystems. *Nature Communications*, 4. DOI: 10.1038/ncomms3972.

Lapierre, J.-F., Seekell, D.A. et del Giorgio, P.A. 2015. Climate and landscape influence on indicators of lake carbon cycling through spatial patterns in dissolved organic carbon. *Global Change Biology*. DOI: 10.1111/gcb.13031.

Larsen, S., Andersen, T. et Hessen, D.O. 2011. The pCO_2 in boreal lakes: Organic carbon as a universal predictor? *Global Biogeochemical Cycles*, 25 (3). DOI: 10.1029/2010GB003864.

Laudon, H., Berggren, M., Ågren, A., Buffam, I., Bishop, K., Grabs, T., Jansson, M. et Köhler, S. 2011. Patterns and Dynamics of Dissolved Organic Carbon (DOC) in Boreal Streams: The Role of Processes, Connectivity, and Scaling. *Ecosystems*, 14 (6), 880-893. DOI: 10.1007/s10021-011-9452-8.

Lindell, M., Granéli, W. et Tranvik, L. 1995. Enhanced bacterial growth in response to photochemical transformation of dissolved organic matter. *Limnology and Oceanography*, 40 (1), 195-199.

Lindell, M.J., Granéli, H.W. et Bertilsson, S. 2000. Seasonal photoreactivity of dissolved organic matter from lakes with contrasting humic content. *Canadian Journal of Fisheries and Aquatic Sciences*, 57 (5), 875-885. DOI: 10.1139/cjfas-57-5-875.

López Bellido, J., Tulonen, T., Kankaala, P. et Ojala, A. 2009. CO_2 and CH_4 fluxes during spring and autumn mixing periods in a boreal lake (Pääjärvi, southern Finland). *Journal of Geophysical Research*, 114 (G4), G04007. DOI: 10.1029/2009JG000923.

Maberly, S. 1996. Diel, episodic and seasonal changes in pH and concentrations of

inorganic carbon in a productive lake. *Freshwater Biology*, 579-598.

Maberly, S.C., Barker, P.A., Stott, A.W. et De Ville, M.M. 2012. Catchment productivity controls CO2 emissions from lakes. *Nature Climate Change*, 3 (4), 391-394. DOI: 10.1038/nclimate1748.

Madronich, S. et Flocke, S. 1997. Theoretical Estimation of Biologically Effective UV Radiation at the Earth's Surface. Dans *Solar Ultraviolet Radiation*, sous la dir. de Christos S. Zerefos et Alkiviadis F. Bais, p. 23-48. Springer Berlin Heidelberg.

Marchand, D., Prairie, Y.T. et del Giorgio, P.A. 2009. Linking forest fires to lake metabolism and carbon dioxide emissions in the boreal region of Northern Quebec. *Global Change Biology*, 15, 2861-2873. DOI: 10.1111/j.1365-2486.2009.01979.x.

Marin-Spiotta, E., Gruley, K.E., Crawford, J., Atkinson, E.E., Miesel, J.R., Greene, S., Cardona-Correa, C. et Spencer, R.G.M. 2014. Paradigm shifts in soil organic matter research affect interpretations of aquatic carbon cycling: transcending disciplinary and ecosystem boundaries. *Biogeochemistry*. DOI: 10.1007/s10533-013-9949-7.

Markager, S. et Vincent, W.F. 2000. Spectral light attenuation and the absorption of UV and blue light in natural waters. *Limnology and Oceanography*, 45 (3), 642-650.

Marschner, B. et Kalbitz, K. 2003. Controls of bioavailability and biodegradability of dissolved organic matter in soils. *Geoderma*, 113 (3-4), 211-235. DOI: 10.1016/S0016-7061(02)00362-2.

McCallister, S.L. et del Giorgio, P.A. 2008. Direct measurement of the d13C signature of carbon respired by bacteria in lakes: Linkages to potential carbon sources, ecosystem baseline metabolism, and CO_2 fluxes. *Limnology and Oceanography*, 53 (4), 1204-1216.

McDonald, C.P., Stets, E.G., Striegl, R.G. et Butman, D. 2013. Inorganic carbon loading as a primary driver of dissolved carbon dioxide concentrations in the lakes and reservoirs of the contiguous United States. *Global Biogeochemical Cycles*, 27, 1-11. DOI: 10.1002/gbc.20032.

McNair, J.N., Gereaux, L.C., Weinke, A.D., Sesselmann, M.R., Kendall, S.T. et Biddanda, B. a. 2013. New methods for estimating components of lake

metabolism based on free-water dissolved-oxygen dynamics. *Ecological Modelling*, 263, 251-263. DOI: 10.1016/j.ecolmodel.2013.05.010.

Meehl, G.A., Arblaster, J.M. et Tebaldi, C. 2005. Understanding future patterns of increased precipitation intensity in climate model simulations. *Geophysical Research Letters*, 32 (18). DOI: 10.1029/2005GL023680.

Minns, C. et Shuter, B. 2012. A semi-mechanistic seasonal temperature-profile model (STM) for the period of stratification in dimictic lakes. *Canadian Journal of Fisheries and Aquatic Sciences*, 181 (December 2012), 169-181.

Molot, L.A. et Dillon, P.J. 1997. Photolyric regulation of dissolved organic carbon in northern lakes. *Global Biogeochemical Cycles*, 11 (3), 357-365.

Monsen, N.E., Cloern, J.E., Lucas, L. V. et Monismith, S.G. 2002. The use of flushing time, residence time, and age as transport time scales. *Limnology and Oceanography*, 47 (5), 1545-1553. DOI: 10.4319/lo.2002.47.5.1545.

Monteith, D.T., Stoddard, J.L., Evans, C.D., de Wit, H.A., Forsius, M., Hogasen, T., Wilander, A., *et al.* 2007. Dissolved organic carbon trends resulting from changes in atmospheric deposition chemistry. *Nature*, 450 (7169), 537-540.

Morales-Pineda, M., Cozar, A., Laiz, I., Ubeda, B. et Galvez, J.A. 2014. Daily, biweekly, and seasonal temporal scales of pCO_2 variability in two stratified Mediterranean reservoirs. *Journal of Geophysical Research: Biogeosciences*. DOI: 10.1002/2013JG002317.Received.

Ojala, A., López Bellido, J., Tulonen, T., Kankaala, P. et Huotari, J. 2011. Carbon gas fluxes from a brown-water and a clear-water lake in the boreal zone during a summer with extreme rain events. *Limnology and Oceanography*, 56 (1), 61-76. DOI: 10.4319/lo.2011.56.01.0061.

OMI Science Team. 2012. OMI/Aura TOMS-Like Ozone, Aerosol Index, Cloud Radiance Fraction Daily L3 Global 1.0x1.0 deg,version 003. *NASA Goddard Space Flight Center*.

Opsahl, S. et Benner, R. 1998. Photochemical reactivity of dissolved lignin in river and ocean waters. *Limnology and Oceanography*, 43 (6), 1297-1304. DOI: 10.4319/lo.1998.43.6.1297.

Öquist, M.G., Wallin, M., Seibert, J., Bishop, K. et Laudon, H. 2009. Dissolved inorganic carbon export across the soil/stream interface and its fate in a boreal

headwater stream. *Environmental science & technology*, 43 (19), 7364-9.

Pace, M. et Prairie, Y.T. 2005. Respiration in lakes. *dans P. A. del Giorgio et P. J. leB. Williams (eds), Respiration inAquatic Ecosystems. Oxford University Press*, sous la dir. de Paul A. del Giorgio et Peter J.L.B. Williams, p. 103:121. New York : Oxford University Press.

Porcal, P., Dillon, P.J. et Molot, L.A. 2013. Seasonal changes in photochemical properties of dissolved organic matter in small boreal streams. *Biogeosciences*, 10 (8), 5533-5543. DOI: 10.5194/bg-10-5533-2013.

Prairie, Y. 2008. Carbocentric limnology: Looking back, looking forward. *Canadian Journal of Fisheries and Aquatic Sciences*, 548 (January 2005), 543-548. DOI: 10.1139/F08-011.

Prairie, Y., Bird, D. et Cole, J. 2002. The summer metabolic balance in the epilimnion of southeastern Quebec lakes. *Limnology and Oceanography*, 47 (1), 316-321.

Pumpanen, J., Ilvesniemi, H., Kulmala, L., Siivola, E., Laakso, H., Kolari, P., Helenelund, C., Laakso, M., Uusimaa, M. et Hari, P. 2008. Respiration in Boreal Forest Soil as Determined from Carbon Dioxide Concentration Profile. *Soil Science Society of America Journal*, 72 (5), 1187. DOI: 10.2136/sssaj2007.0199.

R Development Core Team. 2008. R: A language and environment for statistical computing. Vienna, Austria : R Foundation for Statistical Computing.

Rantakari, M. et Kortelainen, P. 2005. Interannual variation and climatic regulation of the CO_2 emission from large boreal lakes. *Global Change Biology*, 11 (8), 1368-1380. DOI: 10.1111/j.1365-2486.2005.00982.x.

Rasilo, T., Ojala, A., Huotari, J. et Pumpanen, J. 2012. Rain Induced Changes in Carbon Dioxide Concentrations in the Soil–Lake–Brook Continuum of a Boreal Forested Catchment. *Vadose Zone Journal*, 11 (2). DOI: 10.2136/vzj2011.0039.

Rasilo, T., Prairie, Y.T. et Del Giorgio, P.A. 2014. Large-scale patterns in summer diffusive CH4 fluxes across boreal lakes, and contribution to diffusive C emissions. *Global change biology*, 1, 1-16. DOI: 10.1111/gcb.12741.

Raymond, P.A., Hartmann, J., Lauerwald, R., Sobek, S., McDonald, C., Hoover, M., Butman, D., et al. 2013. Global carbon dioxide emissions from inland waters. *Nature*, 503 (7476), 355-9. DOI: 10.1038/nature12760.

Raymond, P.A. et Saiers, J.E. 2010. Event controlled DOC export from forested watersheds. *Biogeochemistry*, 100 (1-3), 197-209. DOI: 10.1007/s10533-010-9416-7.

Read, J.S., Hamilton, D.P., Desai, A.R., Rose, K.C., MacIntyre, S., Lenters, J.D., Smyth, R.L., et al. 2012. Lake-size dependency of wind shear and convection as controls on gas exchange. *Geophysical Research Letters*, 39 (9). DOI: 10.1029/2012GL051886.

Read, J.S., Hamilton, D.P., Jones, I.D., Muraoka, K., Winslow, L. a., Kroiss, R., Wu, C.H. et Gaiser, E. 2011. Derivation of lake mixing and stratification indices from high-resolution lake buoy data. *Environmental Modelling & Software*, 26 (11), 1325-1336. DOI: 10.1016/j.envsoft.2011.05.006.

Riera, J., Schindler, J. et Kratz, T. 1999. Seasonal dynamics of carbon dioxide and methane in two clear-water lakes and two bog lakes in northern Wisconsin, USA. *Canadian Journal of Fisheries and Aquatic Sciences*, 274, 265-274.

Roehm, C.L., Prairie, Y.T. et del Giorgio, P.A. 2009. The pCO_2 dynamics in lakes in the boreal region of northern Québec, Canada. *Global Biogeochemical Cycles*, 23 (3). DOI: 10.1029/2008GB003297.

Rosenberry, D.O., Winter, T.C., Buso, D.C. et Likens, G.E. 2007. Comparison of 15 evaporation methods applied to a small mountain lake in the northeastern USA. *Journal of Hydrology*, 340 (3-4), 149-166. DOI: 10.1016/j.jhydrol.2007.03.018.

Roulet, N. et Moore, T.R. 2006. Browning the waters. *Nature*, 444 (November), 2-3.

Sadro, S. et Melack, J.M. 2012. The Effect of an Extreme Rain Event on the Biogeochemistry and Ecosystem Metabolism of an Oligotrophic High-Elevation Lake. *Arctic, Antarctic, and Alpine Research*, 44 (2), 222-231. DOI: 10.1657/1938-4246-44.2.222.

Sadro, S., Melack, J.M. et MacIntyre, S. 2011. Depth-integrated estimates of ecosystem metabolism in a high-elevation lake (Emerald Lake, Sierra Nevada, California). *Limnology and Oceanography*, 56 (5), 1764-1780. DOI: 10.1007/s10021-011-9471-5.

Salonen, K. et Vähätalo, A. 1994. Photochemical mineralisation of dissolved organic matter in lake Skjervatjern. *Environment International*, 20 (3), 307-312. DOI: http://dx.doi.org/10.1016/0160-4120(94)90114-7.

Sand-Jensen, K. et Staehr, P.A. 2011. CO_2 dynamics along Danish lowland streams: water–air gradients, piston velocities and evasion rates. *Biogeochemistry*, 111 (1-3), 615-628. DOI: 10.1007/s10533-011-9696-6.

Schindler, D.W., Armstrong, F.A.J., Holmgren, S.K. et Brunskill, G.J. 1971. Eutrophication of Lake 227, Experimental Lakes Area, Northwestern Ontario, by Addition of Phosphate and Nitrate. *Journal of the Fisheries Research Board of Canada*, 28 (11), 1763-1782. DOI: 10.1139/f71-261.

Scully, N.M., Cooper, W.J. et Tranvik, L.J. 2003. Photochemical effects on microbial activity in natural waters: the interaction of reactive oxygen species and dissolved organic matter. *FEMS microbiology ecology*, 46 (3), 353-7. DOI: 10.1016/S0168-6496(03)00198-3.

Seekell, D.A., Lapierre, J.-F., Ask, J., Bergström, A.-K., Deininger, A., Rodríguez, P. et Karlsson, J. 2015. The influence of dissolved organic carbon on primary production in northern lakes. *Limnology and Oceanography*. DOI: 10.1002/lno.10096.

Sobek, S., Algesten, G., Bergström, A.-K., Jansson, M. et Tranvik, L.J. 2003. The catchment and climate regulation of *p*CO2 in boreal lakes. *Global Change Biology*, 9, 630-641.

Sobek, S., Durisch-Kaiser, E., Zurbrügg, R., Wongfun, N., Wessels, M., Pasche, N. et Wehrli, B. 2009. Organic carbon burial efficiency in lake sediments controlled by oxygen exposure time and sediment source. *Limnology and Oceanography*, 54 (6), 2243-2254. DOI: 10.4319/lo.2009.54.6.2243.

Sobek, S., Tranvik, L.J. et Cole, J.J. 2005. Temperature independence of carbon dioxide supersaturation in global lakes. *Global Biogeochemical Cycles*, 19 (2), 1-10. DOI: 10.1029/2004GB002264.

Solomon, C.T., Bruesewitz, D.A., Richardson, D.C., Rose, K.C., Van de Bogert, M.C., Hanson, P.C., Kratz, T.K., *et al.* 2013. Ecosystem respiration : Drivers of daily variability and background respiration in lakes around the globe. *Limnology and Oceanography*, 58 (3), 849-866. DOI: 10.4319/lo.2013.58.3.0849.

Solomon, C.T., Jones, S.E., Weidel, B.C., Buffam, I., Fork, M.L., Karlsson, J., Larsen, S., *et al.* 2015. Ecosystem Consequences of Changing Inputs of Terrestrial Dissolved Organic Matter to Lakes: Current Knowledge and Future Challenges. *Ecosystems* (January), 376-389. DOI: 10.1007/s10021-015-9848-y.

Soumis, N., Canuel, R. et Lucotte, M. 2008. Evaluation of Two Current Approaches for the Measurement of Carbon Dioxide Diffusive Fluxes from Lentic Ecosystems. *Environmental science & technology*, 42 (8), 2964-2969.

Soumis, N., Lucotte, M., Larose, C., Veillette, F. et Canuel, R. 2007. Photomineralization in a boreal hydroelectric reservoir: a comparison with natural aquatic ecosystems. *Biogeochemistry*, 86 (2), 123-135. DOI: 10.1007/s10533-007-9141-z.

Sprugel, D.G. 1983. Correcting for bias in log-transformed allometric equations. *Ecology*, 64 (1), 209-210.

Staehr, P.A., Sand-Jensen, K., Raun, A.L., Nilsson, B. et Kidmose, J. 2010a. Drivers of metabolism and net heterotrophy in contrasting lakes. *Limnology and Oceanography*, 55 (2), 817-830. DOI: 10.4319/lo.2009.55.2.0817.

Staehr, P.A., Baastrup-Spohr, L., Sand-Jensen, K. et Stedmon, C. 2011. Lake metabolism scales with lake morphometry and catchment conditions. *Aquatic Sciences*, 74 (1), 155-169. DOI: 10.1007/s00027-011-0207-6.

Staehr, P.A., Bade, D., Van DeBogert, M.C., Koch, G.R., Williamson, C., Hanson, P., Cole, J.J. et Kratz, T. 2010b. Lake metabolism and the diel oxygen technique: State of the science. *Limnology And Oceanography Methods*, 8, 628-644. DOI: 10.4319/lom.2010.8.628.

Staehr, P.A., Christensen, J.P.A., Batt, R.D. et Read, J.S. 2012. Ecosystem metabolism in a stratified lake. *Limnology and Oceanography*, 57 (5), 1317-1330. DOI: 10.4319/lo.2012.57.5.1317.

Staehr, P.A. et Sand-Jensen, K. 2013. Temporal dynamics and regulation of lake metabolism. *Limnology and Oceanography*, 52 (1), 108-120. DOI: 10.4319/lo.2007.52.1.0108.

Stets, E.G., Striegl, R.G. et Aiken, G.R. 2010. Dissolved organic carbon export and internal cycling in small, headwater lakes. *Global Biogeochemical Cycles*, 24 (4). DOI: 10.1029/2010GB003815.

Stets, E.G., Striegl, R.G., Aiken, G.R., Rosenberry, D.O. et Winter, T.C. 2009. Hydrologic support of carbon dioxide flux revealed by whole-lake carbon budgets. *Journal of Geophysical Research*, 114 (G1), G01008. DOI: 10.1029/2008JG000783.

Striegl, R.G., Kortelainen, P., Chanton, J.P., Wickland, K.P., Bugna, G.C. et Rantakari, M. 2001. Carbon dioxide partial pressure and ^{13}C content of north temperate and boreal lakes at spring ice melt. *Limnology and Oceanography*.

Striegl, R.G. et Michmerhuizen, C.M. 1998. Hydrologic influence on methane and carbon dioxide dynamics at two north-central Minnesota lakes. *Limnology and Oceanography*.

Stubbins, A., Hubbard, V., Uher, G., Law, C.S., Upstill-goddard, R.C., Aiken, G.R. et Mopper, K. 2008. Relating Carbon Monoxide Photoproduction to Dissolved Organic Matter Functionality. *Environmental science & technology*, 42 (9), 3271-3276.

Stubbins, A., Law, C.S., Uher, G. et Upstill-Goddard, R.C. 2011. Carbon monoxide apparent quantum yields and photoproduction in the Tyne estuary. *Biogeosciences*, 8 (3), 703-713. DOI: 10.5194/bg-8-703-2011.

Suhett, A.L., Amado, A.M., Enrich-Prast, A., Esteves, F.D.A. et Farjalla, V.F. 2007. Seasonal changes of dissolved organic carbon photo-oxidation rates in a tropical humic lagoon: the role of rainfall as a major regulator. *Canadian Journal of Fisheries and Aquatic Sciences*, 64 (9), 1266-1272. DOI: 10.1139/f07-103.

Teodoru, C.R., del Giorgio, P.A., Prairie, Y.T. et Camire, M. 2009. Patterns in pCO_2 in boreal streams and rivers of northern Quebec, Canada. *Global Biogeochemical Cycles*, 23 (2). DOI: 10.1029/2008GB003404.

Tranvik, L.J., Downing, J.A., Cotner, J.B., Loiselle, S.A., Striegl, R.G., Ballatore, T.J., Dillon, P., et al. 2009. Lakes and reservoirs as regulators of carbon cycling and climate. *Limnology and Oceanography*, 54 (6_part_2), 2298-2314. DOI: 10.4319/lo.2009.54.6_part_2.2298.

Tsai, J.-W., Kratz, T.K., Hanson, P.C., Wu, J.-T., Chang, W.Y.B., Arzberger, P.W., Lin, B.-S., Lin, F.-P., Chou, H.-M. et Chiu, C.-Y. 2008. Seasonal dynamics, typhoons and the regulation of lake metabolism in a subtropical humic lake. *Freshwater Biology*, 53 (10), 1929-1941. DOI: 10.1111/j.1365-2427.2008.02017.x.

Vachon, D. et del Giorgio, P.A. 2014. Whole-lake CO_2 dynamics in response to storm events in two morphologically different lakes. *Ecosystems*, 17 (8), 1338-1353. DOI: 10.1007/s10021-014-9799-8.

Vachon, D. et Prairie, Y.T. 2013. The ecosystem size and shape dependence of gas

transfer velocity versus wind speed relationships in lakes. *Canadian Journal of Fisheries and Aquatic Sciences*, 70 (12), 1757-1764. DOI: 10.1139/cjfas-2013-0241.

Vachon, D., Prairie, Y.T. et Cole, J.J. 2010. The relationship between near-surface turbulence and gas transfer velocity in freshwater systems and its implications for floating chamber measurements of gas exchange. *Limnology and Oceanography*, 55 (4), 1723-1732. DOI: 10.4319/lo.2010.55.4.1723.

Vadeboncoeur, Y., Peterson, G., Zanden, M.J. Vander et Kalff, J. 2008. Benthic algal production across lake size Gradients: Interactions among morphometry, nutrients, and light. *Ecology*, 89 (9), 2542-2552. DOI: 10.1890/07-1058.1.

Vadeboncoeur, Y. et Steinman, A.D. 2002. Periphyton function in lake ecosystems. *TheScientificWorldJournal*, 2, 1449-68. DOI: 10.1100/tsw.2002.294.

Vähätalo, A., Salkinoja-Salonen, M., Taalas, P. et Salonen, K. 2000. Spectrum of the quantum yield for photochemical mineralization of dissolved organic carbon in a humic lake. *Limnology and Oceanography*, 45 (3), 664-676.

Vähätalo, A. V., Aarnos, H. et Mäntyniemi, S. 2010. Biodegradability continuum and biodegradation kinetics of natural organic matter described by the beta distribution. *Biogeochemistry*, 100 (1-3), 227-240. DOI: 10.1007/s10533-010-9419-4.

Venkiteswaran, J.J., Wassenaar, L.I. et Schiff, S.L. 2007. Dynamics of dissolved oxygen isotopic ratios: a transient model to quantify primary production, community respiration, and air-water exchange in aquatic ecosystems. *Oecologia*, 153 (2), 385-98. DOI: 10.1007/s00442-007-0744-9.

Verpoorter, C., Kutser, T., Seekell, D.A. et Tranvik, L.J. 2014. A global inventory of lakes based on high-resolution satellite imagery. *Geophysical Research Letters*, 41. DOI: 10.1002/2014GL060641.

Vogt, R.J., Rusak, J.A., Patoine, A. et Leavitt, P.R. 2011. Differential effects of energy and mass influx on the landscape synchrony of lake ecosystems. *Ecology*, 92 (5), 1104-1114.

von Wachenfeldt, E. et Tranvik, L.J. 2008. Sedimentation in Boreal Lakes—The Role of Flocculation of Allochthonous Dissolved Organic Matter in the Water Column. *Ecosystems*, 11 (5), 803-814. DOI: 10.1007/s10021-008-9162-z.

Wanninkhof, R. 1992. Relationship between wind speed and gas exchange over the ocean. *Journal of Geophysical Research: Oceans*, 97 (92), 7373-7382.

Wetzel, R.R.G., Hatcher, P.P.G. et Bianchi, T.T.S. 1995. Natural photolysis by ultraviolet irradiance of recalcitrant dissolved organic matter to simple substrates for rapid bacterial metabolism. *Limnology and Oceanography*, 40 (8), 1369-1380.

Weyhenmeyer, G.A., Fröberg, M., Karltun, E., Khalili, M., Kothawala, D., Temnerud, J. et Tranvik, L.J. 2012. Selective decay of terrestrial organic carbon during transport from land to sea. *Global Change Biology*, 18 (1), 349-355. DOI: 10.1111/j.1365-2486.2011.02544.x.

Weyhenmeyer, G.A., Kortelainen, P., Sobek, S., Müller, R. et Rantakari, M. 2012. Carbon Dioxide in Boreal Surface Waters: A Comparison of Lakes and Streams. *Ecosystems*, 15 (8), 1295-1307. DOI: 10.1007/s10021-012-9585-4.

White, E.M., Kieber, D.J., Sherrard, J., Miller, W.L. et Mopper, K. 2010. Carbon dioxide and carbon monoxide photoproduction quantum yields in the Delaware Estuary. *Marine Chemistry*, 118 (1-2), 11-21. DOI: 10.1016/j.marchem.2009.10.001.

Wickland, K.P., Neff, J.C. et Aiken, G.R. 2007. Dissolved Organic Carbon in Alaskan Boreal Forest: Sources, Chemical Characteristics, and Biodegradability. *Ecosystems*, 10 (8), 1323-1340. DOI: 10.1007/s10021-007-9101-4.

Wilkinson, G.M., Pace, M.L. et Cole, J.J. 2013. Terrestrial dominance of organic matter in north temperate lakes. *Global Biogeochemical Cycles*, 27 (November 2012). DOI: 10.1029/2012GB004453.

Wilson, H.F., Saiers, J.E., Raymond, P.A. et Sobczak, W. V. 2013. Hydrologic Drivers and Seasonality of Dissolved Organic Carbon Concentration, Nitrogen Content, Bioavailability, and Export in a Forested New England Stream. *Ecosystems*, 604-616. DOI: 10.1007/s10021-013-9635-6.

Worrall, F., Burt, T. et Adamson, J. 2005. Fluxes of dissolved carbon dioxide and inorganic carbon from an upland peat catchment: implications for soil respiration. *Biogeochemistry*, 73 (3), 515-539. DOI: 10.1007/s10533-004-1717-2.

Xie, H., Bélanger, S., Demers, S., Vincent, W.F. et Papakyriakou, T.N. 2009. Photobiogeochemical cycling of carbon monoxide in the southeastern Beaufort

Sea in spring and autumn. *Limnology and Oceanography*, 54 (1), 234-249. DOI: 10.4319/lo.2009.54.1.0234.

Yin, J.H. 2005. A consistent poleward shift of the storm tracks in simulations of 21st century climate. *Geophysical Research Letters*, 32 (18). DOI: 10.1029/2005GL023684.

Yvon-Durocher, G., Caffrey, J.M., Cescatti, A., Dossena, M., del Giorgio, P., Gasol, J.M., Montoya, J.M., et al. 2012. Reconciling the temperature dependence of respiration across timescales and ecosystem types. *Nature*, 487 (7408), 472-6. DOI: 10.1038/nature11205.

Zepp, R.G. 1978. Quantum Yields for Reaction of Pollutants in Dilute Aqueous Solution, 12 (85), 1976-1978.

Zwart, J.A., Craig, N., Kelly, P.T., Sebestyen, S.D., Solomon, C.T., Weidel, B.C. et Jones, S.E. 2015. Metabolic and physiochemical responses to a whole-lake experimental increase in dissolved organic carbon in a north-temperate lake. *Limnology and Oceanography*. DOI: 10.1002/lno.10248.